Vibrio cholerae's ToxRS Bile Sensing System

N. Gubensäk[1*], T. Sagmeister[1], C. Buhlheller[1], B. D. Geronimo[2], G. E. Wagner[3,4], L. Petrowitsch[1], M. Gräwert[5], M. Rotzinger[3], T. M. I. Berger[1], J. Schäfer[6], I. Usón[7,8], J. Reidl[1,9,10], P. A. Sánchez-Murcia[2], K. Zangger[3,9,10] and T. Pavkov-Keller[1,9,10]*

1 Institute of Molecular Biosciences; University of Graz, Graz, Austria.
2 Laboratory of Computer-Aided Molecular Design, Division of Medicinal Chemistry, Otto-Loewi Research Center; Medical University of Graz, Graz, Austria.
3 Institute of Chemistry / Organic and Bioorganic Chemistry; University of Graz, Graz, Austria.
4 Diagnostic and Research Institute of Hygiene, Microbiology and Environmental Medicine, Medical University of Graz, Graz, Austria.
5 EMBL Hamburg; Hamburg, Germany.
6 RedShiftBio; Boxborough, Massachusetts, United States.
7 Institute of Molecular Biology of Barcelona (IBMB–CSIC); Barcelona, Spain.
8 ICREA, Institució Catalana de Recerca i Estudis Avançats; Barcelona, Spain.
9 BioHealth Field of Excellence, University of Graz; Graz, Austria.
10 BioTechMed-Graz; Graz, Austria..

*Nina Gubensäk, Tea Pavkov-Keller

Email: nina.gubensaek@uni-graz.at, tea.pavkov@uni-graz.at

Competing Interest Statement: Authors declare that they have no competing interests.

Classification: Biological Sciences – Biochemistry

Keywords: Vibrio cholerae – protein interaction – virulence regulation – transcription factor - ToxRS

This PDF file includes:

Main Text
Figures 1 to 11
References

Abstract

The seventh pandemic of the diarrheal cholera disease, which began in 1960, is caused by the Gram-negative bacterium *Vibrio cholerae*. Its environmental persistence provoking recurring sudden outbreaks is enabled by *V. cholerae's* rapid adaption to changing environments involving sensory proteins like ToxR and ToxS. Located at the inner membrane, ToxR and ToxS react to environmental stimuli like bile acid, thereby inducing survival strategies e.g. bile resistance and virulence regulation. The presented crystal structure of the sensory domains of ToxR and ToxS in combination with multiple bile acid interaction studies, reveals that a bile binding pocket of ToxS is only properly folded upon binding to ToxR. Our data proposes an interdependent functionality between ToxR transcriptional activity and ToxS sensory function. These findings support the previously suggested link between ToxRS and VtrAC-like co-component systems. Besides VtrAC, ToxRS is now the only experimentally determined structure within this recently defined superfamily, further emphasizing its significance.

In-depth analysis of the ToxRS complex reveals its remarkable conservation across various *Vibrio* species, underlining the significance of conserved residues in the ToxS barrel and the more diverse ToxR sensory domain. Unravelling the intricate mechanisms governing ToxRS's environmental sensing capabilities, provides a promising tool for disruption of this vital interaction, ultimately inhibiting *Vibrio's* survival and virulence. Our findings hold far-reaching implications for all *Vibrio* strains that rely on the ToxRS system as a shared sensory cornerstone for adapting to their surroundings.

Main Text

Introduction

The Gram-negative bacterium *Vibrio cholerae* is the causative agent of the diarrheal cholera disease, which is pandemic since 1960 (***Hu et al., 2016***). Its dangerousness is highlighted by its sudden outbreaks and environmental persistence causing 21 000 to 143 000 deaths worldwide per year (***Ali et al., 2015***) including long-lasting environmental and economic damage (***Kanungo et al., 2022***).

V. cholerae exhibits a life cycle between dormant and virulent state, enabled by its rapid adaption to changing environments (***Almagro-Moreno et al., 2015b; Bari et al., 2013***). This survival mechanism is maintained via sensory proteins reacting to environmental conditions and substances (***DiRita et al., 1991; Hung and Mekalanos, 2005***). For entero-pathogens like *V. cholerae*, bile acid represents one of the major components for virulence activation, pressuring survival strategies (***Hung et al., 2006; Hung and Mekalanos, 2005; Li et al., 2016; Midgett et al., 2017***).

ToxR is a transmembrane transcription factor (Fig. Figure 1-figure supplement 1) involved in the regulation of numerous genes, not only virulence associated, and can function as an activator, co-activator and repressor (***Bina et al., 2003; Champion et al., 1997; Lee et al., 2000; Morgan et al., 2011; Skorupski and Taylor, 1997; Wang et al., 2002; Welch and Bartlett, 1998***). ToxR periplasmic domain is proposed to act as environmental sensor, being able to bind bile acids (***Midgett et al., 2017; Midgett et al., 2020***) and consequently activate transcription with its cytoplasmic DNA binding domain (***Gubensäk et al., 2021a; Morgan et al., 2011; Morgan et al., 2019; Pfau and Taylor, 1996; Withey and DiRita, 2006***), thus inducing a switch of outer membrane proteins from OmpT to OmpU (***Simonet et al., 2003; Wibbenmeyer et al., 2002***). Since OmpU is more efficient in excluding bile salts due to its negatively charged pore (***Duret and Delcour, 2006; Simonet et al., 2003***), bile-induced ToxR activation enables *V. cholerae* survival in the human gut (***Wibbenmeyer et al., 2002***).

ToxS is built of a periplasmic, a transmembrane and a short cytoplasmic region (Fig. Figure 1-figure supplement 1). The periplasmic domain of ToxS (ToxSp) interacts with the periplasmic domain of ToxR (ToxRp) forming a stable heterodimer (ToxRSp) (***Gubensäk et al., 2021b***) thereby protecting ToxR from periplasmic proteolysis and enhancing its activity (***Almagro-Moreno et al., 2015a; Almagro-Moreno et al., 2015c; Gubensäk et al., 2021b; Lembke et al., 2018; Pennetzdorfer et al., 2019***).

The exact mechanism of ToxR functionality is not clear yet, it was proposed that ToxR binds DNA as a homodimer at the so called 'tox-boxes' which represent direct repeat DNA motifs (***Crawford et al., 1998; Goss et al., 2013; Krukonis and DiRita, 2003; Ottemann and Mekalanos, 1996; Pfau and Taylor, 1996; Withey and DiRita, 2006***). Recently it was shown that ToxR uses a topological DNA recognition mechanism by recognizing DNA structural elements rather than base sequences (***Canals et al., 2023***). Also, it is suggested that by multiple binding events of ToxR to promoter regions, membrane attached transcription regulation of ToxR is enabled (***Canals et al., 2023***). The versatile functionality of ToxR suggests a general role of ToxRS in *Vibrio* strains, e.g. the sensing and

consequent adaption to changing environmental conditions (***Chen et al., 2018; Provenzano et al., 2000***).

Bile significantly alters the virulence factor production. Nevertheless, the exact mechanism remains unclear. Studies showed opposite outcomes in regard of up- or downregulation of virulence factors by bile (***Bina et al., 2021; Gupta and Chowdhury, 1997; Hung and Mekalanos, 2005; Midgett et al., 2017; Xue et al., 2016; Yang et al., 2013***). On the one hand a bile induced reduction of virulence factor production was observed (***Gupta and Chowdhury, 1997***) via inhibiting ToxT DNA binding ability (***Plecha and Withey, 2015***). On the other hand bile seems to enhance TcpP and ToxR activity (***Yang et al., 2013***) and even induce ToxR ability to activate *ctx* without ToxT in classical biotype *V. cholerae* strains (***Hung and Mekalanos, 2005***). Nevertheless, direct activation of *ctx* by ToxRS by bile acids is dependent on *ctx* promotors, differing between strains (***Hung and Mekalanos, 2005***). Concluding, the effect of bile on *V. cholerae* virulence seems to be complex and probably dependent on multiple other factors e.g. calcium concentration and oxygen levels (***Hay et al., 2017; Sengupta et al., 2014***).

The presented crystal structure of sensory domains of *V. cholerae* ToxR and ToxS reveals ToxS as a main environmental sensor in *V. cholerae*. The ToxRS complex exposes a bile binding pocket inside ToxS lipocalin-like barrel that is only properly built via stabilization by newly formed structural elements of ToxR. We performed multiple interaction experiments combined with extensive molecular dynamic MD simulations, to eventually present a bile binding ToxRSp complex, revealing contributions from both proteins to the interaction with bile acid. ToxRSp shows structural and functional similarities with bile sensing complex VtrAC from *V. parahaemolyticus* (***Alnouti, 2009; Li et al., 2016; Tomchick et al., 2016***) thus supporting a common superfamily of co-component signal transduction systems whose sensory function is strictly connected to an obligate heterodimer formation (***Kinch et al., 2022***). AlphaFold-Multimer (***Evans et al., 2021; Jumper et al., 2021***) structure predictions furthermore reveal a conserved fold of ToxS in different *Vibrio* species, in contrast to ToxR exhibiting a structural variability among different *Vibrio* strains.

Results

Periplasmic domains of *V. cholerae* ToxRS form an obligate dimer.

The crystal structure of ToxRp and ToxSp reveals the formation of a heterodimer, with ToxRp contributing secondary structure elements to ToxSp otherwise unstable ß-barrel fold (Fig. 1, Fig. 2, pdb: 8ALO). The complex forms spontaneously upon addition of both proteins.

ToxRp in the complex has an αß fold which is formed by an α-helix flanked by an anti-parallel hairpin and a three-stranded anti-parallel ß-sheet, followed by a C-terminal helix (Fig. 1). Together, the ß-strands form a five-stranded anti-parallel ß-sheet. The C-terminal $Cys293_{ToxRp}$ is involved in a solution-oriented disulphide bond with $Cys236_{ToxRp}$ of the N-terminal helix (Fig. 3).

ToxSp forms a lipocalin-like fold consisting of an eight-stranded ß-barrel stabilized by intermolecular H-bond network and flanked by two α-helices located at the openings of the barrel (Fig. 2, Supplementary File 3). For a correct barrel formation ToxSp ß1 and ß8 would need to be close enough for building main chain interactions. However, ToxSp ß8 contacts only the first three residues of nine residues long ToxSp ß1 (Fig. 2). ToxRp ß5 is positioned into this gap and forms main chain H-bonds with remaining ToxSp ß1 residues. Additionally, close side-chain interactions between ToxRp ß4 and ToxSp ß8 further stabilize ToxSp ß8 positioning (Fig. 2). ToxRp ß4 and ß3 are also involved in side-chain interactions with ToxSp ß7 and ß6 completing the strong complex formation. The residue Arg281 located in ToxRp ß5 forms an intermolecular salt bridge with Asp142 of ToxSp α2, which restricts the opening of the barrel (Fig. 2).

DSSP secondary structure analysis (***Kabsch and Sander, 1983; Touw et al., 2015***) indicates a ten-stranded intermolecular ß-sheet consisting of ß1-ß5 of ToxSp and ß1-ß5 of ToxRp. ToxSp five stranded ß-sheet (ß1-ß5) and three-stranded ß-sheet (ß6-ß8), result in a ß-barrel formation, which is stabilized mainly via hydrophobic core interactions and interactions with ToxRp ß5. (Fig.1).

Mutational studies reveal that ToxSp mutant L33S results in increased proteolysis of ToxRp indicating a loss of function of ToxS (***Pfau and Taylor, 1998***). The crystal structure of ToxRSp shows that L33 is located at ToxSp α1 at the N-terminal membrane-oriented opening of the barrel of ToxSp (Figure 1-figure supplement 2). L33 forms central hydrophobic interactions with apolar residues of ToxSp ß strands stabilizing the core of the barrel (Figure 1-figure supplement 2.). A serine to leucine mutation probably disrupts the hydrophobic interactions and may result in a loss of structure, thus explaining the inability of ToxSp L33S mutant to protect ToxR from proteolysis (***Pfau and Taylor, 1998***).

There are currently no structures of proteins with significant sequence homology to the ToxRSp complex available in the protein data bank. However, despite the lack of sequence identity the VtrAC complex of *V. parahaemolyticus* (***Tomchick et al., 2016***) (pdb code: 5KEV, 5KEW) has striking structural and functional similarities with ToxRSp from *V. cholerae* (Figure 1-figure supplement 3, all-atom RMSD 5.348 Å calculated for 836 atoms; sequence identity: ToxRp-VtrA: 8.1%; ToxSp-VtrC: 11.7%). Similar to ToxRS, the bile sensing functionality of VtrAC induces an essential step for virulence activation upon human gastro-intestinal infection. VtrAC activates the production of main virulence factor VtrB which enables the production of a type III secretion system 2 (T3SS2) for the injection of virulence factors into host cells (***Kaval et al., 2023; Zou et al., 2023***).

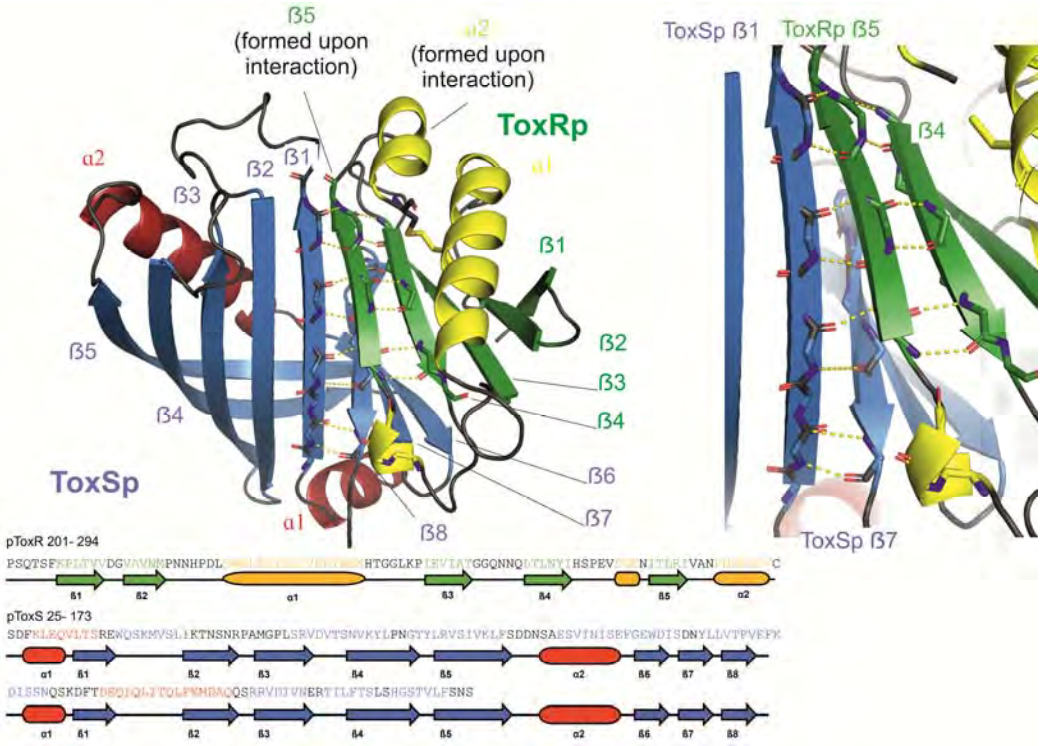

Fig. 1 Heterodimer formation of ToxRSp (pdb: 8ALO). ToxRp ß strand 5 completes main chain hydrogen bond network of ToxSp ß-barrel formation, by interaction with ToxSp ß1. ToxSp ß8 position is stabilized by main chain hydrogen bonds with ToxSp ß1, as well as side chain interactions with ToxRp ß5 and ß4. ToxRp ß5 and α2 are formed upon ToxSp interaction. ToxRSp crystal structure was determined by molecular replacement using an AlphaFold (***Evans et al., 2021; Jumper et al., 2021***) model as template.

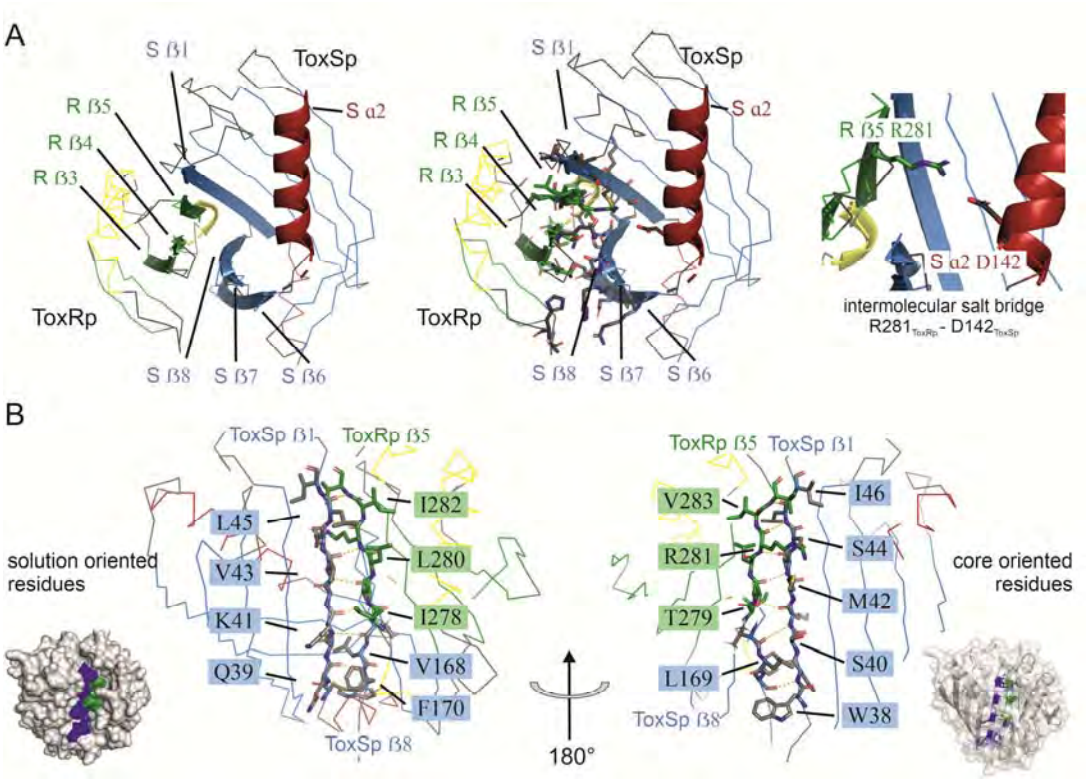

Fig. 2 Detailed description of ToxRSp interface. (A) Overview of ToxRSp interface. The interaction is mainly established via ToxRp ß strands 3, 4 and 5, and ToxSp ß strands 6, 7 and 8. Additionally, an intermolecular salt bridge is formed between ToxRp R281 and ToxSp D142 located at the opening of ToxSp barrel. **(B) The intermolecular main chain H-bond pattern of ToxRSp.** The interprotein H-bond network is established between ToxRp ß5 and ToxSp ß1 thereby filling the gap between ToxSp ß1 and ß8, which interact only in the C-terminal region of the strands.

Intrinsically disordered ToxRp C-terminus folds into structural elements essential for the complex formation with ToxSp.

Small-angle X-ray scattering (SAXS) experiments indicate a dimer formation of ToxSp in the absence of ToxRp (Figure 6-figure supplement 1, Figure 6-figure supplement 2, Supplementary File 1c) supporting the recently proposed HDOCK ToxS-ToxS dimer (***Canals et al., 2023***). Nevertheless, aggregation of ToxSp in solution occurs rapidly suggesting an unstable dimer formation (***Gubensäk et al., 2021b***) (Figure 6-figure supplement 3). The instability of ToxSp can be explained by the inability of the first and the last ß strand of the barrel to form strong hydrogen bonding, thus resulting in an unstable hydrophobic core and consequently aggregation. Interaction with ToxRp likely protects otherwise exposed hydrophobic regions of ToxSp (Fig. 1, Fig. 2).

Comparison of the ToxRSp crystal structure with our previously determined NMR structure of ToxRp (pdb: 7NN6) (***Gubensäk et al., 2021b***), shows the formation of additional secondary structure elements upon complex formation (Fig. 3). Unbound ToxRp has a long intrinsically disordered C-terminus in solution, containing the second cysteine $Cys293_{ToxRp}$ forming a disulphide bond with $Cys236_{ToxRp}$ located in the middle of helix 1 (***Gubensäk et al., 2021b***). When bound to ToxSp, the unstructured region of the C-terminus of ToxRp performs a disorder to order transition, by forming two additional structural elements: short α helix 2 and ß strand 5 (Fig. 3). The newly formed short α helix 2 contacts the turn between ToxSp ß1 and ß2, as well as residues $Leu45_{ToxSp}$ and $Ile46_{ToxSp}$ located at the C-terminal part of ToxSp ß1 thus increasing the interaction interface and further stabilizing the fold. Although the C-terminal region undergoes extreme structural changes upon complex formation, the orientation of the disulphide bond does not change drastically.

ToxRp ß strand 5 is only formed upon complex formation with ToxSp and forms the essential basis for the interaction by building a stabilizing hydrogen bonding network with ß strands 1 and 8 of ToxSp (Fig. 2). Newly formed ToxRp ß5 also forms hydrogen bonds with ToxRp ß4. In unbound ToxRp, polar

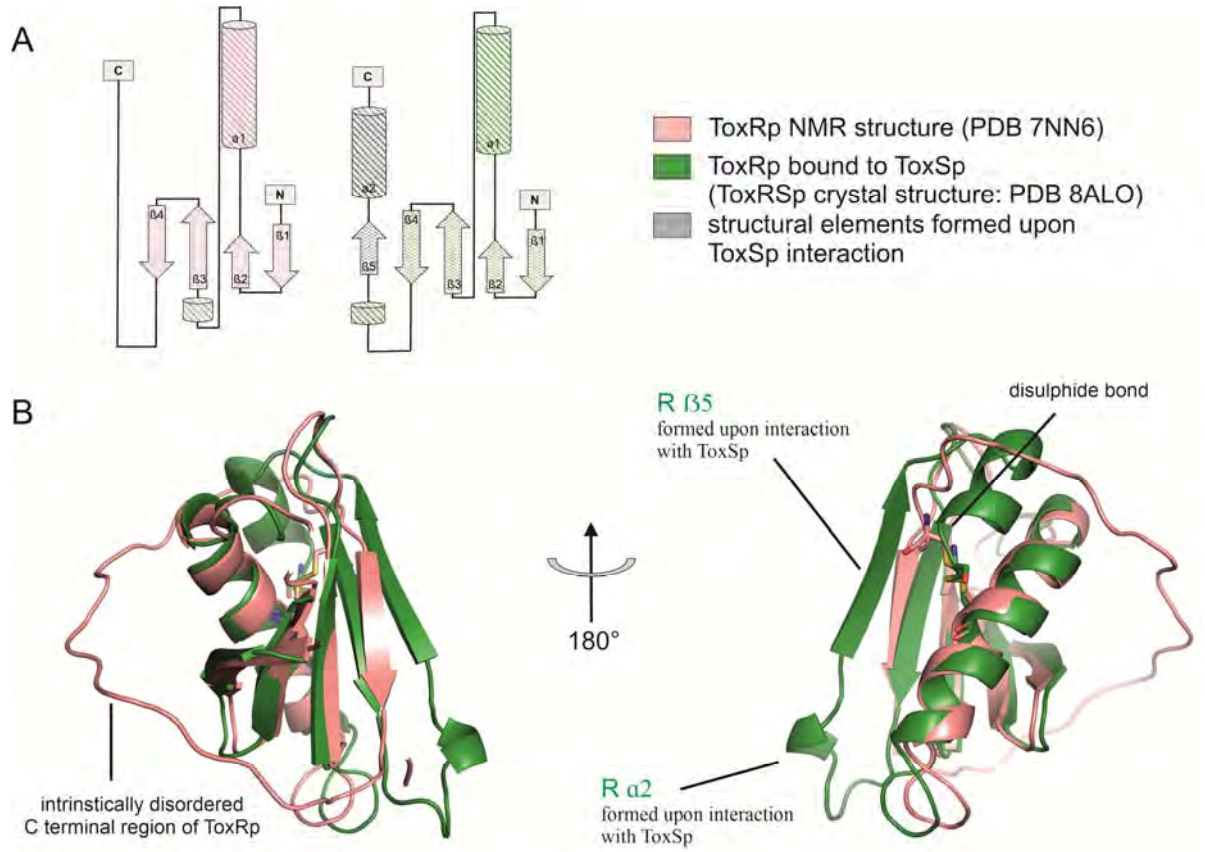

residues of ß4 are pointing towards solution, whereas hydrophobic parts contribute to the hydrophobic core. Nevertheless, ToxRp ß4 does not reveal significant conformational changes upon ToxRSp complex formation.

Fig. 3. Comparison of ToxRp NMR structure (salmon) to ToxRp bound to ToxSp (green). Upon binding to ToxSp, ToxRp intrinsically disordered C-terminal region forms ß5 and α2. **(A)** Topology diagram of ToxRp and ToxRp bound to ToxSp. Newly formed structural elements are highlighted in grey. **(B)** Structural alignment between ToxRp (PDB 7NN6) and ToxRp in complex with ToxSp (PDB 8ALO). The C-terminal disulphide bond is shown in sticks.

ToxSp in complex with ToxRp contains a bile binding pocket.

ToxRSp bile interaction was tested using NMR (***Becker et al., 2018***) (saturation transfer difference STD (Figure 6-figure supplement 3, Figure 6-figure supplement 4), chemical shift perturbation CSP (Fig. 7, Figure 6-figure supplement 5) and diffusion ordered spectroscopy DOSY (Fig. 6B, Figure 6-figure supplement 6), as well microfluidic modulation spectroscopy MMS (Fig. 4, Figure 4-figure supplement 1), size exclusion chromatography (Fig. 6C) and SAXS (Fig. 6A, Figure 6-figure supplement 1, Figure 6-figure supplement 2, Supplementary File 1c). Interaction experiments were performed with bile acid sodium cholate hydrate S-CH. All mentioned experiments confirm an interaction of the ToxRSp complex with bile.

The lipocalin-like fold of ToxSp forms a hydrophobic cavity (Fig. 5, Figure 5-figure supplement 1), similar to the bile binding pocket of VtrC in complex with VtrA from *V. parahaemolyticus (**Tomchick et al., 2016**).* Using extensive MD simulations enabled a detailed analysis of the protein-ligand interface. Upon binding of bile acid mainly loop regions undergo major conformational changes (Fig. 4, Fig. 5). Comparison of ToxRSp apo and bile-bound state reveals that ToxSp β1/β2 loop and ToxRp α1/β2 loop experience strongest rearrangements, whereas loop $\beta3/\beta4_{ToxSp}$, $\alpha1_{ToxSp}$, $\alpha2_{ToxSp}$ and loop

β3/β4$_{ToxRp}$ reveal only minor structural changes (Fig. 5C). Similarly, MMS spectra show significant spectral changes in disordered, turn and helical regions (Fig. 4).

The nature of the interactions of bile acid with the protein complex are mostly hydrophobic. The carboxylic moiety forms a strong interaction with Arg52$_{ToxSp}$. Additionally, cholate interacts with residues Ser44$_{ToxSp}$, Ile135$_{ToxSp}$, Leu138$_{ToxSp}$, Phe139$_{ToxSp}$, Val283$_{ToxRp}$ and Arg281$_{ToxRp}$ (Fig. 5). Both proteins contribute to the bile acid interaction, although ToxSp residues are forming a major part of the interface.

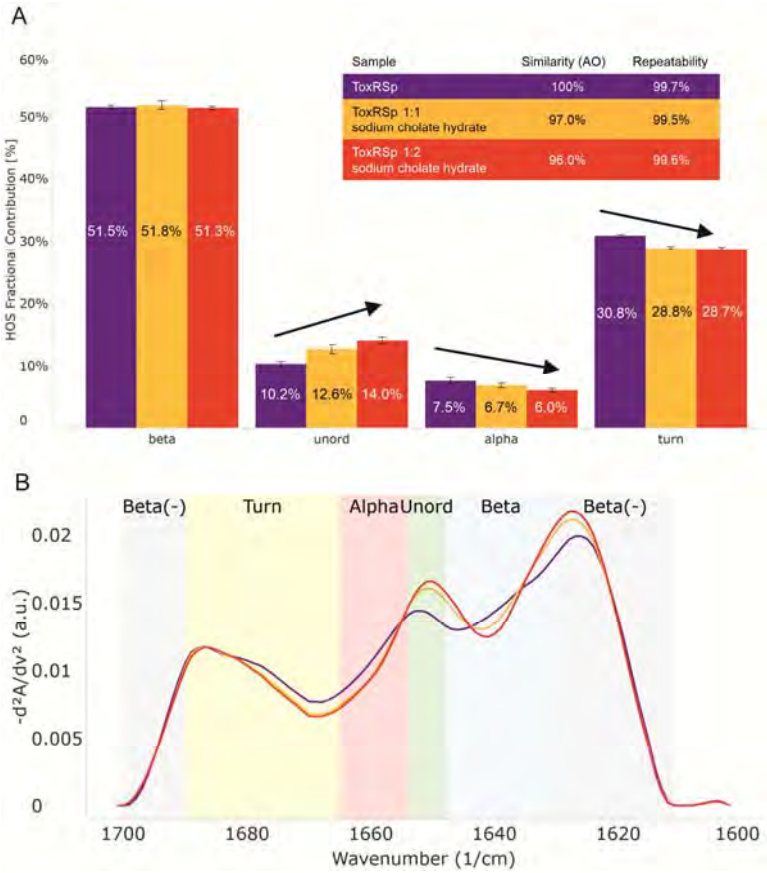

Fig. 4 Analysis of microfluidic modulation spectroscopy MMS experiments. MMS experiments of ToxRSp with different S-CH concentrations show conformational changes upon binding of bile to ToxRSp. Additional structural rearrangements could be detected upon higher additions of bile. **(A)** Bar chart of the relative abundance of secondary structural motifs based on Gaussian deconvolution of the corresponding spectra. **(B)** MMS spectra (baselined, inverted 2nd Derivative) of ToxRSp with and without bile, showing spectral changes upon higher bile additions.

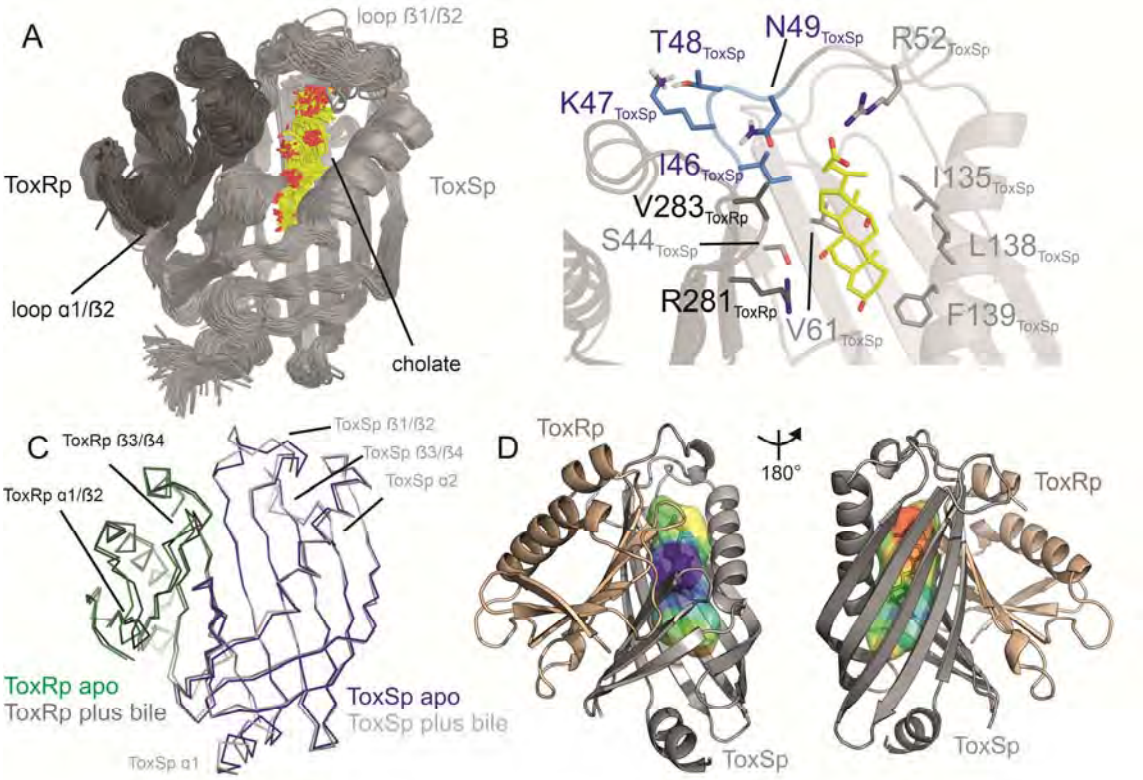

Fig. 5 ToxRSp binding pocket for bile acid. (A) Superimposition of 100 structures of the ToxRSp complex (dark grey/light grey cartoons) with cholate (sticks, C-atoms in yellow) along one representative classical MD simulation. (**B)** Detailed view of the binding mode of cholate to ToxRSp. The residues with the larger contribution to the binding of the ligand are highlighted as well as residues 46-49 of ToxSp located on loop β1/β2. **(C)** Overlay of ToxRSp apo and bile-bound structures. Conformational changes mainly occur in ToxSp loop β1/β2 and ToxRp loop α1/β2. ToxSp helices α1 and α2 and ToxRp loop β3/β4, both close to the ToxRSp interface, experience minor conformational rearrangements upon bile interaction. (**D)** Hydrophobic properties of the bile binding cavity calculated with the CavMan (v. 0.1, 2019, Innophore GmbH plugin in PyMOL). The entrance of the cavity (blue to green) faces the solvent exhibiting a hydrophilic environment, in contrast to the buried hydrophobic areas (yellow to red). For the analysis of the hydrophobicity of the cavities the program VASCo (***Steinkellner et al., 2009***) was used; cavities were calculated using a LIGSITE algorithm (***Hendlich et al., 1997***).

ToxRSp has additional surface exposed bile binding patches.

ToxRSp interaction experiments propose an increase of molecular weight upon bile addition as shown in Fig. 6. SEC-SAXS experiments indicate an increase of molecular weight, radius of gyration and effective maximum particle dimension of ToxRSp upon addition of equimolar amounts of bile acid (Fig. 6A, Figure 6-figure supplement 1, Figure 6-figure supplement 2, Supplementary File 1c). Similar outcomes are observed by SEC runs of ToxRSp with and without bile acid using a Superdex200 column resulting in a broadening of ToxRSp-bile acid peak and slightly decreased retention times (Fig. 6C, Figure 6-figure supplement 7). NMR DOSY experiments of ToxRSp bound to bile acid clearly show a decrease of the diffusion coefficient, which is linked to an increase of size and weight (Fig. 6B, Figure 6-figure supplement 5). Via MMS experiments conformational changes could be detected upon bile acid binding but clearly indicate that no severe structural rearrangements e.g., aggregation events occur (Fig. 4, Figure 4-figure supplement 1).

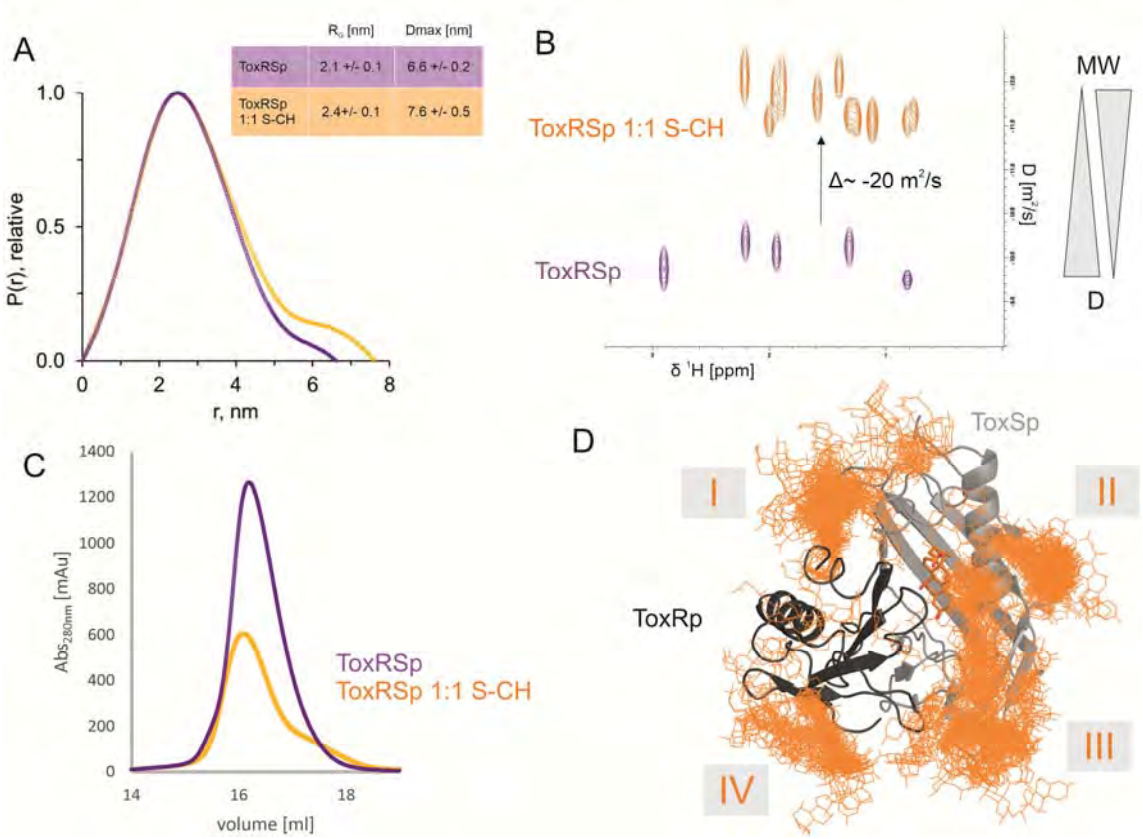

Fig. 6 ToxRSp bile interaction experiments propose additional bile interaction areas I-IV. (A) SEC-SAXS experiments with ToxRSp and S-CH reveal an increase of the radius of gyration R_G and the effective maximum particle dimension Dmax upon bile addition. **(B)** Superimposed NMR DOSY spectra of ToxRSp with and without bile acid S-CH. Addition of bile acid causes a decrease of the diffusion coefficient due to an increase of molecular weight. **(C)** SEC experiments with ToxRSp and S-CH reveal a slight decrease of retention volume upon bile acid presence from 16.19 ml to to 16.08 ml and a broadening of the peak. **(D)** MD determined surface exposed bile interacting regions of ToxRSp. Besides the bile binding cavity of ToxSp, four regions (marked as I-IV) on the ToxRSp surface could be mapped as additional bile binding areas. Region I and III involves both proteins, whereas region II is located on ToxSp and region IV on ToxRp. The representative structure of the ToxRSp complex (ToxRp: dark grey, ToxSp: light grey) is shown with cholate bound at the cavity (orange) and additional cholate molecules attach to surface exposed regions of ToxRSp.

Due to a loss of signals upon equimolar additions of bile acid caused by the previously mentioned increase of molecular weight, NMR titration experiments were performed using small additions of S-CH (Fig. 7). Spectra were recorded with ToxRp and ToxSp both ^{15}N isotopically labelled. An overlay of spectra of only ToxRp or ToxSp ^{15}N labelled enabled the ascription of signals to each of the proteins (Fig. 7A). Even small additions of bile (0.1 molar ratio) to ToxRSp results in a significant decrease of signal intensity. ToxSp seems to be mostly affected by the addition of bile acid, causing a disappearance of ToxSp signals indicating direct interaction events (Fig. 7B-D). ToxRp signals are also affected by decreased signal intensities but to a lower extent when compared to ToxSp. Upon bile additions higher than a molar ratio of 0.6, mostly signals from ToxRp are visible (Fig. 7D). In general, all ToxRSp peaks experience decreased signal intensities caused by fast T_2 relaxation.

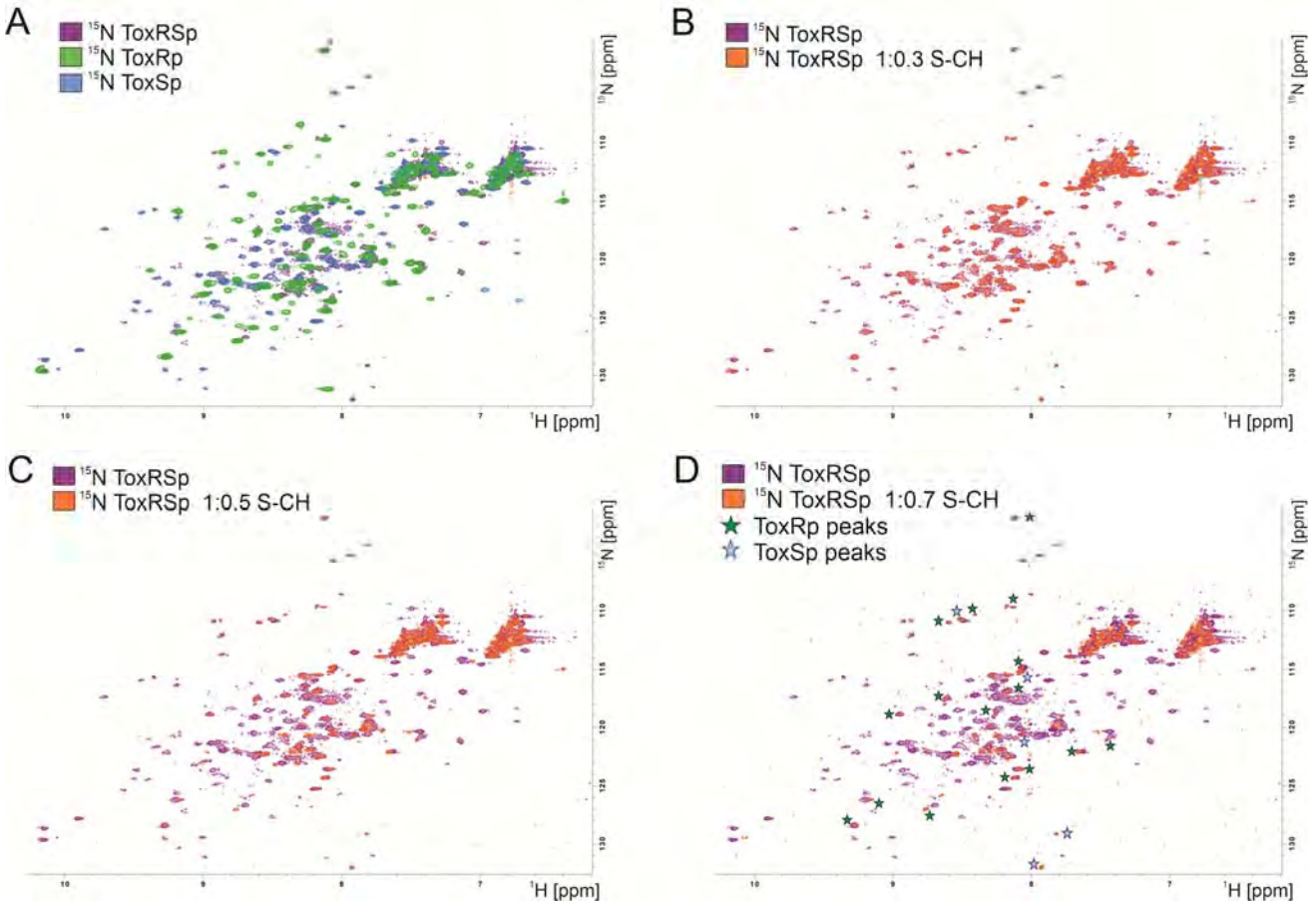

Fig. 7 NMR titration of S-CH to ^{15}N labelled ToxRSp. (A) Overlay of ^{15}N-HSQC spectra of ^{15}N labelled ToxRSp (purple) with ^{15}N labelled ToxRp (green) and ToxSp (blue) for ascription of peaks to each of the proteins. **(B-D)** Overlay of ^{15}N-HSQC spectra of ^{15}N labelled ToxRSp before (purple) and after the addition of increasing ratios of S-CH (orange): 0.3 (B), 0.5 (C), 0.7 (D). Upon bile acid addition signal intensities significantly decrease. Upon higher additions of bile acid mainly ToxRp peaks are visible indicated by green asterisk in **(D),** whereas most ToxSp signals disappear indicating direct interaction with S-CH. Remaining ToxSp signals are marked with blue asterisk.

Interestingly, MMS experiments show additional structural changes of ToxRSp upon higher bile acid concentrations, with maximum changes achieved at a double molar excess of bile acid suggesting the presence of additional binding sites on ToxRSp (Fig. 4, Figure 4-figure supplement 1). Prompted by this evidences, further MD simulations of the complex ToxRSp were performed with one cholate molecule at the binding cavity in the presence of 14 additional cholate molecules randomly positioned in the solvent (Fig. 6D). Four solvent exposed regions of the protein, which show a transient binding of cholate molecules could be identified (Fig. 6D). Three are located on ToxSp, of which two implicate interactions with ToxRp. One interaction site is exclusively located on ToxRp. These results support the experimental finding of an increase of the molecular weight by binding of more than one cholate molecule.

The active state of ToxR is proposed to be dimeric due to its binding to direct repeat DNA sequences (***Canals et al., 2023; Gubensäk et al., 2021a; Krukonis and DiRita, 2003; Withey and DiRita, 2006***). Nevertheless, the increase of molecular weight observed in the interaction experiments is significantly lower than 30 kDa (Fig. 6A-C), which corresponds to the molecular weight of ToxRSp. Interaction experiments therefore do not implement a bile induced dimerization or oligomerization event. A bile induced formation of trimers involving two ToxRp and one ToxSp or two ToxSp and one ToxRp molecules also seems unlikely. A described trimer formation would involve the disruption of ToxRSp heterodimer complexes, which exhibits a dissociation constant at nanomolar range (***Gubensäk et al., 2021b***), and includes aggregation of unstable ToxSp. Also, MMS experiments

reveal subtle conformational changes of ToxRSp upon bile interaction and do not support extreme structural rearrangements. Instead of major structural changes like dimerization or loss of structure due to aggregation, the experimental results more likely indicate that the presence of bile leads to local conformational changes near the binding cavity of the ToxRSp barrel, similar to the VtrAC complex of *V. parahaemolyticus (**Li et al., 2016; Tomchick et al., 2016**)*.

Taken together, we propose that ToxRSp bile sensing functions in a complex manner involving a binding site in ToxRSp barrel as well as surface exposed binding regions for bile acid. Bile acid interaction results in concentration dependent conformational changes of ToxRSp which may be related to ToxR transcriptional activity changes (***Eichinger et al., 2011; Gubensäk et al., 2021a; Kenney, 2002; Martínez-Hackert and Stock, 1997a; Martínez-Hackert and Stock, 1997b***).

ToxRp ß-sheet forms a low-affinity binding region for bile.

The MD determined ToxRp binding region to bile (Fig. 6D) is also confirmed experimentally via chemical shift mapping (Fig. 8, Figure 8-figure supplement 1) (***Becker et al., 2018; Williamson, 2013***). The bile binding area is located at the solution-oriented region of the ß-sheet of ToxRp. The determined dissociation constant of 2.6 ± 1.42 mM (Fig. 8, Supplementary File 1d) exhibits a weak binding affinity of ToxRp to bile but physiologically still relevant (***Qin and Gronenborn, 2014; Sukenik et al., 2017***) since bile acid concentrations in the small intestine vary between 2 and 10 mM (***Hamilton et al., 2007***). Therefore, we propose that ToxRp interaction with bile acid is only relevant upon high bile concentrations and could be linked to an additional bile sensing mechanism not connected to ToxRSp complex formation.

Interaction experiments with ToxSp alone and S-CH did not reveal any binding event (Figure 6-figure supplement 4). Due to ToxSp structural instability (***Gubensäk et al., 2021b***) we propose that without stabilization of ToxRp, the binding pocket is not properly formed and therefore binding to bile cannot occur. Additionally, the presented bile binding complex of ToxRSp shows that residues from ToxRp are also involved in the bile interaction (Fig. 5).

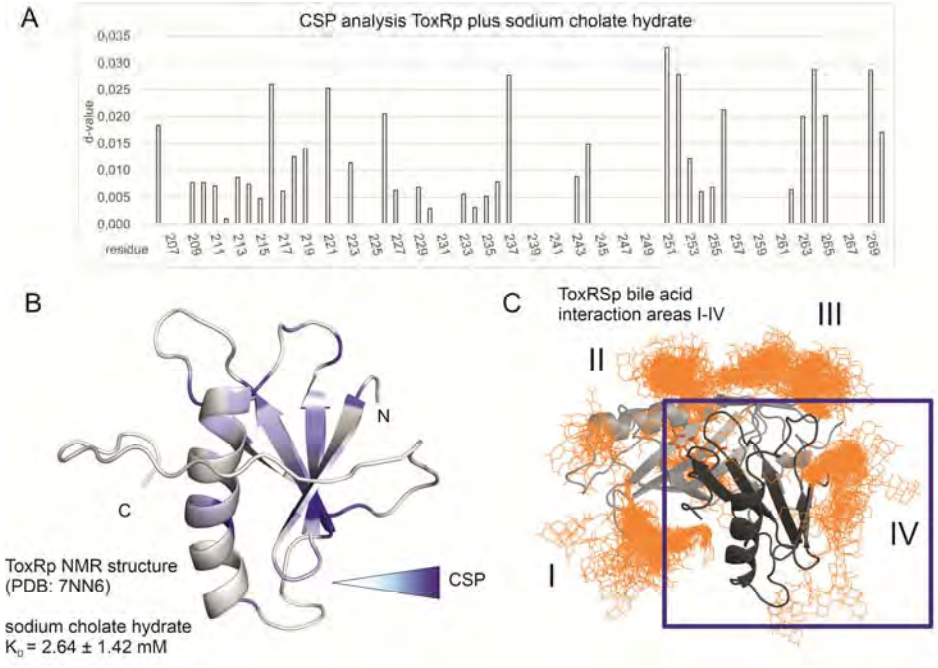

Fig. 8 Binding studies with ToxRp and bile. (A) Chemical shift perturbation experiments expose residues mostly affected upon binding of S-CH. (**B)** Residues which experience a change of their chemical shift upon bile addition are coloured according to a gradient from white to blue. Residues highlighted in dark blue are mostly affected upon bile addition and are therefore most likely located at the interaction area. The calculated dissociation constant of 2.6 mM suggests a low affinity binding of bile to ToxRp. (**C)** Binding area IV determined by MD simulations (Fig. 6) is located at the ß-sheet of ToxRp. Taken together, MD simulation and CSP experiments reveal a bile interacting area located at

the ß-sheet of ToxRp proposing a bile sensing function of ToxRp independent on ToxRSp complex formation relevant only at high bile salt concentrations.

Discussion

Bile induced ToxRS activation enables *V. cholerae* bile resistance.

Sensory proteins represent an indispensable tool for *V. cholerae* to react to changes in its environment and consequently survive in harsh habitats like the human gut (***Almagro-Moreno et al., 2015b***). The interaction of inner membrane proteins ToxR and ToxS initiates a sensing function followed by signal transmission thereby causing immediate changes of the expression system of the bacterium (***Bina et al., 2003; Childers and Klose, 2007; DiRita et al., 1991***). In order to achieve bile resistance, ToxRS bile induced activation leads to a change of outer membrane protein production from OmpT to OmpU (***Morgan et al., 2011; Provenzano and Klose, 2000; Simonet et al., 2003***).

Our studies reveal a crucial heterodimer formation of the periplasmic sensory domains of *V. cholerae* thereby shaping a bile binding pocket which is only properly folded upon the complex formation. Interaction experiments show that correct heterodimer assembly of ToxRSp is critical for efficient bile sensing functionality. *In vivo* these findings suggest that bile-induced virulence regulation and OmpU production occurs only when ToxR and ToxS are both present for forming the obligate heterodimer, thus providing a regulatory restriction in the regulation process by bile. Although a single protein may be more efficient in sensory regulation, a co-component system offers a more strict regulation enabling fine-tuning of transcription levels according to small changes of the pathogen's environment.

A distinctive feature of members of the 'ToxR-like' transcription factor family is the transduction of signals through the membrane without chemical modification, probably via conformational changes (***Eichinger et al., 2011; Gubensäk et al., 2021a; Kenney, 2002; Martínez-Hackert and Stock, 1997a; Martínez-Hackert and Stock, 1997b***). Thus, we suggest that the observed structural changes of the periplasmic domains of ToxRS upon bile recognition are passed on through the ToxR transmembrane domain to its cytoplasmic effector domain, thereby enhancing ToxR binding to recognition sequences and subsequently induction of transcription (Fig. 9).

Higher additions of bile acid induce additional structural changes of ToxRSp as shown by MMS experiments (Fig. 4). A bile acid concentration dependent mechanism could be an efficient tool for *V. cholerae* for sensing its preferred location of infection in the small intestine (SI). Bile acid concentrations also vary within the SI: postprandial bile acid concentrations are around 10 mM in the initial region of the SI, whereas the distal part contains 2 mM bile acids. (***Hamilton et al., 2007***). Still, the exact localization of *V. cholerae* within the SI is not clear (***Millet et al., 2014***). Previous studies revealed higher numbers of colony forming units (cfu) of the pathogen in the middle and distal regions of the SI (***Angelichio et al., 1999***). Nevertheless, *V. cholerae* colonization seems to depend on its motility and host factors e.g. mucins (***Millet et al., 2014***).

The presented experiments reveal that bile sensing of ToxRS functions according to a complex scheme dependent on the concentration of bile acids. ToxRSp interaction involves a binding site of ToxRSp barrel hosting one bile molecule and multiple surface exposed binding regions offering attachment sites for bile acid molecules. Bile interaction with ToxRSp induces concentration dependent conformational changes of ToxRSp probably influencing ToxR transcriptional activity changes (***Eichinger et al., 2011; Gubensäk et al., 2021a; Kenney, 2002; Martínez-Hackert and Stock, 1997a; Martínez-Hackert and Stock, 1997b***). The low affinity binding region of ToxR alone could be connected to another bile sensing mechanism, which is relevant at high concentrations of bile acid and independent on ToxRSp complex formation.

The expression system of *V. cholerae* is complex and sensitively regulated involving numerous factors and depending on environmental conditions and signals. The high-energy consuming virulent state of the pathogen is only switched on when its localization for colonization is reached. Sensing different bile acid concentrations could support the determination of the exact position of the bacterium in the human body and thereby adapting its gene expression according to environmental conditions. Bile resistant associated genes as well as factors essential for colonization are switched on at early stages in order to guarantee the survival of the bacteria, whereas other factors like the cholera toxin are produced later, enabling the spread of the bacteria and causing the main symptoms of the disease (***Almagro-Moreno et al., 2015b; Srivastava et al., 1980***).

The presented experiments do not indicate a bile-induced dimer- or oligomerization of the ToxRS complex, which is currently proposed as the active conformation of ToxR. Nevertheless, since experiments are performed with periplasmic domains only, a different behaviour of full-length proteins

in their natural environment cannot be ruled out. Dimer- and oligomerization events may be dependent on the presence of DNA as suggested recently (***Canals et al., 2023***), and remain to be elucidated.

The strong interaction of periplasmic domains of ToxR and ToxS indicates that complex formation also occurs spontaneously *in-vivo*, and independent on the presence of ligands. Presented experiments were performed with already established ToxRSp complexes, to which bile acid was added after complex formation. Nevertheless, we cannot rule out that a folding-on-binding interaction of ToxRS and bile acid happens *in-vivo*, which remains to be elucidated

Taken together we propose that in regard to *V. cholerae's* virulence expression system 'ToxR-regulon' ToxR transcriptional activity is guided by ToxS sensory function. The heterodimer formation is therefore inevitable for the individual functionality of each protein forming a co-dependent system. Understanding the mechanistic details of the ToxRS complex provides a relevant basis for disruption of the crucial interaction interface and consequently inhibition of *Vibrio's* adaption to its host and its virulent action.

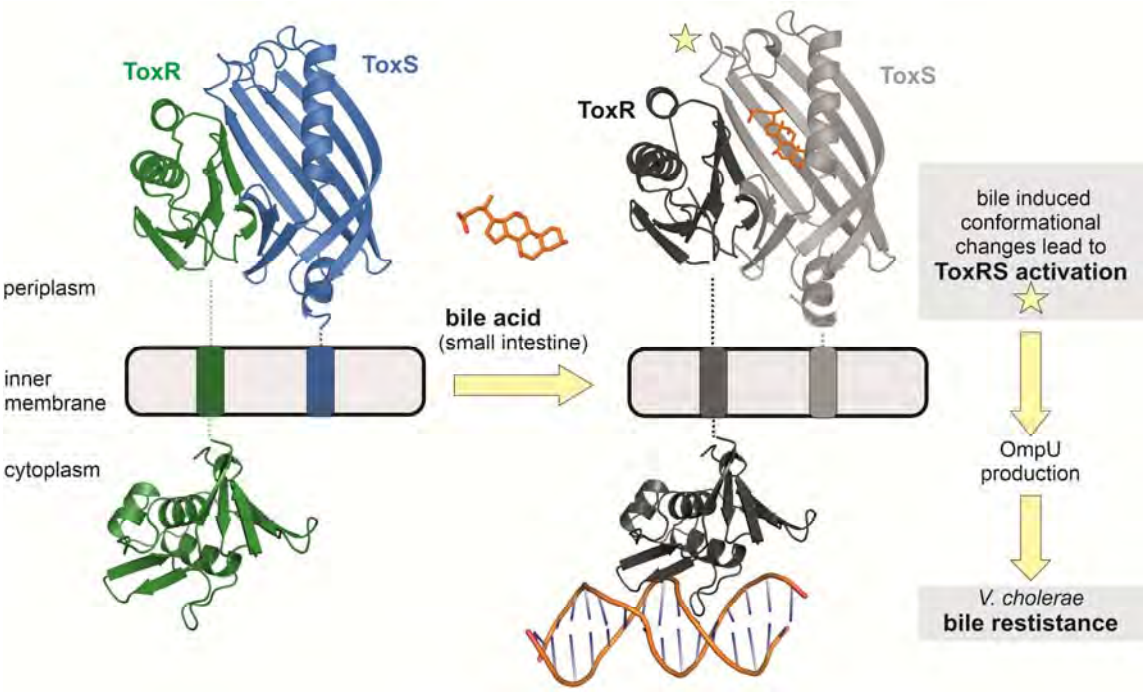

Fig. 9 Model of bile induced activation of *V. cholerae* ToxRS. When entering the human gut *V. cholerae* senses the presence of bile acids by binding of bile to the periplasmic domains of inner membrane proteins ToxR and ToxS. The bile binding pocket is formed by ToxS and stabilized by ToxR. Subsequently, the interaction with bile induces ToxR activation which leads to a change of outer-membrane proteins from OmpT to OmpU. OmpU then provides bile resistance and thus enables the bacterium's survival in the human body. PDB accession codes: ToxRSp crystal structure: 8ALO, cytoplasmic domain of ToxR: 7NMB. The cytoplasmic domain of ToxR bound to *ompU* operon is a NMR guided HADDOCK model (***Gubensäk et al., 2021a***).

ToxRS belongs to the superfamily of VtrAC-like co-component signal transduction systems.

Vibrio pathogens have a complex regulatory mechanism that allows them to survive and cause disease. ToxRS and VtrAC (***Tomchick et al., 2016***) are both *Vibrio* protein complexes fulfilling an essential function since they induce virulence by sensing bile via direct interaction (***Bina et al., 2021; Hay et al., 2017; Hung and Mekalanos, 2005; Tomchick et al., 2016***). Bile sensing is inevitable for the survival of gastro-entero pathogens (***Gunn, 2000; Tomchick et al., 2016***). On one hand outer membrane proteins need to be adapted to bile stress in order to guarantee the survival of the bacteria (***Sistrunk et al., 2016***). On the other hand, the presence of bile signals the environment of the host and therefore the virulence activating state needs to be induced in order to effectively colonize the gut.

Structurally, the protein complexes share the ß-barrel lipocalin-like formation of ToxSp/VtrC completed by a ß strand of ToxRp/VtrA, together forming a bile binding pocket (Figure 1-figure supplement 3). Similar to ToxSp, VtrC is not stable without its interaction partner and tends to aggregate easily (***Tomchick et al., 2016***). There is no structure of unbound VtrA available yet, so we cannot compare if VtrA also forms new structural elements upon complex formation like ToxRp (pdb code: 7NN6). Another difference between the complexes is that VtrA does not contain cysteine residues like ToxRp. The disulphide linkage represents another option for regulation in *V. cholerae*. Also, bile interaction occurs in a different manner. Whereas in ToxRSp both proteins contribute to the direct interaction with bile, in VtrAC bile binding strictly involves only VtrC (***Li et al., 2016; Tomchick et al., 2016; Zou et al., 2023***). If VtrC, in contrast to ToxS, is capable of binding bile acid on its own remains to be elucidated.

Recently, *V. cholerae* ToxRS was proposed as a distant homolog to VtrAC, forming together a superfamily of co-component signalling systems which are not linked to sequence homology (***Kinch et al., 2022***). Bacterial two-component systems typically enable signal transduction via chemical modification e.g. phosphorylation of a response regulator (***Mitrophanov and Groisman, 2008***). In the case of VtrAC and ToxRS signal transduction is achieved via binding of signalling molecules like bile acid, thereby inducing conformational changes which likely facilitate transcription regulation (***Eichinger et al., 2011; Gubensäk et al., 2021a; Kenney, 2002; Li et al., 2016; Martínez-Hackert and Stock, 1997a; Martínez-Hackert and Stock, 1997b; Tomchick et al., 2016***).

Although the eight-stranded ß-barrel fold of ToxS and VtrC shows similarities with the calycin superfamily (including fatty acid binding proteins FABP and lipocalins) (Supplementary File 1f) (***Kinch et al., 2022; Tomchick et al., 2016***), the formation of an obligate heterodimer to fold the barrel including the binding pocket is unique for ToxRSp and VtrAC (***Tomchick et al., 2016***).

Despite the obligate heterodimerization and the structural similarities, another feature of this protein family is the arrangement of a two-gene cassette encoding the two proteins (***Kinch et al., 2022***). Using this information, genetic cluster analysis recently revealed additional members of the VtrAC-like superfamily including BqrP/BqrQ from enteric *Burkholderia pseudomallei,* as well as GrvA/FidL from pathogenic *E. coli* O157:H7 Sakai strain (***Kinch et al., 2022***).

The distinctive structural and functional features of ToxRS and VtrAC support a common superfamily of co-component signalling systems of VtrAC-like protein complexes, whose sensory function is strictly linked to dimerization and ligand binding (***Kinch et al., 2022***). So far VtrAC and ToxRSp remain the only experimentally solved structures of this relatively new defined superfamily.

ToxRSp obligate dimer formation is conserved among *Vibrio* strains.

The predicted protein structures of ToxRSp proteins from different *Vibrio* strains (Supplementary File 1e) share the distinctive ToxRSp fold consisting of a ß-barrel ToxSp and an αß folded ToxRp (Fig. 10, Fig. Figure 10-figure supplement 1). Whereas ToxRp structure varies among the strains, the barrel shaped lipocalin-like structure of ToxSp is consistent, clearly visible in the alignment of all structures (Fig. 11, Figure 11-figure supplement 1, Figure 11-figure supplement 2).

Sequence alignments (Figure 11-figure supplement 1, Figure 11-figure supplement 2) reveal numerous conserved residues of ToxSp compared to more diverse ToxRp (Fig. 11). Most of the conserved residues of ToxSp are located at the openings of the barrel as well as ß strands 8, 7 and 6 which are involved in ToxRp interaction (Fig. 11). Also, residues near the N-terminus, which is probably located near the membrane, seem to be highly conserved in *Vibrio* species. The aspartate residue which is involved in the intermolecular salt bridge with ToxRp is also one of the conserved residues of ToxSp (Figure 10-figure supplement 1). The high content of conserved residues in the binding pocket of ToxSp proposes that its general function is to bind to small hydrophobic molecules similar to bile acids.

Compared to ToxSp, ToxRp sequence seems to be only conserved between human colonizing strains (Figure 11-figure supplement 2). Most of ToxRp conserved residues are involved in the formation of the hydrophobic core, as well as the ToxSp interface (Fig. 11). Additionally, two cysteine residues are conserved, as well as an arginine/lysine residue involved in the formation of the intermolecular salt bridge with the conserved aspartate residue of ToxSp. ToxRp residues involved in the binding to S-CH are also conserved ($Val283_{ToxRp}$, $Arg281_{ToxRp}$).

In conclusion, the sequential and structural alignments reveal that ToxSp is conserved among different *Vibrio* species, whereas ToxRp shows significant sequence similarities only among human colonizing

strains. The high number of conserved residues involved in the direct interaction with bile acid furthermore proposes that ToxRSp complex has a common sensory function in *Vibrio*'s.

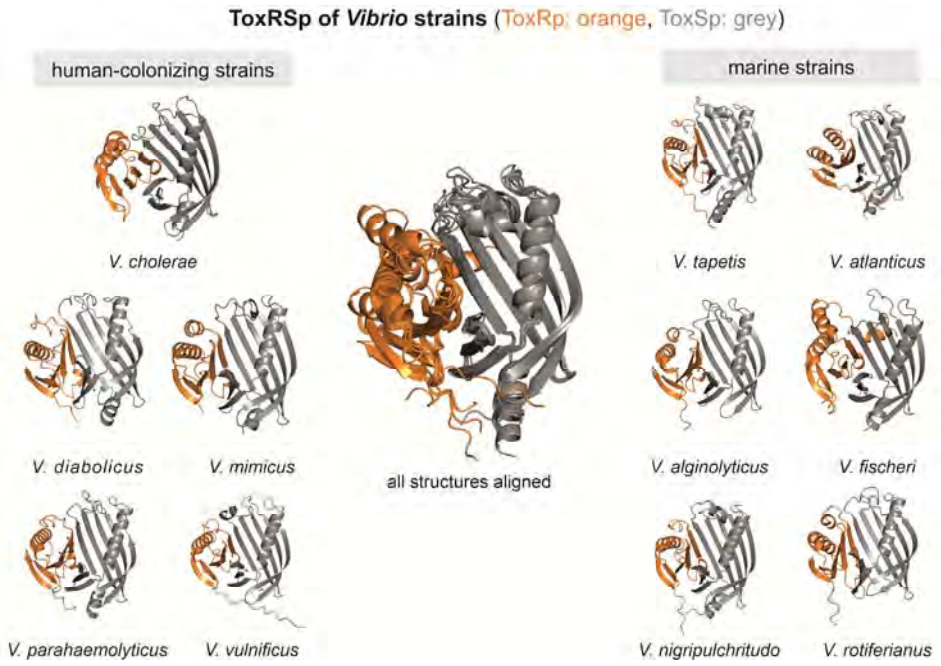

Fig. 10 Heterodimer structures of periplasmic sensory domains of ToxRS from *Vibrio* organisms calculated using AlphaFold-Multimer (***Evans et al., 2021; Jumper et al., 2021***). ToxRSp dimer formation occurs in different *Vibrio* strains. The structural alignment of all models reveal that the ToxSp fold is highly similar in whereas ToxRp seems to be more diverse.

A

Vibrio strains	% identity to V. cholerae ToxSp	% identity to V. cholerae ToxRp	
V. fischeri	48.6	45.7	luminescent marine bacteria
V. tapetis	58.5	48.4	marine mussel pathogen
V. nigripulchritudo	61.1	44.8	marine shrimp pathogen
V. atlanticus	59.9	23.4	marine pathogen
V. mimicus	93.2	93.3	human entero-pathogen
V. vulnificus	68.7	54.3	human entero-pathogen
V. rotiferianus	69.9	50.0	marine pathogen
V. parahaemolyticus	67.1	50.5	human entero-pathogen
V. diabolicus	64.4	48.4	prebiotic bacterium
V. alginolyticus	65.1	50.5	human and marine pathogen

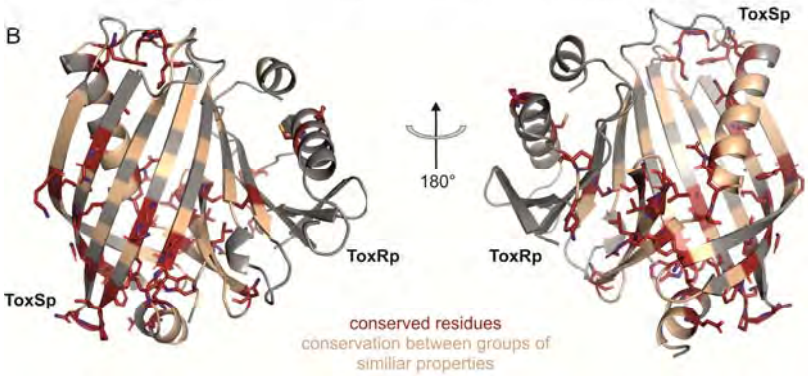

Fig. 11 Sequential and structural analysis of sensory domains of ToxRS from different *Vibrio* strains. ToxRSp from different *Vibrio* species exhibit similar heterodimer formations. Especially ToxSp ß-barrel structure, which forms the binding cavity, seems to be conserved. **(A)** Sequential analysis of conserved residues of ToxRSp. Sequential alignment was done using ToxRS amino acid sequences from *Vibrio* species (Supplementary File 1e). The sequence identity (%) of ToxR and ToxS proteins from different strains to *V. cholerae* is shown in the table above the structures. **(B)** Conserved residues

are highlighted on the ToxRSp structure. Conserved residues are coloured in red and shown in sticks, residues which are conserved between groups of similar properties are coloured in gold. Most conserved regions could be found in ToxSp, especially at the openings of the barrel. ToxRp seems to have a higher sequential variability.

Conclusion

Cholera represents a dangerous disease which leads to sudden epidemic outbreaks due to the perseverance of the causative *V. cholerae* in aqueous environments (***Ahmed and Nashwan, 2022; Ali et al., 2015***). The bacterium has an immense ability to adapt to challenging conditions due to its sensitive sensory systems. Herein, we present insights into the regulatory bile binding protein complex of *V. cholerae* involving sensory proteins ToxR and ToxS. Our analysis reveals ToxS as a conserved environmental sensor in *Vibrio* strains, functionally effective only in complex with transcription factor ToxR. Targeting the disruption of this vital binding mechanism provides a powerful tool for inhibiting *Vibrio's* adaption to its host and consequently its virulent action.

Materials and Methods

Protein expression and purification

All constructs listed in table Supplementary File 1a were generated by using standard procedures and verified via automated sequencing. For protein expression *E. coli* BL21 DE cells were used. Cells were grown under shaking at 180 rpm and induced with 1 mM IPTG when the OD_{600} reached 0.6 to 0.8. ToxRp producing cultures were incubated at 37°C overnight, ToxSp was expressed at 37°C before induction, after growth at 20°C overnight. For production of non-isotopically labelled proteins LB media was used. For isotopically labelled proteins cells were grown in M9 minimal media containing ^{15}N labelled $(NH_4)_2SO_4$ and ^{13}C labelled glucose as the sole nitrogen and carbon sources, respectively.
After overnight expression, cell cultures were centrifuged, and the pellet dissolved in 20 ml of loading buffer containing either 8 M urea, 300 mM sodium chloride, 10 mM imidazole pH 8 for ToxRp, or 20 mM Tris, 300 mM sodium chloride, 10 mM imidazole pH 8 for ToxSp. Protease inhibitor mix (Serva, Protease Inhibitor Mix HP) was added to the loading buffer. The cells were disrupted via sonication. The lysate was centrifuged, and the supernatant was loaded on a gravity column containing 2 ml of Ni-NTA agarose beads. The column was washed with 15 column volumes (CV) of loading buffer followed by 5 CV of the loading buffers containing 1 M sodium chloride and 5 CV of the loading buffer containing 20 mM imidazole. His-tagged proteins were eluted with 5 CV elution buffer containing 330 mM imidazole. ToxRp constructs were refolded overnight by dialysis at 4°C in 50 mM Na_2HPO_4, 300 mM sodium chloride, pH 8. The final purification step includes purification by FPLC using a HiLoad 26/600 Superdex 75 pg column in 50 mM sodium phosphate, 300 mM sodium chloride, pH 8.

Crystallization & Data Acquisition

Periplasmic protein domains were expressed separately and added in a 1:2 ratio, with excess of ToxSp. Due to ToxSp instability saturation of ToxRp binding sites is only achieved when ToxSp is added in two molar excess. Unbound ToxSp was eliminated by SEC. The protein complex was dialyzed against crystallization buffer (20 mM Tris, 150 mM NaCl, 0.02 % NaN_3, pH 8) and concentrated to 30 mg/ml using an Amicon Ultra-15 Centricon (Millipore Merck, Darmstadt, Germany). Crystallization experiments were performed with ORYX8 pipetting robot (Douglas Instruments, Hungerford, UK) and sitting drop vapor-diffusion method using 96-well 3-drop plates (SwissCI AG, Neuheim, Switzerland). Initial crystallizations were setup using commercially available screens: Index (Hampton Research, United States), JCSG+ and Morpheus (Molecular Dimensions, United states). Each drop was set up with 0.5 µl protein mix and 0.5 µl of the screen condition. Crystallization plates were incubated at 16° C and H11 condition JCSG+ containing 0.2 M magnesium chloride hexahydrate, 0.1 M Bis-Tris pH 5.5 and 25 % w/v PEG3350 yielded the best diffracting single crystals after two months. The crystals were stored in liquid nitrogen until screening and data collection at the ID30A-3 beamline at the ESRF (Grenoble, France) using a PILATUS detector. Data were collected at 100° K at 0.96770 Å wavelength with 0.20° oscillation range and a total of 700 images.
Data were processed using XDS (***Kabsch, 2010***) and AIMLESS (v.0.7.7.) (***Evans and Murshudov, 2013***). Crystals diffracted up to 3 Å and belong to the space group $P6_5$ with cell constants of 72.5 Å, 72.5 Å, 79.4 Å and 90°, 90° and 120°. The structure was solved with molecular replacement using Phaser (2.8.3) (***McCoy et al., 2007***). A partial *ab initio* model of the assembled complex of ToxSp and ToxRp predicted by AlphaFold-Multimer (***Evans et al., 2021***) was used as a template. Employing the complete predicted model of the complex for phasing failed, hence only the larger part of it, ToxSp, was used for initial phasing with Phaser. Furthermore, the predicted model of the ToxSp part was trimmed down at parts below 0.7 predicted lDDT score. The trimmed partial model of ToxSp was suitable to position the model correctly, solve the phase problem and obtain phases that were

sufficient enough to place the second molecule, ToxRp, using Phaser. The solved structure was rebuilt and improved in Coot (v.0.9.6.) (***Emsley et al., 2010***) and with ChimeraX (v.1.3.) (***Pettersen et al., 2021***) using the ISOLDE plugin (***Croll, 2018***). Waters were placed manually within Coot. Refinement was performed with REFMAC5 (***Murshudov et al., 2011***). The final refined model was analysed and validated with PISA (***Krissinel and Henrick, 2007***), MolProbity (***Chen et al., 2010***) and PDB. Data collection and refinement statistics (Supplementary File 1b) were generated within Phenix Table1 (***Liebschner et al., 2019***). The structure was deposited at the PDB with the DOI: https://doi.org/10.2210/pdb8ALO/pdb and the PDB accession code 8ALO.

Ab initio Models of ToxRp, ToxSp and Dimers with AlphaFold

Ab initio models of ToxRp and ToxSp (*V. cholerae*) were calculated using an AlphaFold 2.1 (***Jumper et al., 2021***) installation with full databases in standard configuration for procaryotes. The search models used for molecular replacement of the heterodimer ToxRSp (*V. cholerae*) as well as the models of the proposed homodimer ToxSp (*V. cholerae*) were calculated on an AlphaFold-Multimer 2.1 (***Evans et al., 2021***) installation with full databases in standard configuration for procaryotes.
For calculation of ToxRSp Heterodimers from various *Vibrio* Species shown in Supplementary File 1e, an AlphaFold-Multimer 2.2 (*31*) installation in standard configuration with full databases and v2 model weights was used. For all species, 5 models were generated and ranked by the highest model confidence metric (0.8·ipTM + 0.2·pTM).

NMR experiments

All NMR spectra were recorded on a Bruker Avance III 700 MHz spectrometer equipped with a cryogenically cooled 5 mm TCI probe using z-axis gradients at 25° C. All NMR samples were prepared in 90% H_2O/10 % D_2O. The total sample volume was 600 µL. Spectra were processed with NMRPipe (***Delaglio et al., 1995***).

Diffusion-Ordered NMR Spectroscopy DOSY

For DOSY experiments all samples were dissolved in the exact same buffer (20 mM Tris, 100 mM NaCl pH 6.5). Sodium cholate hydrate S-CH was added to ToxRSp samples from a 20mM stock dissolved in the same buffer. The concentration of ToxRSp was 360 µM. The DOSY spectra were recorded using the Bruker dstebpgp3s pulse sequence employing a solvent suppression via presaturation and 3 spoil gradients (***Johnson, 1999; Morris and Johnson, 1992***). Relevant parameters include a gradient duration of 1.4 ms, a diffusion time of 70 ms and a linear 32-step gradient ramp profile from 1.06 to 51.84 G/cm. Due to phase errors in the first gradient steps, the initial measurement points could not be used, thus the series of points was truncated to afford only the stable signal attenuation. The spectra were processed with Bruker Dynamics Center using standard parameters.

Saturation Transfer Difference STD

Samples for STD experiments (***Mayer and Meyer, 1999***) contained an excess of S-CH compared to protein (protein to ligand ratios: ToxRp 1:50, ToxRSp 1:20, ToxSp 1:20). Protein concentrations of samples were: 50µM ToxRp, 300µM ToxRSp, 30 µM ToxSp. Three protein selective regions were chosen for saturation: 6000 Hz (amide region), 5000 Hz (amide region) and -5000 Hz (negative control). Experiments with ToxRp and bile were done in two buffers: 20 mM Tris, 100 mM NaCl pH 6.5. Reference spectrum of S-CH was recorded in the exact same buffer at a concentration of 2mM. Additionally, experiments were repeated in buffer 20 mM Kpi, 200 mM NaCl, pH 8 according to previously published NMR experiments (***Midgett et al., 2017***)

NMR titration experiments

Titration experiments with ToxRSp (360 µM) and ToxRp (200 µM) were performed in 50 mM Na_2HPO_4, 100 mM NaCl at pH 6.5. Additionally, experiments were repeated in buffer 20 mM Kpi, 200 mM NaCl, pH 8 according to previously published NMR experiments (***Midgett et al., 2017***). S-CH was titrated using a 20 mM stock solution prepared in the exact same buffer. 1D ^{1}H proton spectra as well as 2D ^{1}H-^{15}N-HSQC spectra (***Davis et al., 1992***) were recorded for each step of the titrations. Due to the disappearance of ToxRSp peaks upon bile addition, bile interaction experiments were performed using low amounts of S-CH. Following protein-to-ligand ratios of S-CH were used for ToxRSp experiments: 0.1, 0.2, 0.3, 0.4, 0.5, 0.7, 0.8, 1, 1.5, 2, 4. For Fig. 7 only ratios 0.3, 0.5, and 0.7 are shown. Regarding ToxRp-bile titration following protein-to-ligand ratios of S-CH were used: 1, 3, 13, 50, 100, 150, 200, shown in supplementary figure S.13.

Size Exclusion Chromatography SEC

SEC experiments were carried out on an ÄKTA pure 25 (Cytavi, Marlborough, USA) using a Superdex 200 Increase 10/300 column (Cytiva) with a flowrate of 0.4 ml/min. As sample and running buffer a phosphate buffer (50 mM Na_2HPO_4, 300 mM NaCl, pH 8, supplemented with 0.02% NaN_3) was used. 100 µl of ToxRS without and with bile acid S-CH were measured. Sample 1 was 1 mM of ToxRSp complex, sample 2 was 300µM of ToxRSp with equimolar amount (1:1) of S-CH.

Microfluidic Modulation Spectroscopy (MMS)

For initial MMS measurements three 1 ml ToxRSp samples of 5 mg/ml were prepared in 50 mM Na_2HPO_4, 300 mM NaCl pH 8.0. A 20 mM stock of S-CH was made in the exact same buffer and added to the protein complex for final protein to ligand ratios of 1:1 and 1:2. Also, a ToxRSp sample without ligand was measured. Results are shown in Fig.4. For each sample a reference buffer, containing the same amount of S-CH was used.

Additionally, measurements with increasing protein-to-ligand ratios were performed with 4.5 mg/ml ToxRSp complex in 50 mM Na_2HPO_4, 300 mM NaCl pH 8. A 20 mM stock of S-CH was made in the exact same buffer and added to the protein complex for final protein to ligand ratios of: 1:0, 1:1, 1:2, 1:3, 1:5, 1:20. For each sample a reference buffer, containing the same amount of S-CH was used. Results are shown in supplementary figure S.11.

Samples were measured and analysed with a RedShiftBio AQS3®pro MMS production system equipped with sweep scan capability (RedShiftBio, Boxborough, MA, US). For background subtraction, chemically identical buffer and buffer-bile mixtures were loaded pairwise with the corresponding sample onto a 96-well plate. The instrument was run at a modulation frequency of 1 Hz and with a microfluidic transmission cell of 23.5 µm optical pathlength. The differential absorbance spectra of the sample against its buffer reference were measured across the amide I band (1,714 – 1,590 cm-1). For each spectrum, triplicate measurements were collected and averaged. The data were analysed on the RedShiftBio *delta* analysis software.

SEC-SAXS

SEC-SAXS was performed at the EMBL P12 bioSAXS beamline (PETRA III, Hamburg, Germany). Samples were dissolved in 50 mM Na_2HPO_4, 300 mM NaCl pH 8.0 and 3% glycerol to prevent radiation damage. For the single proteins, ToxSp (10 mg/ml), ToxRp (10 mg/ml) and ToxRSp (14 mg/ml), a Superdex 75 Increase 10/300 column was used. For the ToxRS complex in the presence of bile acid S-CH (10 mg/ml), a Superdex 75 Increase 5/150 column was used. The column outlet was connected to the flow-through SAXS cell.

Throughout the elution, frames (I(q) vs q, where $q = 4\pi\sin\theta/\lambda$, and 2θ is the scattering angle) were collected successively. The data were normalized to the intensity of the transmitted beam and radially averaged; the scattering of the solvent was subtracted from the sample frames using frames corresponding to the scattering of the solvent. For optimized selection of buffer and sample frames the program CHROMIXS was employed. Data were further analysed and prepared via PRIMUS from the ATSAS software (***Manalastas-Cantos et al., 2021***), model preparation was done using DAMMIF at the online ATSAS server provided by EMBL Hamburg (https://www.embl-hamburg.de/biosaxs/atsas-online/). Comparison to theoretical scattering curves was performed with CRYSOL. Figures were done using PyMOL (***The PyMOL Molecular Graphics System, Version 1.2r3pre, Schrödinger, LLC.***).

The data have been deposited in the SASBDB databank. Accession codes: SASDR25, SASDR35, SASDR45, SASDR55.

MD simulations

The Cartesian coordinates of the complex between ToxRp and ToxSp were used as initial structure for our MD simulations. The minimum energy structure of the ligand cholate was first of all minimized with the GFN2-xTB (***Bannwarth et al., 2019***) using CREST, (***Grimme, 2019***), minimized with r^2SCAN (***Furness et al., 2020***) and the RESP point charges for all atoms of cholate were derived from the electrostatic potential computed at the HF-6-31G* level of theory with Gaussian16 v. C. (***Gaussian 16 Rev. C.01, 2016***). The protonation states of the titritable residues on the protein complex were calculated via the H^{++} web server (***Anandakrishnan et al., 2012; Gordon et al., 2005; Myers et al., 2006***) assuming a pH value of 8.0. Cholate was manually docked at the hydrophobic inner chamber of the ToxRSp complex guided by the superimposition of the crystallographic structure of *Vibrio parahaemolyticus* VtrA/VtrC complex in the presence of taurodeoxycholate (PDB id. 5KEW) (***Alnouti, 2009; Li et al., 2016***).

MD simulations were carried out using the suite of programs AMBER20 (***Amber20, 2022***) Protein residues and solvated ions were treated with the AMBER ff19SB force-field (***Ponder and Case, 2003***) and cholate was described as AMBER atoms types following the standard procedure in antechamber. We simulated two systems: the apo complex (ToxRSp) and the cholate-bound complex (ToxRSp +

cholate). The two systems were then energetically minimized to avoid close contacts, and then placed in the center of a cubic box filled with OPC water molecules (***Izadi et al., 2014***). Then, the solvated systems were minimized in three consecutive steps (all protons, solvent and all system) and heated up in 50 ps to from 100 k to 300 K in a NVT ensemble using the Langevin thermostat (gamma friction coefficient of 1.0). Care was taken to constraint the solute during the heating step by imposition of a harmonic force on each atom of the solute of 40 kcal mol^{-1} $Å^{-2}$. Afterwards, these harmonic constraints were gradually reduced up to a value of 10 kcal mol^{-1} $Å^{-2}$ in 4 simulation stages (NVT, 300 K). Then, the systems were switched to constant pressure (NPT scheme, 300 K) and the imposed constraints during the heating step were totally removed. Finally, each of the systems was submitted to three independent MD simulations of 0.8 μs (total simulation time per system: 2.4 μs). Atom-pair distance cut-offs were applied at 10.0 Å to compute the van der Waals interactions and long-range electrostatics by means of Particle-Mesh Ewald (PME) method. SHAKE algorithm was applied to restrain the hydrogen atoms on water molecules. MD trajectory analysis was carried out using the CPPTRAJ (***Roe and Cheatham, 2013***) module from AMBER20 for monitoring the root-mean-square distance (RMSD) and root-mean-square fluctuation (RMSF), amongst other parameters.

Acknowledgments

We are grateful for the beam time on ID30A-3 at ESRF (Grenoble, France) for intensive diffraction screening and data collection, as well as for staff support during data collection measurements (BAG mx-1740). J.R., K.Z. and T.P.K. acknowledge the support of the field of excellence BioHealth at the University of Graz. We also thank the interuniversity programs NAWI Graz and BioTechMed for financial support. Financial contributions by the Land Steiermark infrastructure grant “Frontier NMR”, project number 1109 are also gratefully acknowledged. B.D.G. thanks Fundación Martínez Escudero for a postdoctoral grant.

Supplementary files 1 a-f

- **Supplementary File 1a**: Description of expression constructs. List of plasmids and amino acid sequences used for the expression of ToxRp and ToxSp.
- **Supplementary File 1b**: Crystal data and structure refinement table of ToxRSp.
- **Supplementary File 1c:** Analysis of size-exclusion chromatography coupled with solution small-angle X-ray scattering SEC-SAXS. According to SAXS curves, ToxRp is monomeric in solution, whereas ToxSp seems to form dimers. Upon bile addition, the radius of gyration RG, the maximum particle size Dmax and the molecular weight of the ToxRSp complex increases.
- **Supplementary File 1d:** NMR derived dissociation constants for ToxRp and sodium cholate hydrate. NMR titration experiments reveal a weak binding of bile to ToxRp with a dissociation constant of 2.6 mM. Table S5 includes ToxRp residue number, chemical shift distance, dissociation constant Kd [M], error of Kd. The calculated average Kd is 2.7 ± 1.4 mM.
- **Supplementary File 1e:** List of amino acid sequences of sensory domains of ToxRS proteins from different Vibrio species. Table S5 includes UniProt ID of the used sequences as well as sequence identity values to ToxRSp from V. cholerae.
- **Supplementary File 1f:** Structural homology search of ToxSp bound to ToxRp using Dali server (Holm, 2022).

Supplementary File 2 – ToxRSp atom-atom interactions:

List of all atom interactions of ToxRSp (pdb: 8ALO). The list was created using PDBsum online server (Laskowski et al., 2018).

Supplement figures

- **Figure 1-figure supplement 1.** Inner membrane spanning domains of Vibrio cholerae regulators ToxR and ToxS. ToxRp, ToxSp stand for the periplasmic domains of ToxR and ToxS, respectively. ToxRSp is the complex formation of periplasmic domains of ToxR and ToxS.
- **Figure 1-figure supplement 2**. ToxRSp structure highlighting L33ToxSp core stabilizing hydrophobic network. According to previous studies ToxSp L33S mutant results in a loss of ToxSp protective function against ToxRp proteolysis (***Pfau and Taylor, 1998***). According to ToxRSp crystal structure ToxSp L33 has a central function in stabilizing the N-terminal membrane oriented core visible in the zoomed region.
- **Figure 1-figure supplement 3.** Structural alignment of bile interacting protein complexes ToxRS *V. cholerae* and VtrAC *V. parahaemolyticus*. VtrAC (gold; pdb: 5KEV) and ToxRSp (dark blue; pdb: 8ALO) reveal a similar fold (RMSD: 3.8Å). VtrC and ToxSp form a ß-barrel fold, which is stabilized by ß-strand 5 from VtrA and ToxRp, resulting in an obligate heterodimer formation including a binding pocket in the barrel cavity.
- **Figure 4-figure supplement 1.** MMS titration experiment with ToxRSp and S-CH. Six samples were measured with increasing molar ratios of S-CH to ToxRSp: 0, 1, 2, 3, 5, 20. Significant conformational changes occur within 1:1 and 1:2 samples whereas higher bile to protein ratios does not seem to induce additional significant spectral changes.
- **Figure 5-figure supplement 1.** Hydrophobic cleft of ToxSp binding pocket in complex with ToxRp. Hydrophobic (ochre) and hydrophilic (teal) surface representation of ToxS calculated with ChimeraX mlp. The bile binding cavity is highly hydrophobic (arrow).
- **Figure 6-figure supplement 1.** Analysis of size-exclusion chromatography coupled with solution small-angle X-ray scattering SEC-SAXS experiments. ToxRp (green), ToxSp (blue), ToxRSp (purple) and ToxRSp:bile (orange). **A:** The SEC-SAXS profiles are compared to the theoretical scattering curves (Crysol). Chi² values are indicated. Profiles are shifted along the y-axis for clarity. The following models were used ToxRp – NMR structure pdb: 7NN6; ToxSp – the dimeric model (AlphaFold-Multimer); ToxRSp – crystal structure pdb (8ALO); ToxRSp plus bile acid (1:1)- MD complex (Fig. 2). **B:** p(r) functions. **C:** Overlay of the models listed in (A) with the respective bead models calculated from the SAXS profiles. Note, for ToxRp and ToxRSp:bile an excess of volume indicates overall larger size. **D:** Dimensionless Kratkyplot ((qRG)2I(q)/I(0) vs qRG) . Note, dotted lines are drawn at y=1.104 and x = √ 3. Folded proteins have a local maximum where the two lines intersect. Here, the maxima of ToxRp and ToxRSp:bile are shifted, indicating a flexible/elongated structure.
- **Figure 6-figure supplement 2.** SAXS-derived chromatogram showing Integrated intensities (0.1 nm−1 < s < 0.8 nm−1) vs. elution of indicated samples. Note, the bile complex was separated on a Superdex 75 increase 5/150 column; the other samples on the larger Superdex 75 10/300 column.
- **Figure 6-figure supplement 3.** Saturation transfer difference STD NMR spectra of ToxRSp with S-CH. STD experiments reveal a binding of ToxRSp to bile acid S-CH. Saturation of the amide region of ToxRSp resulted in signals of the ligand in the STD spectra. **(A)** Overlay of ToxRSp spectra with and without S-CH. **(B-D)** STD spectra after saturation of different regions: (B) amide region 5000 Hz, (C) amide region 6000 Hz, (D) negative control -5000 Hz. **(E)** Reference spectrum for S-CH 2mM.
- **Figure 6-figure supplement 4.** Saturation transfer difference NMR spectra of ToxSp with sodium cholate hydrate. Spectra does not show an interaction between ToxSp and bile. No ligand signals could be observed upon saturation of amide signals of ToxSp. **(A)** Overlay of ToxSp spectra with and without S-CH. **(B-D)** STD spectra after saturation of different regions: (B) amide region 5000 Hz, (C) amide region 6000 Hz, (D) negative control -5000 Hz.
- **Figure 6-figure supplement 5.**
- **^{1}H NMR spectrum of ToxRSp upon S-CH addition.** Addition of increasing amounts of bile acid S-CH causes broadening of peaks and chemical shift changes indicating a binding event and increase of molecular weight. Reference spectrum of ToxRSp is shown in purple, spectrum recorded after addition of 0.5 and equimolar molar ratios of S-CH to ToxRSp is shown in orange and green, respectively.

- **Figure 6-figure supplement 6.** Superimposed NMR DOSY spectra of ToxRSp with and without bile acid sodium cholate hydrate. X-axis represents ^{1}H chemical shift, y-axis the determined diffusion coefficient D [m²/s]. Three samples were measured: ToxRSp (purple), ToxRSp 1:1 bile acid (orange), ToxRSp 1:20 bile acid (green). Addition of bile acid causes a decrease of the diffusion coefficient due to an increase of molecular weight. Higher bile acid concentrations result in higher diffusion coefficients via averaging due to exchange of bound and free bile molecules.
- **Figure 6-figure supplement 7.** SEC runs of ToxRSp with and without bile acid S-CH. x-axis represents the retention volume in ml, y-axis shows the absorption at 280 nm [mAU]. Maximum absorption of ToxRSp (purple) and ToxRSp with bile acid (1:1) (orange) is observed at 16.19 ml and 16.08 ml, respectively. Bile addition leads to a slight decrease of the retention volume and peak broadening.
- **Figure 6 -figure supplement 8.** NMR interaction experiment of ToxRSp with cyclo-PhePro (cFP). Previous experiments revealed a ToxR dependent downregulation of virulence factor production in response to cFP (***Bina et al., 2013; Bina and Bina, 2010***). NMR interaction experiments with ToxRSp do not indicate a binding event between ToxRSp and cFP since upon cFP addition no significant changes of chemical shift or intensity of ToxRSp signals could be observed.
- **Figure 8-figure supplement 1.** NMR titration experiment with ToxRp and S-CH. Overlay of ^{15}N-HSQC spectra of ToxRp with increasing amounts of bile acid S-CH proposes a weak interaction event. Significant chemical shift changes of ToxRp could be observed with high ligand concentrations of 1:50-1:200.
- **Figure 10-figure supplement 1.** Overlay of ToxRSp from different *Vibrio* species. Structures are calculated using AlphaFold-Multimer (***Evans et al., 2021; Jumper et al., 2021***). The structural alignment reveals a conserved fold of ToxSp (grey), whereas ToxRp (orange) varies among different *Vibrio* strains. The intermolecular salt bridge between ToxRp and ToxSp is highlighted, and residues types involved are mentioned in the table beside the aligned structures. ToxSp salt bridge forming aspartate residue is strictly conserved.
- **Figure 11-figure supplement 1.** Sequential analysis of ToxSp proteins from different *Vibrio* species. Analysis was performed with Clustal2.1 (***Madeira et al., 2022***). Strongly conserved residues are marked with an asterisk (*), conserved residues with colon (:) and period (.). Below the sequence identities are shown in percent.
- **Figure 11-figure supplement 2.** Sequential analysis of ToxRp proteins from different *Vibrio* species. Analysis was performed with Clustal2.1 (***Madeira et al., 2022***). Strongly conserved residues are marked with an asterisk (*), conserved residues with colon (:) and period (.). Below the sequence identities are shown in percent. Due to the higher variability of ToxRp in *Vibrio's* an additional analysis was performed for closely related strains, which are mostly human colonizing.

Source files:

- Figure 10 source data 1 – coordinate files of *Vibrio* AlphaFold models
- Figure 5 source data 1 – ToxRSp MD data
- Figure 6 source data 1 – SEC data
- Figure 4 source data 1 – MMS data
- Figure 8 source data 1 – NMR titration ToxRp plus S-CH
- Figure 6- figure supplement 3 source data 1 – STD ToxRSp plus S-CH
- Figure 6- figure supplement 4 source data 1 – STD ToxSp plus S-CH
- Figure 7 source data 1 – NMR titration 1 ToxRSp plus S-CH
- Figure 7 source data 2 – NMR titration 2 ToxRSp plus S-CH

References

Ahmed SH, Nashwan AJ. 2022. Cholera outbreak amid civil war: A public health crisis in Syria. *Journal of infection and public health* **15**:1484–1485. doi: 10.1016/j.jiph.2022.11.013.

Ali M, Nelson AR, Lopez AL, Sack DA. 2015. Updated global burden of cholera in endemic countries. *PLoS neglected tropical diseases* **9**:e0003832. doi: 10.1371/journal.pntd.0003832.

Almagro-Moreno S, Kim TK, Skorupski K, Taylor RK. 2015a. Proteolysis of virulence regulator ToxR is associated with entry of Vibrio cholerae into a dormant state. *PLoS genetics* **11**:e1005145. doi: 10.1371/journal.pgen.1005145.

Almagro-Moreno S, Pruss K, Taylor RK. 2015b. Intestinal Colonization Dynamics of Vibrio cholerae. *PLoS pathogens* **11**:e1004787. doi: 10.1371/journal.ppat.1004787.

Almagro-Moreno S, Root MZ, Taylor RK. 2015c. Role of ToxS in the proteolytic cascade of virulence regulator ToxR in Vibrio cholerae. *Molecular microbiology* **98**:963–976. doi: 10.1111/mmi.13170.

Alnouti Y. 2009. Bile Acid sulfation: a pathway of bile acid elimination and detoxification. *Toxicological sciences : an official journal of the Society of Toxicology* **108**:225–246. doi: 10.1093/toxsci/kfn268.

Amber20. 2022. University of California, San Francisco.

Anandakrishnan R, Aguilar B, Onufriev AV. 2012. H++ 3.0: automating pK prediction and the preparation of biomolecular structures for atomistic molecular modeling and simulations. *Nucleic acids research* **40**:W537-41. doi: 10.1093/nar/gks375.

Angelichio MJ, Spector J, Waldor MK, Camilli A. 1999. Vibrio cholerae Intestinal Population Dynamics in the Suckling Mouse Model of Infection. *Infection and Immunity* **67**:3733–3739.

Bannwarth C, Ehlert S, Grimme S. 2019. GFN2-xTB-An Accurate and Broadly Parametrized Self-Consistent Tight-Binding Quantum Chemical Method with Multipole Electrostatics and Density-Dependent Dispersion Contributions. *Journal of chemical theory and computation* **15**:1652–1671. doi: 10.1021/acs.jctc.8b01176.

Bari SMN, Roky MK, Mohiuddin M, Kamruzzaman M, Mekalanos JJ, Faruque SM. 2013. Quorum-sensing autoinducers resuscitate dormant Vibrio cholerae in environmental water samples. *Proceedings of the National Academy of Sciences of the United States of America* **110**:9926–9931. doi: 10.1073/pnas.1307697110.

Becker W, Bhattiprolu KC, Gubensäk N, Zangger K. 2018. Investigating Protein-Ligand Interactions by Solution Nuclear Magnetic Resonance Spectroscopy. *ChemPhysChem* **19**:894. doi: 10.1002/cphc.201800256.

Bina J, Zhu J, Dziejman M, Faruque S, Calderwood S, Mekalanos J. 2003. ToxR regulon of Vibrio cholerae and its expression in vibrios shed by cholera patients. *Proceedings of the National Academy of Sciences of the United States of America* **100**:2801–2806. doi: 10.1073/pnas.2628026100.

Bina TF, Kunkle DE, Bina XR, Mullett SJ, Wendell SG, Bina JE. 2021. Bile Salts Promote ToxR Regulon Activation during Growth under Virulence-Inducing Conditions. *Infection and Immunity* **89**:e0044121. doi: 10.1128/IAI.00441-21.

Bina XR, Bina JE. 2010. The Cyclic Dipeptide Cyclo(Phe-Pro) Inhibits Cholera Toxin and Toxin-Coregulated Pilus Production in O1 El Tor Vibrio cholerae ▿ . *Journal of bacteriology* **192**:3829–3832. doi: 10.1128/JB.00191-10.

Bina XR, Taylor DL, Vikram A, Ante VM, Bina JE. 2013. Vibrio cholerae ToxR downregulates virulence factor production in response to cyclo(Phe-Pro). *mBio* **4**:e00366-13. doi: 10.1128/mBio.00366-13.

Canals A, Pieretti S, Muriel-Masanes M, El Yaman N, Plecha SC, Thomson JJ, Fàbrega-Ferrer M, Pérez-Luque R, Krukonis ES, Coll M. 2023. ToxR activates the Vibrio cholerae virulence genes by tethering DNA to the membrane through versatile binding to multiple sites. *Proceedings of the National Academy of Sciences of the United States of America* **120**:e2304378120. doi: 10.1073/pnas.2304378120.

Champion GA, Neely MN, Brennan MA, DiRita VJ. 1997. A branch in the ToxR regulatory cascade of Vibrio cholerae revealed by characterization of toxT mutant strains. *Molecular microbiology* **23**:323–331. doi: 10.1046/j.1365-2958.1997.2191585.x.

Chen L, Qiu Y, Tang H, Hu LF, Yang WH, Zhu XJ, Huang XX, Wang T, Zhang YQ. 2018. ToxR Is Required for Biofilm Formation and Motility of Vibrio Parahaemolyticus. *Biomedical and environmental sciences : BES* **31**:848–850. doi: 10.3967/bes2018.112.

Chen VB, Arendall WB, Headd JJ, Keedy DA, Immormino RM, Kapral GJ, Murray LW, Richardson JS, Richardson DC. 2010. MolProbity: all-atom structure validation for macromolecular crystallography. *Acta crystallographica. Section D, Biological crystallography* **66**:12–21. doi: 10.1107/S0907444909042073.

Childers BM, Klose KE. 2007. Regulation of virulence in Vibrio cholerae: the ToxR regulon. *Future microbiology* **2**:335–344. doi: 10.2217/17460913.2.3.335.

Crawford JA, Kaper JB, DiRita VJ. 1998. Analysis of ToxR-dependent transcription activation of ompU, the gene encoding a major envelope protein in Vibrio cholerae. *Molecular microbiology* **29**:235–246. doi: 10.1046/j.1365-2958.1998.00925.x.

Croll TI. 2018. ISOLDE: a physically realistic environment for model building into low-resolution electron-density maps. *Acta crystallographica. Section D, Structural biology* **74**:519–530. doi: 10.1107/S2059798318002425.

Davis AL, Keeler J, Laue ED, Moskau D. 1992. Experiments for recording pure-absorption heteronuclear correlation spectra using pulsed field gradients. *Journal of Magnetic Resonance (1969)* **98**:207–216. doi: 10.1016/0022-2364(92)90126-R.

Delaglio F, Grzesiek S, Vuister GW, Zhu G, Pfeifer J, Bax A. 1995. NMRPipe: a multidimensional spectral processing system based on UNIX pipes. *Journal of biomolecular NMR* **6**:277–293. doi: 10.1007/BF00197809.

DiRita VJ, Parsot C, Jander G, Mekalanos JJ. 1991. Regulatory cascade controls virulence in Vibrio cholerae. *Proceedings of the National Academy of Sciences of the United States of America* **88**:5403–5407. doi: 10.1073/pnas.88.12.5403.

Duret G, Delcour AH. 2006. Deoxycholic acid blocks vibrio cholerae OmpT but not OmpU porin. *The Journal of biological chemistry* **281**:19899–19905. doi: 10.1074/jbc.M602426200.

Eichinger A, Haneburger I, Koller C, Jung K, Skerra A. 2011. Crystal structure of the sensory domain of Escherichia coli CadC, a member of the ToxR-like protein family. *Protein science : a publication of the Protein Society* **20**:656–669. doi: 10.1002/pro.594.

Emsley P, Lohkamp B, Scott WG, Cowtan K. 2010. Features and development of Coot. *Acta crystallographica. Section D, Biological crystallography* **66**:486–501. doi: 10.1107/S0907444910007493.

Evans PR, Murshudov GN. 2013. How good are my data and what is the resolution? *Acta crystallographica. Section D, Biological crystallography* **69**:1204–1214. doi: 10.1107/S0907444913000061.

Evans R, O'Neill M, Pritzel A, Antropova N, Senior A, Green T, Žídek A, Bates R, Blackwell S, Yim J, Ronneberger O, Bodenstein S, Zielinski M, Bridgland A, Potapenko A, Cowie A, Tunyasuvunakool K, Jain R, Clancy E, Kohli P, Jumper J, Hassabis D. 2021. *Protein complex prediction with AlphaFold-Multimer*.

Furness JW, Kaplan AD, Ning J, Perdew JP, Sun J. 2020. Accurate and Numerically Efficient r2SCAN Meta-Generalized Gradient Approximation. *The journal of physical chemistry letters* **11**:8208–8215. doi: 10.1021/acs.jpclett.0c02405.

Gaussian 16 Rev. C.01. 2016. Wallingford, CT.

Gordon JC, Myers JB, Folta T, Shoja V, Heath LS, Onufriev A. 2005. H++: a server for estimating pKas and adding missing hydrogens to macromolecules. *Nucleic acids research* **33**:W368-71. doi: 10.1093/nar/gki464.

Goss TJ, Morgan SJ, French EL, Krukonis ES. 2013. ToxR recognizes a direct repeat element in the toxT, ompU, ompT, and ctxA promoters of Vibrio cholerae to regulate transcription. *Infection and Immunity* **81**:884–895. doi: 10.1128/IAI.00889-12.

Grimme S. 2019. Exploration of Chemical Compound, Conformer, and Reaction Space with Meta-Dynamics Simulations Based on Tight-Binding Quantum Chemical Calculations. *Journal of chemical theory and computation* **15**:2847–2862. doi: 10.1021/acs.jctc.9b00143.

Gubensäk N, Schrank E, Hartlmüller C, Göbl C, Falsone FS, Becker W, Wagner GE, Pulido S, Meyer NH, Pavkov-Keller T, Madl T, Reidl J, Zangger K. 2021a. Structural and DNA-binding properties of the cytoplasmic domain of Vibrio cholerae transcription factor ToxR. *The Journal of biological chemistry* **297**:101167. doi: 10.1016/j.jbc.2021.101167.

Gubensäk N, Wagner GE, Schrank E, Falsone FS, Berger TMI, Pavkov-Keller T, Reidl J, Zangger K. 2021b. The periplasmic domains of Vibriocholerae ToxR and ToxS are forming a strong heterodimeric complex independent on the redox state of ToxR cysteines. *Molecular microbiology* **115**:1277–1291. doi: 10.1111/mmi.14673.

Gunn JS. 2000. Mechanisms of bacterial resistance and response to bile. *Microbes and Infection* **2**:907–913. doi: 10.1016/S1286-4579(00)00392-0.

Gupta S, Chowdhury R. 1997. Bile affects production of virulence factors and motility of Vibrio cholerae. *Infection and Immunity* **65**:1131–1134. doi: 10.1128/iai.65.3.1131-1134.1997.

Hamilton JP, Xie G, Raufman J-P, Hogan S, Griffin TL, Packard CA, Chatfield DA, Hagey LR, Steinbach JH, Hofmann AF. 2007. Human cecal bile acids: concentration and spectrum. *American journal of physiology. Gastrointestinal and liver physiology* **293**:G256-63. doi: 10.1152/ajpgi.00027.2007.

Hay AJ, Yang M, Xia X, Liu Z, Hammons J, Fenical W, Zhu J. 2017. Calcium Enhances Bile Salt-Dependent Virulence Activation in Vibrio cholerae. *Infection and Immunity* **85**. doi: 10.1128/IAI.00707-16.

Hendlich M, Rippmann F, Barnickel G. 1997. LIGSITE: automatic and efficient detection of potential small molecule-binding sites in proteins. *Journal of molecular graphics & modelling* **15**:359-63, 389. doi: 10.1016/s1093-3263(98)00002-3.

Holm L. 2022. Dali server: structural unification of protein families. *Nucleic acids research* **50**:W210-5. doi: 10.1093/nar/gkac387.

Hu D, Liu B, Feng L, Ding P, Guo X, Wang M, Cao B, Reeves PR, Wang L. 2016. Origins of the current seventh cholera pandemic. *Proceedings of the National Academy of Sciences of the United States of America* **113**:E7730-E7739. doi: 10.1073/pnas.1608732113.

Hung DT, Mekalanos JJ. 2005. Bile acids induce cholera toxin expression in Vibrio cholerae in a ToxT-independent manner. *Proceedings of the National Academy of Sciences of the United States of America* **102**:3028–3033. doi: 10.1073/pnas.0409559102.

Hung DT, Zhu J, Sturtevant D, Mekalanos JJ. 2006. Bile acids stimulate biofilm formation in Vibrio cholerae. *Molecular microbiology* **59**:193–201. doi: 10.1111/j.1365-2958.2005.04846.x.

Izadi S, Anandakrishnan R, Onufriev AV. 2014. Building Water Models: A Different Approach. *The journal of physical chemistry letters* **5**:3863–3871. doi: 10.1021/jz501780a.

Johnson CS. 1999. Diffusion ordered nuclear magnetic resonance spectroscopy: principles and applications. *Progress in nuclear magnetic resonance spectroscopy* **34**:203–256. doi: 10.1016/S0079-6565(99)00003-5.

Jumper J, Evans R, Pritzel A, Green T, Figurnov M, Ronneberger O, Tunyasuvunakool K, Bates R, Žídek A, Potapenko A, Bridgland A, Meyer C, Kohl SAA, Ballard AJ, Cowie A, Romera-Paredes B, Nikolov S, Jain R, Adler J, Back T, Petersen S, Reiman D, Clancy E, Zielinski M, Steinegger M, Pacholska M, Berghammer T, Bodenstein S, Silver D, Vinyals O, Senior AW, Kavukcuoglu K, Kohli P, Hassabis D. 2021. Highly accurate protein structure prediction with AlphaFold. *Nature* **596**:583–589. doi: 10.1038/s41586-021-03819-2.

Kabsch W. 2010. XDS. *Acta crystallographica. Section D, Biological crystallography* **66**:125–132. doi: 10.1107/S0907444909047337.

Kabsch W, Sander C. 1983. Dictionary of protein secondary structure: pattern recognition of hydrogen-bonded and geometrical features. *Biopolymers* **22**:2577–2637. doi: 10.1002/bip.360221211.

Kanungo S, Azman AS, Ramamurthy T, Deen J, Dutta S. 2022. Cholera. *Lancet (London, England)* **399**:1429–1440. doi: 10.1016/S0140-6736(22)00330-0.

Kaval KG, Chimalapati S, Siegel SD, Garcia N, Jaishankar J, Dalia AB, Orth K. 2023. Membrane-localized expression, production and assembly of Vibrio parahaemolyticus T3SS2 provides evidence for transertion. *Nature communications* **14**:1178. doi: 10.1038/s41467-023-36762-z.

Kenney L. 2002. Structure/function relationships in OmpR and other winged-helix transcription factors. *Current Opinion in Microbiology* **5**:135–141. doi: 10.1016/S1369-5274(02)00310-7.

Kinch LN, Cong Q, Jaishankar J, Orth K. 2022. Co-component signal transduction systems: Fast-evolving virulence regulation cassettes discovered in enteric bacteria. *Proceedings of the National Academy of Sciences of the United States of America* **119**:e2203176119. doi: 10.1073/pnas.2203176119.

Krissinel E, Henrick K. 2007. Inference of macromolecular assemblies from crystalline state. *Journal of molecular biology* **372**:774–797. doi: 10.1016/j.jmb.2007.05.022.

Krukonis ES, DiRita VJ. 2003. DNA Binding and ToxR Responsiveness by the Wing Domain of TcpP, an Activator of Virulence Gene Expression in Vibrio cholerae. *Molecular Cell* **12**:157–165. doi: 10.1016/S1097-2765(03)00222-3.

Laskowski RA, Jabłońska J, Pravda L, Vařeková RS, Thornton JM. 2018. PDBsum: Structural summaries of PDB entries. *Protein science : a publication of the Protein Society* **27**:129–134. doi: 10.1002/pro.3289.

Lee SE, Shin SH, Kim SY, Kim YR, Shin DH, Chung SS, Lee ZH, Lee JY, Jeong KC, Choi SH, Rhee JH. 2000. Vibrio vulnificus has the transmembrane transcription activator ToxRS stimulating the expression of the hemolysin gene vvhA. *Journal of bacteriology* **182**:3405–3415. doi: 10.1128/jb.182.12.3405-3415.2000.

Lembke M, Pennetzdorfer N, Tutz S, Koller M, Vorkapic D, Zhu J, Schild S, Reidl J. 2018. Proteolysis of ToxR is controlled by cysteine-thiol redox state and bile salts in Vibrio cholerae. *Molecular microbiology* **110**:796–810. doi: 10.1111/mmi.14125.

Li P, Rivera-Cancel G, Kinch LN, Salomon D, Tomchick DR, Grishin NV, Orth K. 2016. Bile salt receptor complex activates a pathogenic type III secretion system. *eLife* **5**. doi: 10.7554/eLife.15718.

Liebschner D, Afonine PV, Baker ML, Bunkóczi G, Chen VB, Croll TI, Hintze B, Hung LW, Jain S, McCoy AJ, Moriarty NW, Oeffner RD, Poon BK, Prisant MG, Read RJ, Richardson JS, Richardson DC, Sammito MD, Sobolev OV, Stockwell DH, Terwilliger TC, Urzhumtsev AG, Videau LL, Williams CJ, Adams PD. 2019. Macromolecular structure determination using X-rays, neutrons and electrons: recent developments in

Phenix. *Acta crystallographica. Section D, Structural biology* **75**:861–877. doi: 10.1107/S2059798319011471.

Madeira F, Pearce M, Tivey ARN, Basutkar P, Lee J, Edbali O, Madhusoodanan N, Kolesnikov A, Lopez R. 2022. Search and sequence analysis tools services from EMBL-EBI in 2022. *Nucleic acids research* **50**:W276-9. doi: 10.1093/nar/gkac240.

Manalastas-Cantos K, Konarev PV, Hajizadeh NR, Kikhney AG, Petoukhov MV, Molodenskiy DS, Panjkovich A, Mertens HDT, Gruzinov A, Borges C, Jeffries CM, Svergun DI, Franke D. 2021. ATSAS 3.0: expanded functionality and new tools for small-angle scattering data analysis. *Journal of applied crystallography* **54**:343–355. doi: 10.1107/S1600576720013412.

Martínez-Hackert E, Stock AM. 1997a. Structural relationships in the OmpR family of winged-helix transcription factors. *Journal of molecular biology* **269**:301–312. doi: 10.1006/jmbi.1997.1065.

Martínez-Hackert E, Stock AM. 1997b. The DNA-binding domain of OmpR: crystal structures of a winged helix transcription factor. *Structure* **5**:109–124. doi: 10.1016/s0969-2126(97)00170-6.

Mayer M, Meyer B. 1999. Characterization of Ligand Binding by Saturation Transfer Difference NMR Spectroscopy. *Angewandte Chemie International Edition in English* **38**:1784–1788. doi: 10.1002/(SICI)1521-3773(19990614)38:12<1784::AID-ANIE1784>3.0.CO;2-Q.

McCoy AJ, Grosse-Kunstleve RW, Adams PD, Winn MD, Storoni LC, Read RJ. 2007. Phaser crystallographic software. *Journal of applied crystallography* **40**:658–674. doi: 10.1107/S0021889807021206.

Midgett CR, Almagro-Moreno S, Pellegrini M, Taylor RK, Skorupski K, Kull FJ. 2017. Bile salts and alkaline pH reciprocally modulate the interaction between the periplasmic domains of Vibrio cholerae ToxR and ToxS. *Molecular microbiology* **105**:258–272. doi: 10.1111/mmi.13699.

Midgett CR, Swindell RA, Pellegrini M, Jon Kull F. 2020. A disulfide constrains the ToxR periplasmic domain structure, altering its interactions with ToxS and bile-salts. *Scientific reports* **10**:9002. doi: 10.1038/s41598-020-66050-5.

Millet YA, Alvarez D, Ringgaard S, Andrian UH von, Davis BM, Waldor MK. 2014. Insights into Vibrio cholerae Intestinal Colonization from Monitoring Fluorescently Labeled Bacteria. *PLoS pathogens* **10**. doi: 10.1371/journal.ppat.1004405.

Mitrophanov AY, Groisman EA. 2008. Signal integration in bacterial two-component regulatory systems. *Genes & development* **22**:2601–2611. doi: 10.1101/gad.1700308.

Morgan SJ, Felek S, Gadwal S, Koropatkin NM, Perry JW, Bryson AB, Krukonis ES. 2011. The two faces of ToxR: activator of ompU, co-regulator of toxT in Vibrio cholerae. *Molecular microbiology* **81**:113–128. doi: 10.1111/j.1365-2958.2011.07681.x.

Morgan SJ, French EL, Plecha SC, Krukonis ES. 2019. The wing of the ToxR winged helix-turn-helix domain is required for DNA binding and activation of toxT and ompU. *PloS one* **14**:e0221936. doi: 10.1371/journal.pone.0221936.

Morris KF, Johnson CS. 1992. Diffusion-ordered two-dimensional nuclear magnetic resonance spectroscopy. *Journal of the American Chemical Society* **114**:3139–3141. doi: 10.1021/ja00034a071.

Murshudov GN, Skubák P, Lebedev AA, Pannu NS, Steiner RA, Nicholls RA, Winn MD, Long F, Vagin AA. 2011. REFMAC5 for the refinement of macromolecular crystal structures. *Acta crystallographica. Section D, Biological crystallography* **67**:355–367. doi: 10.1107/S0907444911001314.

Myers J, Grothaus G, Narayanan S, Onufriev A. 2006. A simple clustering algorithm can be accurate enough for use in calculations of pKs in macromolecules. *Proteins* **63**:928–938. doi: 10.1002/prot.20922.

Ottemann KM, Mekalanos JJ. 1996. The ToxR protein of Vibrio cholerae forms homodimers and heterodimers. *Journal of bacteriology* **178**:156–162. doi: 10.1128/jb.178.1.156-162.1996.

Pennetzdorfer N, Lembke M, Pressler K, Matson JS, Reidl J, Schild S. 2019. Regulated Proteolysis in Vibrio cholerae Allowing Rapid Adaptation to Stress Conditions. *Frontiers in cellular and infection microbiology* **9**:214. doi: 10.3389/fcimb.2019.00214.

Pettersen EF, Goddard TD, Huang CC, Meng EC, Couch GS, Croll TI, Morris JH, Ferrin TE. 2021. UCSF ChimeraX: Structure visualization for researchers, educators, and developers. *Protein science : a publication of the Protein Society* **30**:70–82. doi: 10.1002/pro.3943.

Pfau JD, Taylor RK. 1996. Genetic footprint on the ToxR-binding site in the promoter for cholera toxin. *Molecular microbiology* **20**:213–222. doi: 10.1111/j.1365-2958.1996.tb02502.x.

Pfau JD, Taylor RK. 1998. Mutations in toxR and toxS that separate transcriptional activation from DNA binding at the cholera toxin gene promoter. *Journal of bacteriology* **180**:4724–4733. doi: 10.1128/JB.180.17.4724-4733.1998.

Plecha SC, Withey JH. 2015. Mechanism for inhibition of Vibrio cholerae ToxT activity by the unsaturated fatty acid components of bile. *Journal of bacteriology* **197**:1716–1725. doi: 10.1128/JB.02409-14.

Ponder JW, Case DA. 2003. Force fields for protein simulations. *Advances in protein chemistry* **66**:27–85. doi: 10.1016/s0065-3233(03)66002-x.

Provenzano D, Klose KE. 2000. Altered expression of the ToxR-regulated porins OmpU and OmpT diminishes Vibrio cholerae bile resistance, virulence factor expression, and intestinal colonization. *Proceedings of the National Academy of Sciences of the United States of America* **97**:10220–10224. doi: 10.1073/pnas.170219997.

Provenzano D, Schuhmacher DA, Barker JL, Klose KE. 2000. The virulence regulatory protein ToxR mediates enhanced bile resistance in Vibrio cholerae and other pathogenic Vibrio species. *Infection and Immunity* **68**:1491–1497. doi: 10.1128/IAI.68.3.1491-1497.2000.

Qin J, Gronenborn AM. 2014. Weak protein complexes: challenging to study but essential for life. *The FEBS journal* **281**:1948–1949. doi: 10.1111/febs.12744.

Roe DR, Cheatham TE. 2013. PTRAJ and CPPTRAJ: Software for Processing and Analysis of Molecular Dynamics Trajectory Data. *Journal of chemical theory and computation* **9**:3084–3095. doi: 10.1021/ct400341p.

Sengupta C, Ray S, Chowdhury R. 2014. Fine tuning of virulence regulatory pathways in enteric bacteria in response to varying bile and oxygen concentrations in the gastrointestinal tract. *Gut pathogens* **6**:38. doi: 10.1186/s13099-014-0038-9.

Simonet VC, Baslé A, Klose KE, Delcour AH. 2003. The Vibrio cholerae porins OmpU and OmpT have distinct channel properties. *The Journal of biological chemistry* **278**:17539–17545. doi: 10.1074/jbc.M301202200.

Sistrunk JR, Nickerson KP, Chanin RB, Rasko DA, Faherty CS. 2016. Survival of the Fittest: How Bacterial Pathogens Utilize Bile To Enhance Infection. *Clinical microbiology reviews* **29**:819–836. doi: 10.1128/CMR.00031-16.

Skorupski K, Taylor RK. 1997. Control of the ToxR virulence regulon in Vibrio cholerae by environmental stimuli. *Molecular microbiology* **25**:1003–1009.

Srivastava R, Sinha VB, Srivastava BS. 1980. Events in the pathogenesis of experimental cholera: role of bacterial adherence and multiplication. *Journal of medical microbiology* **13**:1–9. doi: 10.1099/00222615-13-1-1.

Steinkellner G, Rader R, Thallinger GG, Kratky C, Gruber K. 2009. VASCo: computation and visualization of annotated protein surface contacts. *BMC bioinformatics* **10**:32. doi: 10.1186/1471-2105-10-32.

Sukenik S, Ren P, Gruebele M. 2017. Weak protein-protein interactions in live cells are quantified by cell-volume modulation. *Proceedings of the National Academy of Sciences of the United States of America* **114**:6776–6781. doi: 10.1073/pnas.1700818114.

The PyMOL Molecular Graphics System, Version 1.2r3pre, Schrödinger, LLC.

Tomchick DR, Orth K, Rivera-Cancel G. 2016. *Vibrio parahaemolyticus VtrA/VtrC complex*.

Touw WG, Baakman C, Black J, te Beek TAH, Krieger E, Joosten RP, Vriend G. 2015. A series of PDB-related databanks for everyday needs. *Nucleic acids research* **43**:D364-8. doi: 10.1093/nar/gku1028.

Wang S-Y, Lauritz J, Jass J, Milton DL. 2002. A ToxR homolog from Vibrio anguillarum serotype O1 regulates its own production, bile resistance, and biofilm formation. *Journal of bacteriology* **184**:1630–1639. doi: 10.1128/jb.184.6.1630-1639.2002.

Welch TJ, Bartlett DH. 1998. Identification of a regulatory protein required for pressure-responsive gene expression in the deep-sea bacterium Photobacterium species strain SS9. *Molecular microbiology* **27**:977–985. doi: 10.1046/j.1365-2958.1998.00742.x.

Wibbenmeyer JA, Provenzano D, Landry CF, Klose KE, Delcour AH. 2002. Vibrio cholerae OmpU and OmpT porins are differentially affected by bile. *Infection and Immunity* **70**:121–126. doi: 10.1128/IAI.70.1.121-126.2002.

Williamson MP. 2013. Using chemical shift perturbation to characterise ligand binding. *Progress in nuclear magnetic resonance spectroscopy* **73**:1–16. doi: 10.1016/j.pnmrs.2013.02.001.

Withey JH, DiRita VJ. 2006. The toxbox: specific DNA sequence requirements for activation of Vibrio cholerae virulence genes by ToxT. *Molecular microbiology* **59**:1779–1789. doi: 10.1111/j.1365-2958.2006.05053.x.

Xue Y, Tu F, Shi M, Wu C-Q, Ren G, Wang X, Fang W, Song H, Yang M. 2016. Redox pathway sensing bile salts activates virulence gene expression in Vibrio cholerae. *Molecular microbiology* **102**:909–924. doi: 10.1111/mmi.13497.

Yang M, Liu Z, Hughes C, Stern AM, Wang H, Zhong Z, Kan B, Fenical W, Zhu J. 2013. Bile salt-induced intermolecular disulfide bond formation activates Vibrio cholerae virulence. *Proceedings of the National Academy of Sciences of the United States of America* **110**:2348–2353. doi: 10.1073/pnas.1218039110.

Zou AJ, Kinch L, Chimalapati S, Garcia N, Tomchick DR, Orth K. 2023. Molecular determinants for differential activation of the bile acid receptor from the pathogen Vibrio parahaemolyticus. *The Journal of biological chemistry* **299**:104591. doi: 10.1016/j.jbc.2023.104591.

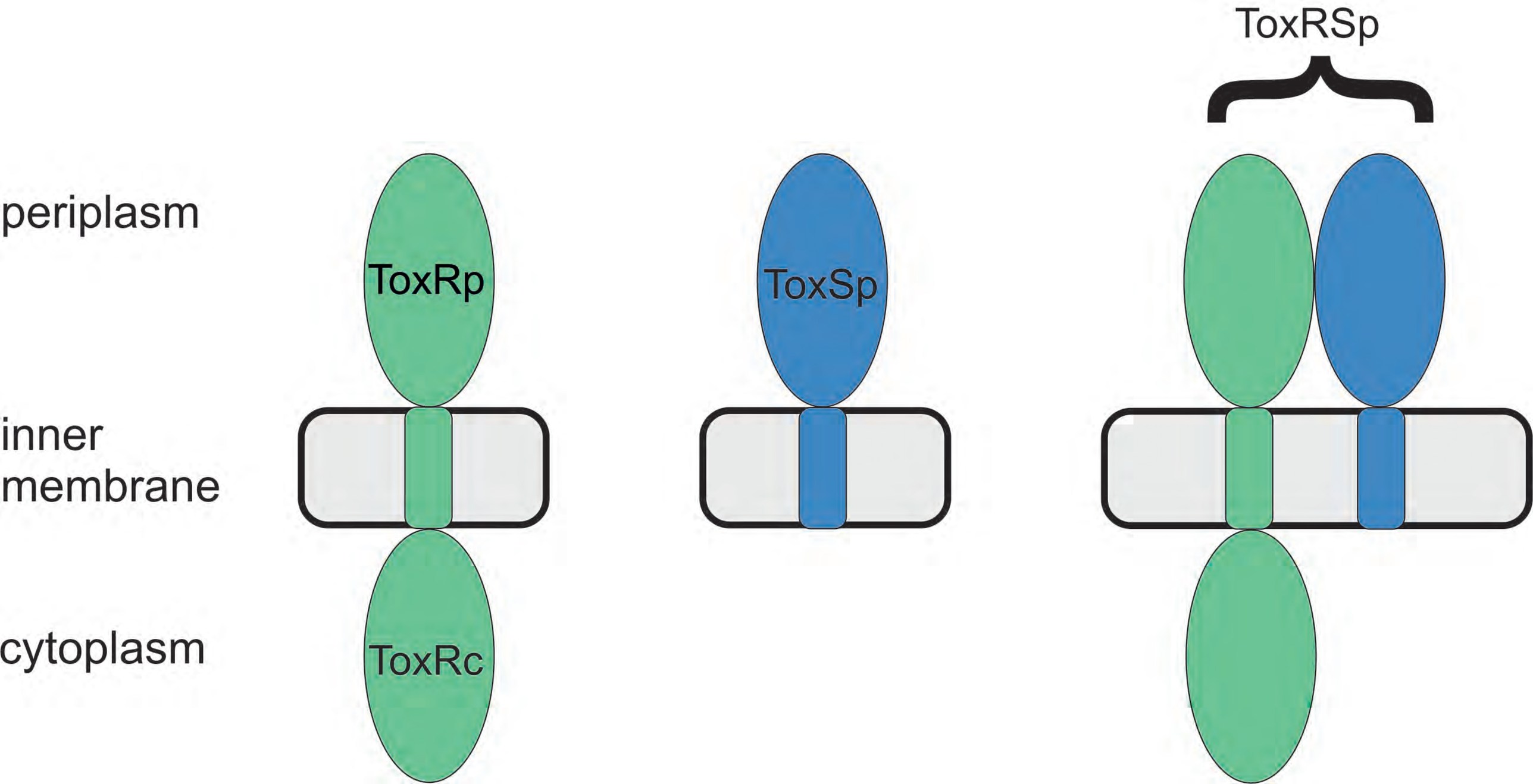
ToxRSp
periplasm
ToxRp
ToxSp
inner
membrane
cytoplasm
ToxRc

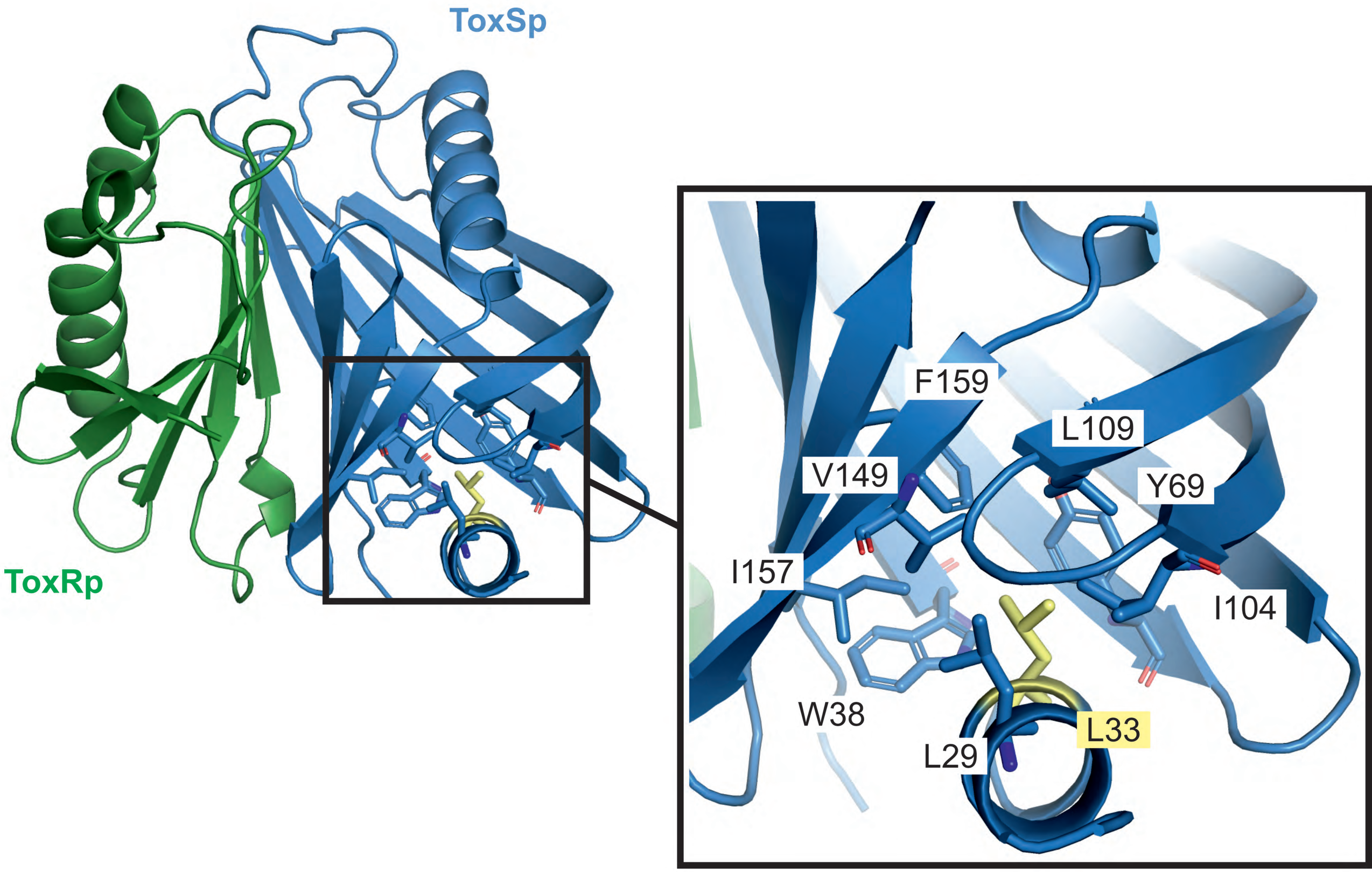
ToxSp
ToxRp
F159
L109
V149
Y69
I157
I104
W38
L33
L29

ToxRSp (pdb:8alo) vs. VtrAC (pdb: 5kev)

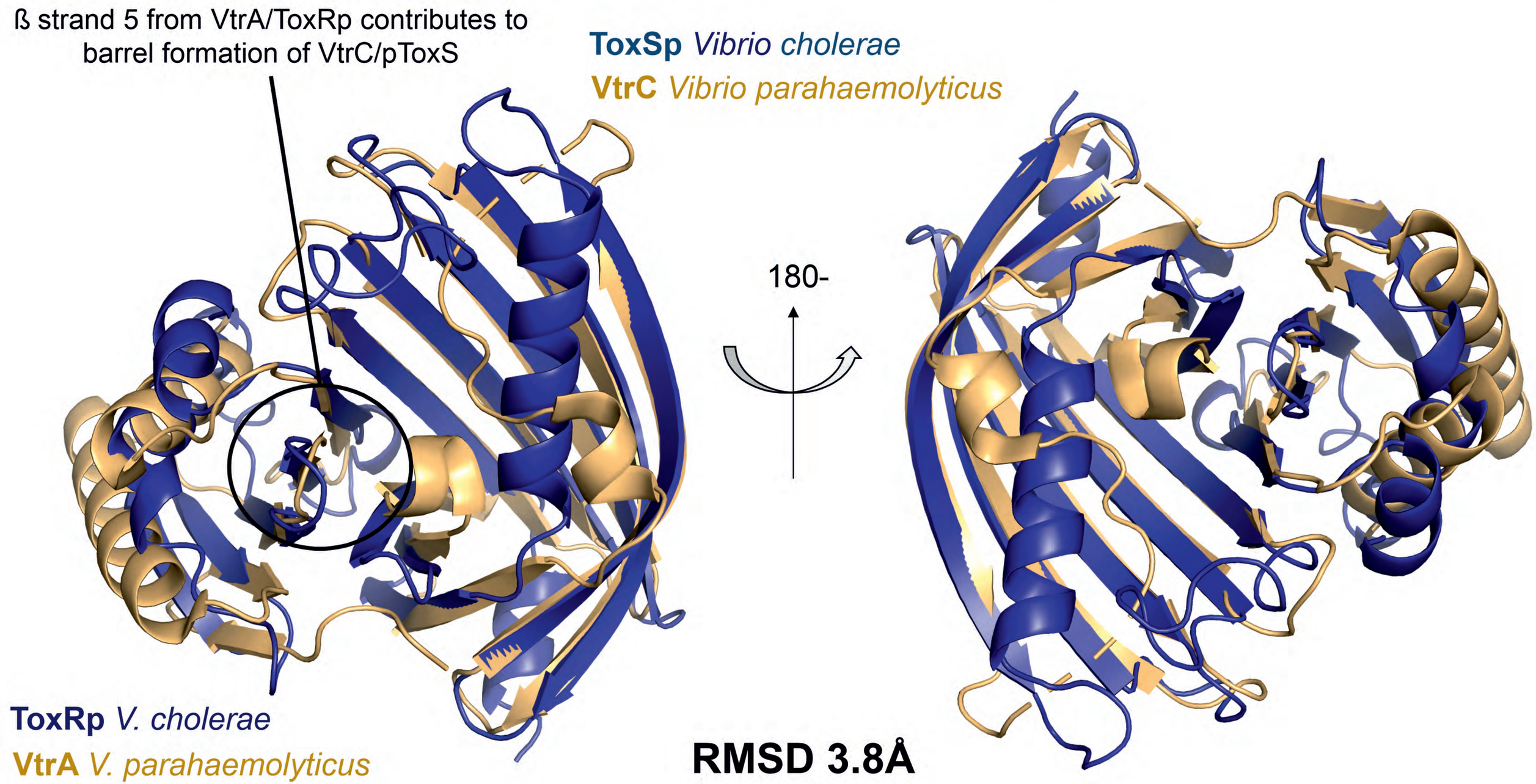

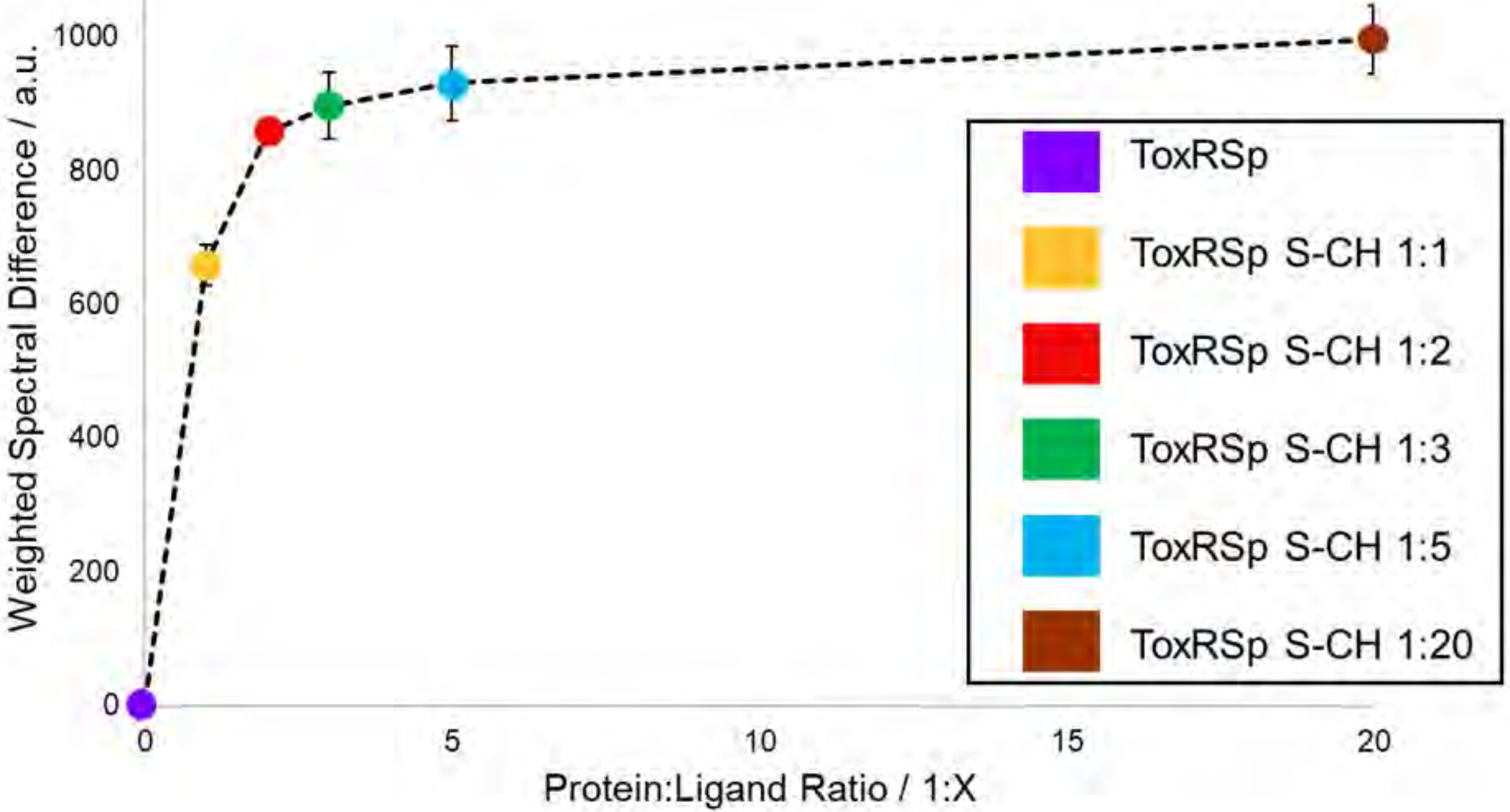
Weighted Spectral Difference / a.u.
1000
800
600
400
200
0
0
5
10
15
20
Protein:Ligand Ratio / 1:X
ToxRSp
ToxRSp S-CH 1:1
ToxRSp S-CH 1:2
ToxRSp S-CH 1:3
ToxRSp S-CH 1:5
ToxRSp S-CH 1:20

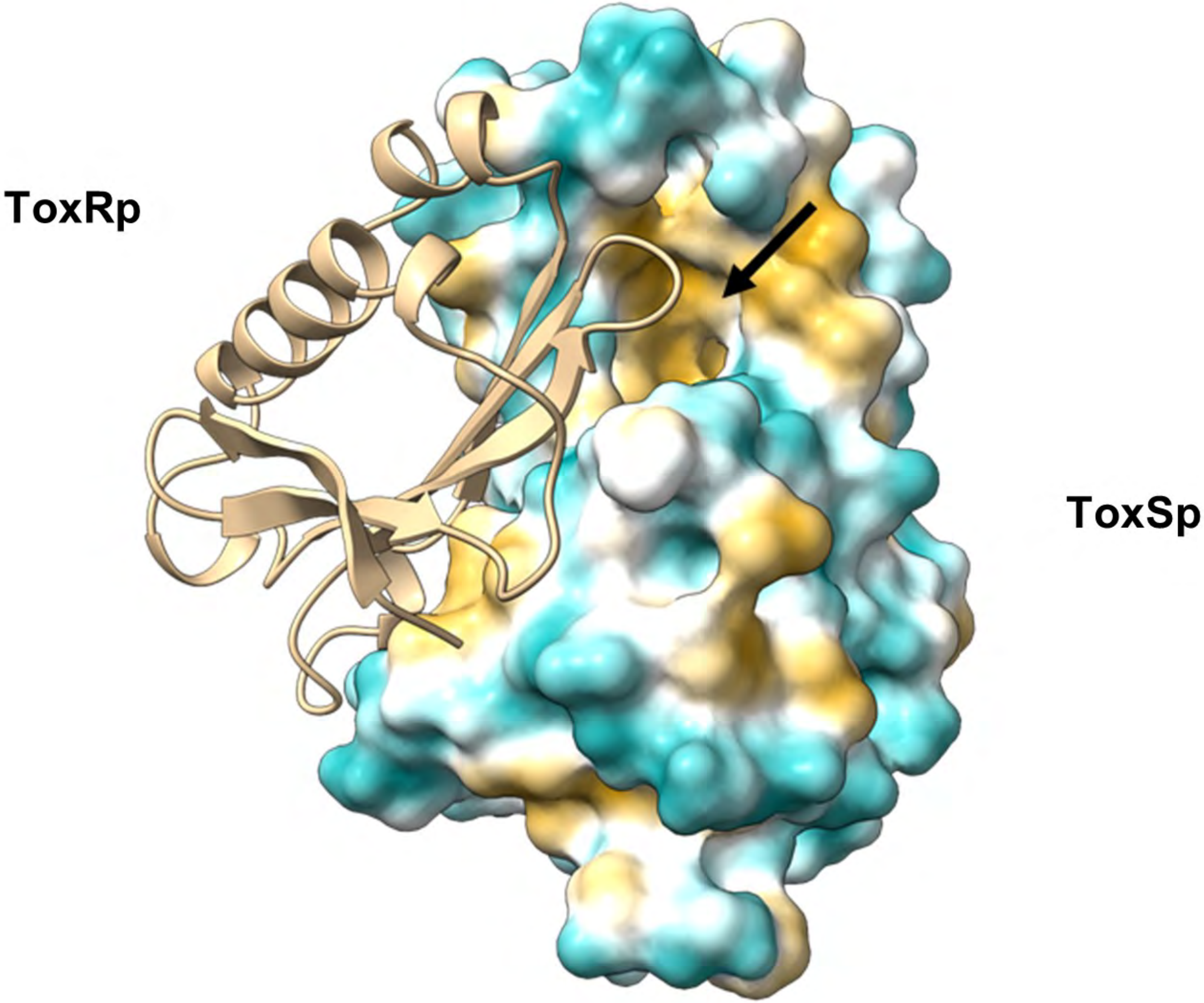
ToxRp
ToxSp

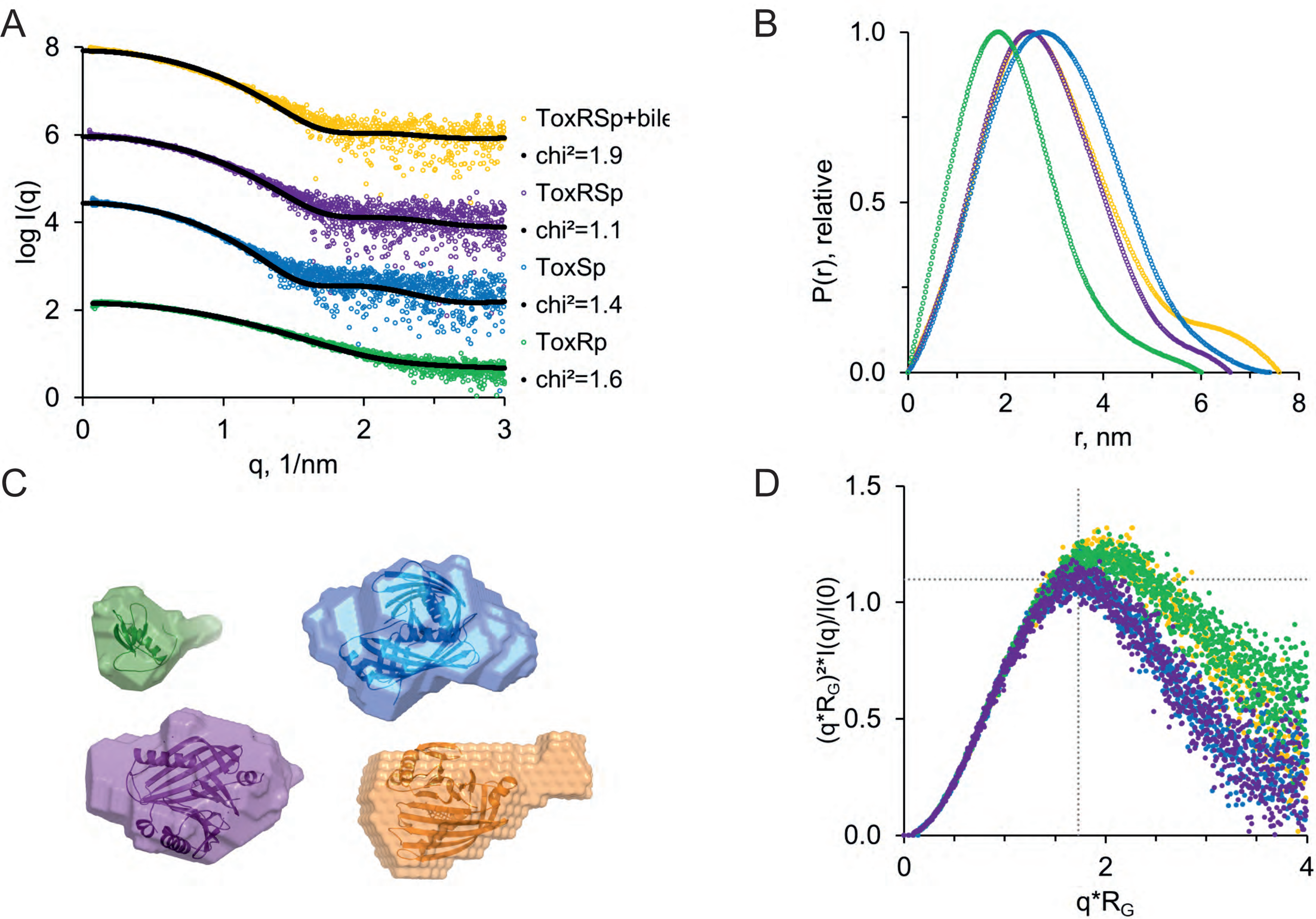
A
log I(q)
q, 1/nm
ToxRSp+bile
chi²=1.9
ToxRSp
chi²=1.1
ToxSp
chi²=1.4
ToxRp
chi²=1.6
B
P(r), relative
r, nm
C
D
(q*R_G)²*I(q)/I(0)
q*R_G

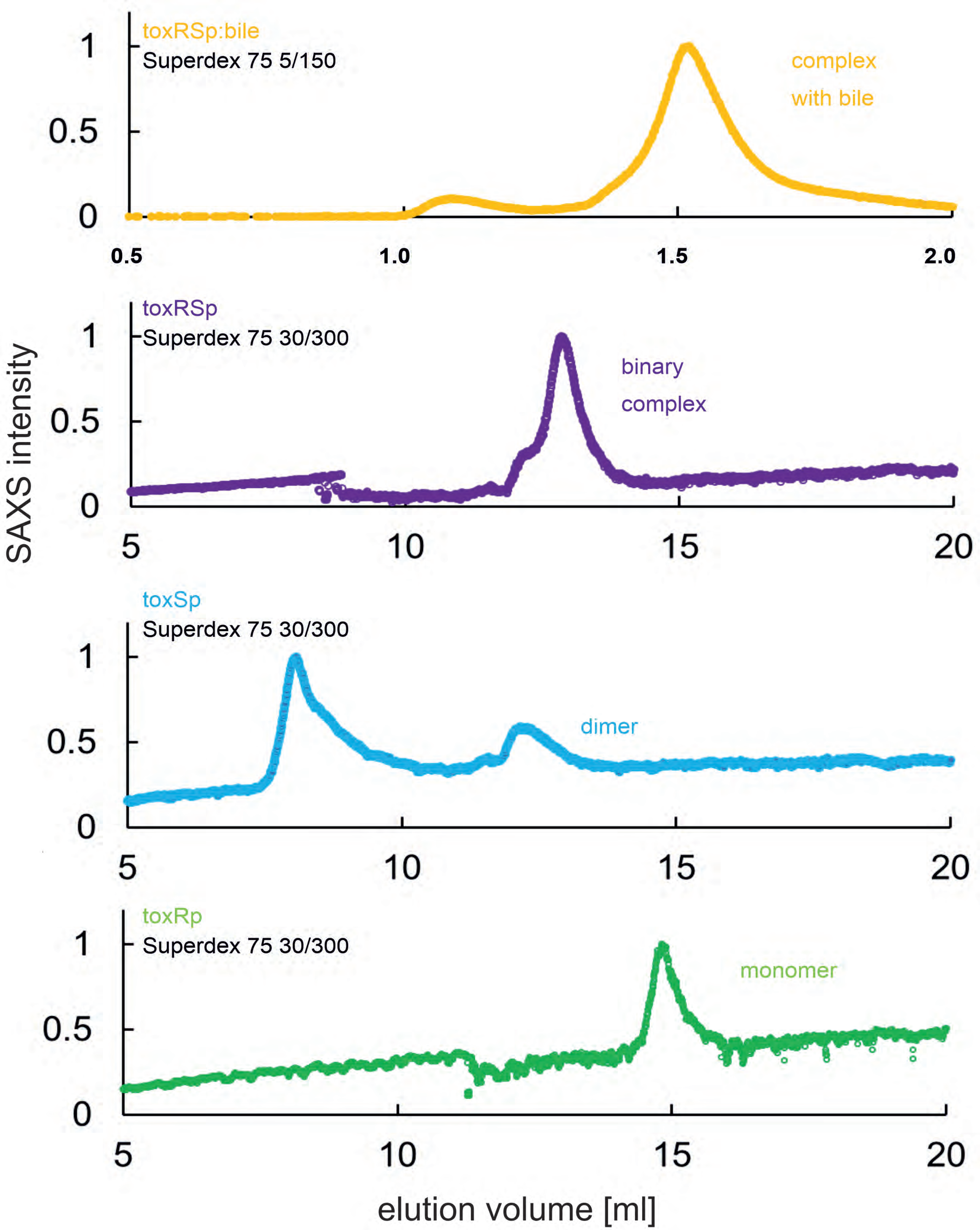
toxRSp:bile
Superdex 75 5/150
complex
with bile
toxRSp
Superdex 75 30/300
binary
complex
toxSp
Superdex 75 30/300
dimer
toxRp
Superdex 75 30/300
monomer
SAXS intensity
elution volume [ml]
0
0.5
1
5
10
15
20
0.5
1.0
1.5
2.0

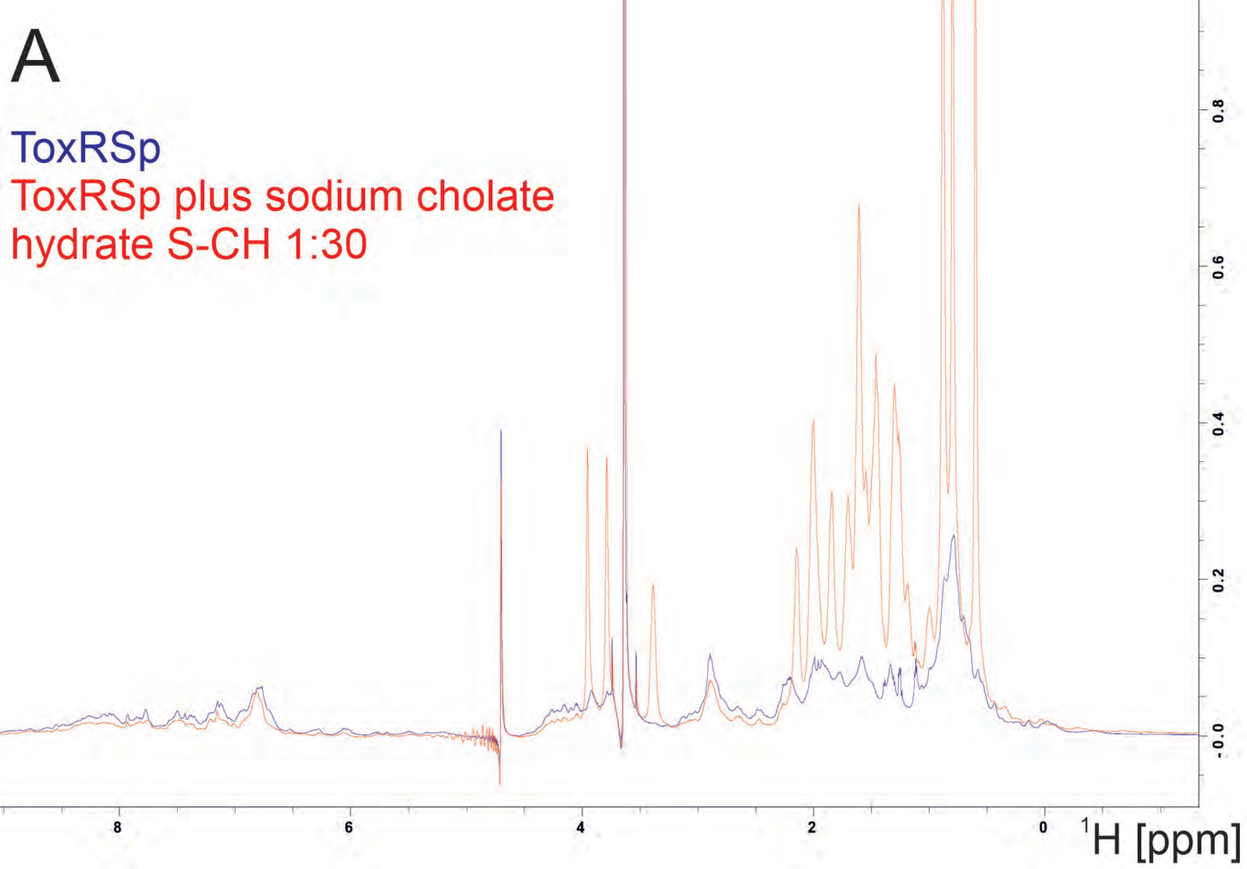
A
ToxRSp
ToxRSp plus sodium cholate hydrate S-CH 1:30
^{1}H [ppm]

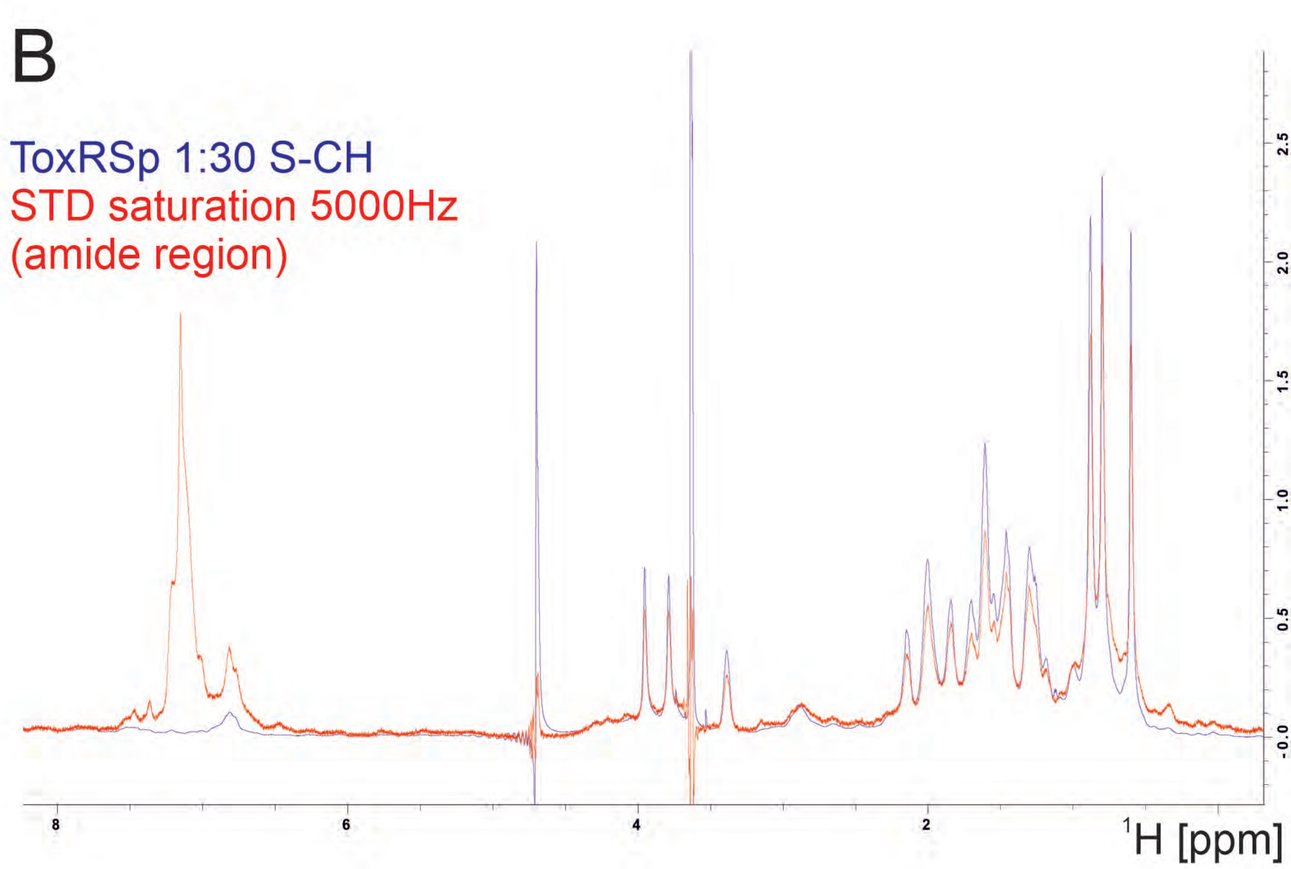
B
ToxRSp 1:30 S-CH
STD saturation 5000Hz (amide region)
^{1}H [ppm]

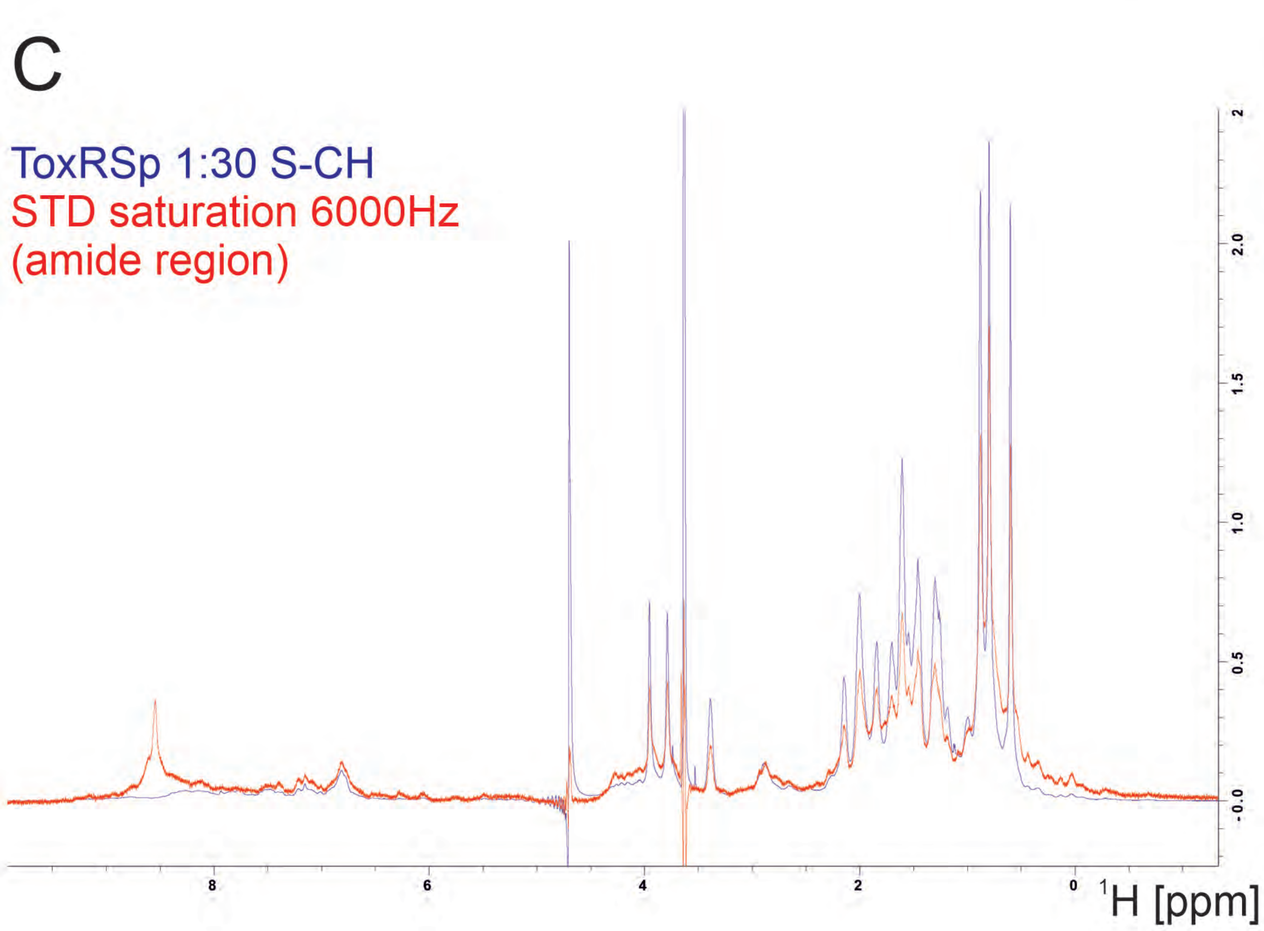
C
ToxRSp 1:30 S-CH
STD saturation 6000Hz (amide region)
^{1}H [ppm]

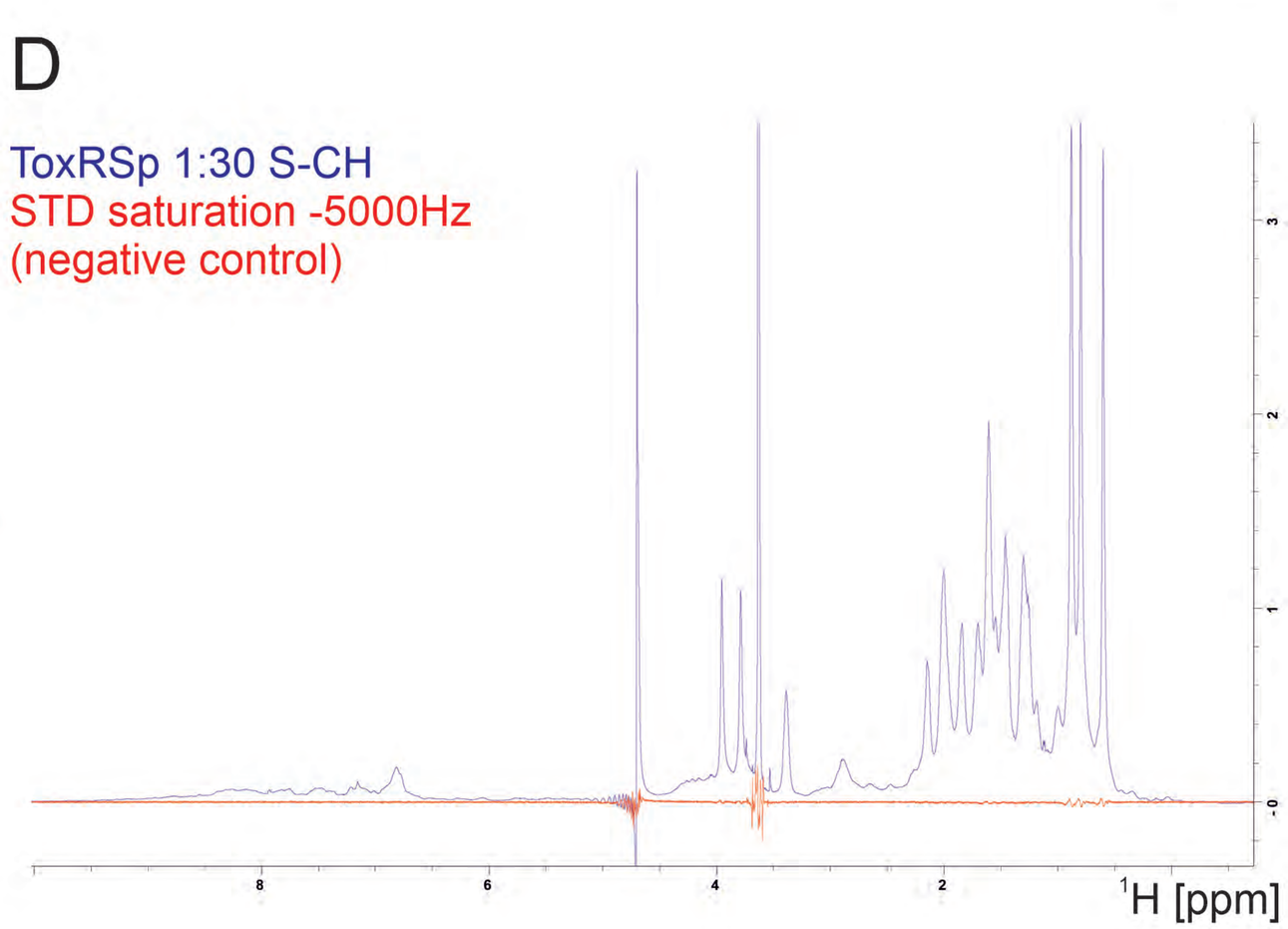
D
ToxRSp 1:30 S-CH
STD saturation -5000Hz (negative control)
^{1}H [ppm]

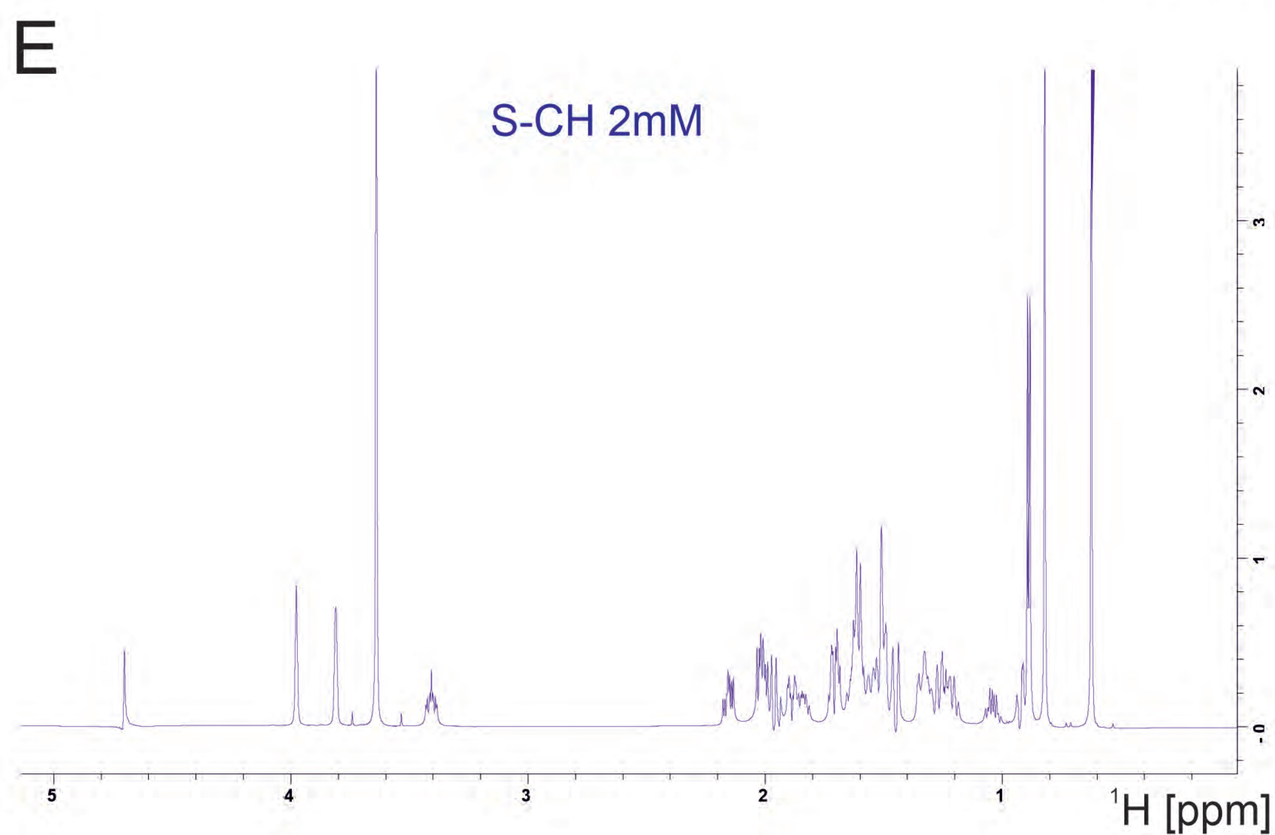
E
S-CH 2mM
^{1}H [ppm]

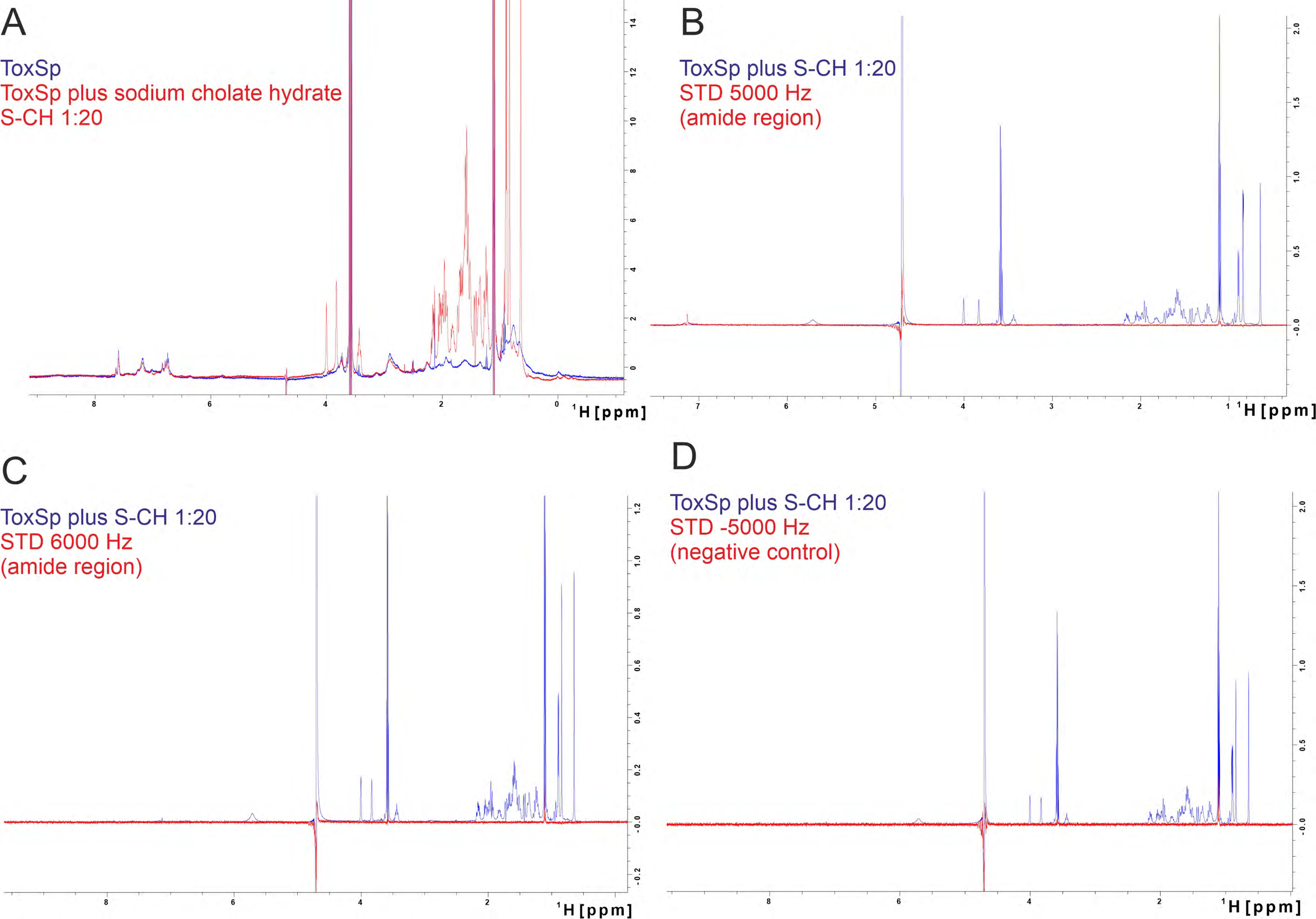
A
ToxSp
ToxSp plus sodium cholate hydrate
S-CH 1:20
^{1}H [ppm]
B
ToxSp plus S-CH 1:20
STD 5000 Hz
(amide region)
^{1}H [ppm]
C
ToxSp plus S-CH 1:20
STD 6000 Hz
(amide region)
^{1}H [ppm]
D
ToxSp plus S-CH 1:20
STD -5000 Hz
(negative control)
^{1}H [ppm]

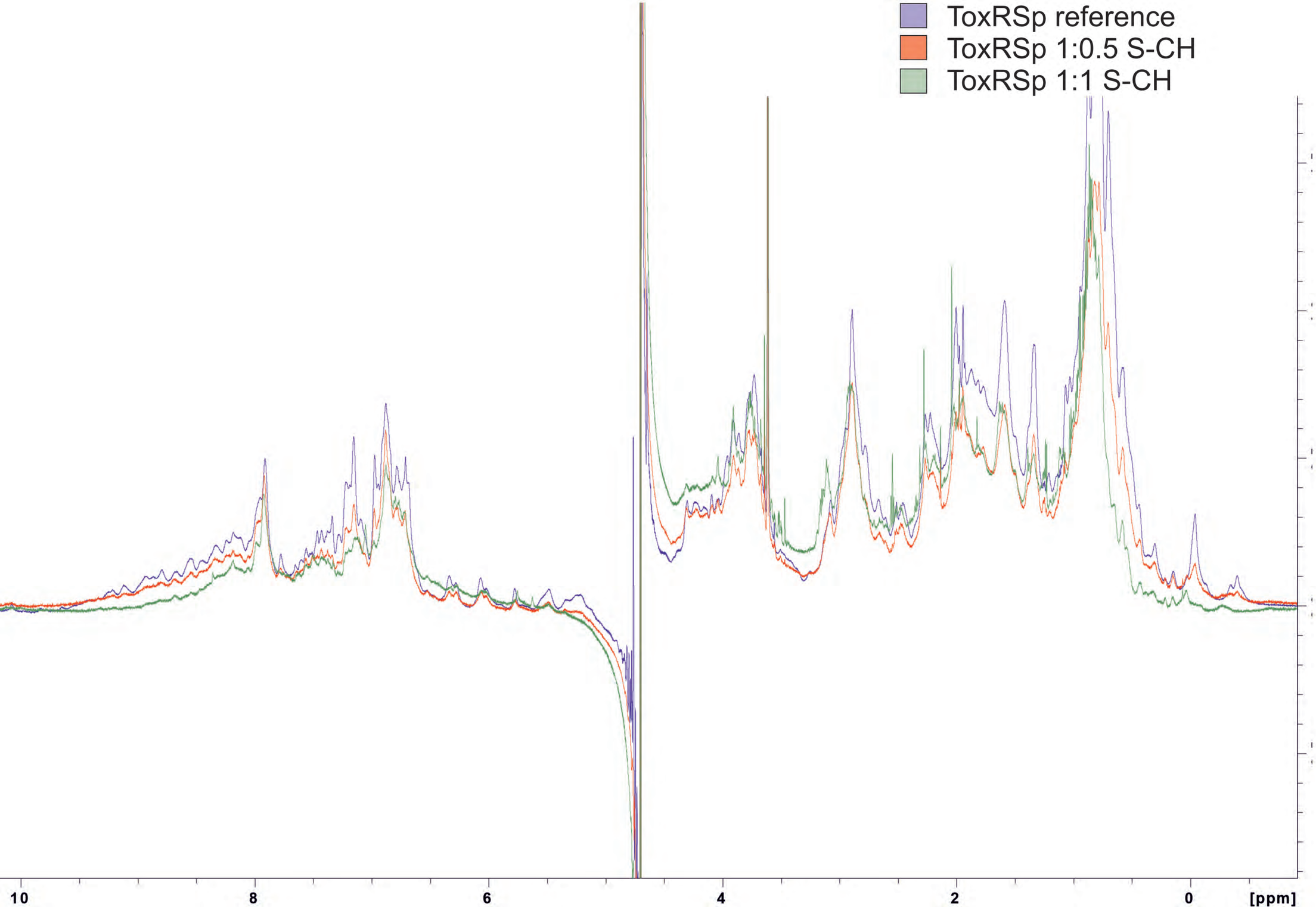
ToxRSp reference
ToxRSp 1:0.5 S-CH
ToxRSp 1:1 S-CH
10
8
6
4
2
0
[ppm]

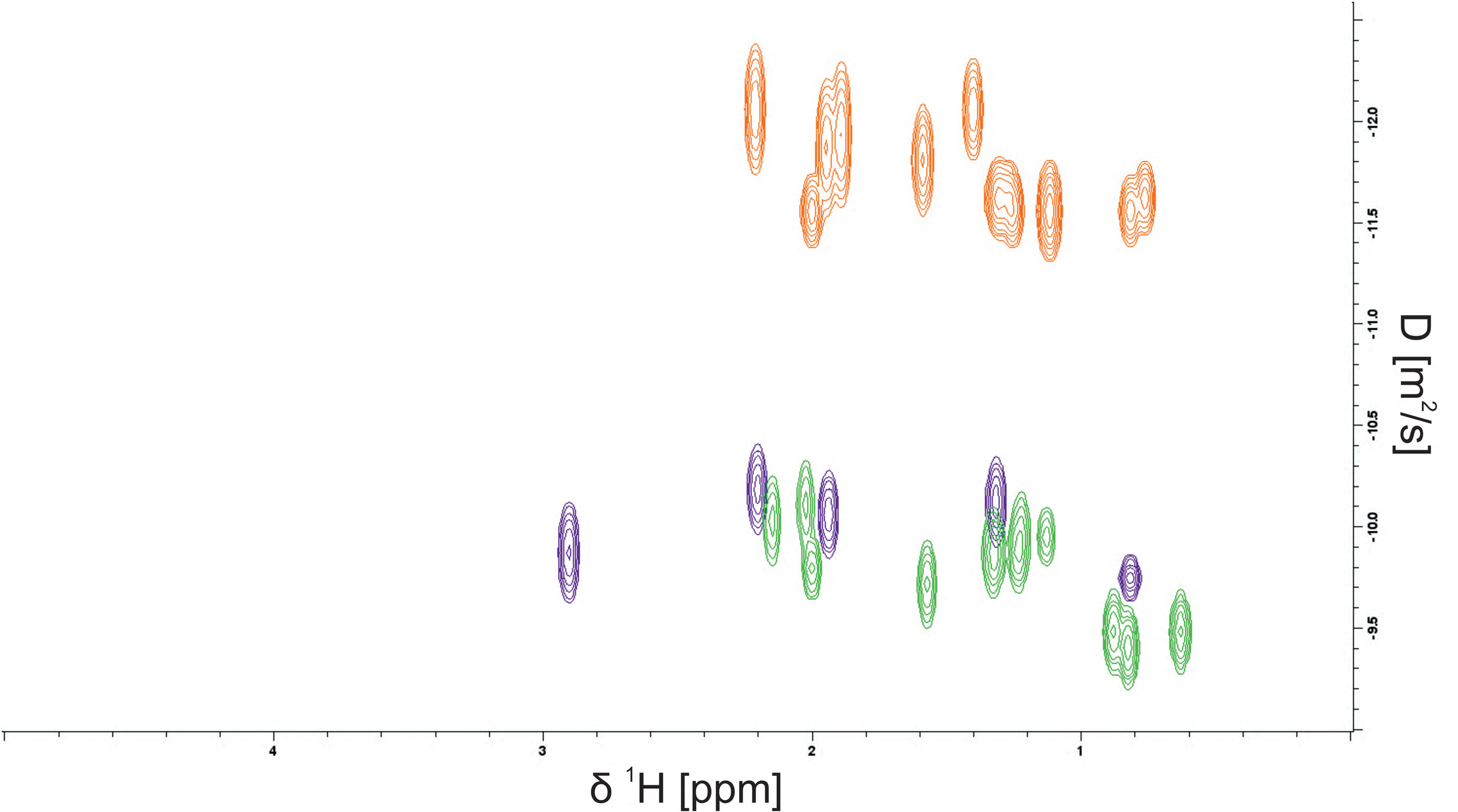
D [m²/s]
-12.0
-11.5
-11.0
-10.5
-10.0
-9.5
δ ¹H [ppm]
4
3
2
1

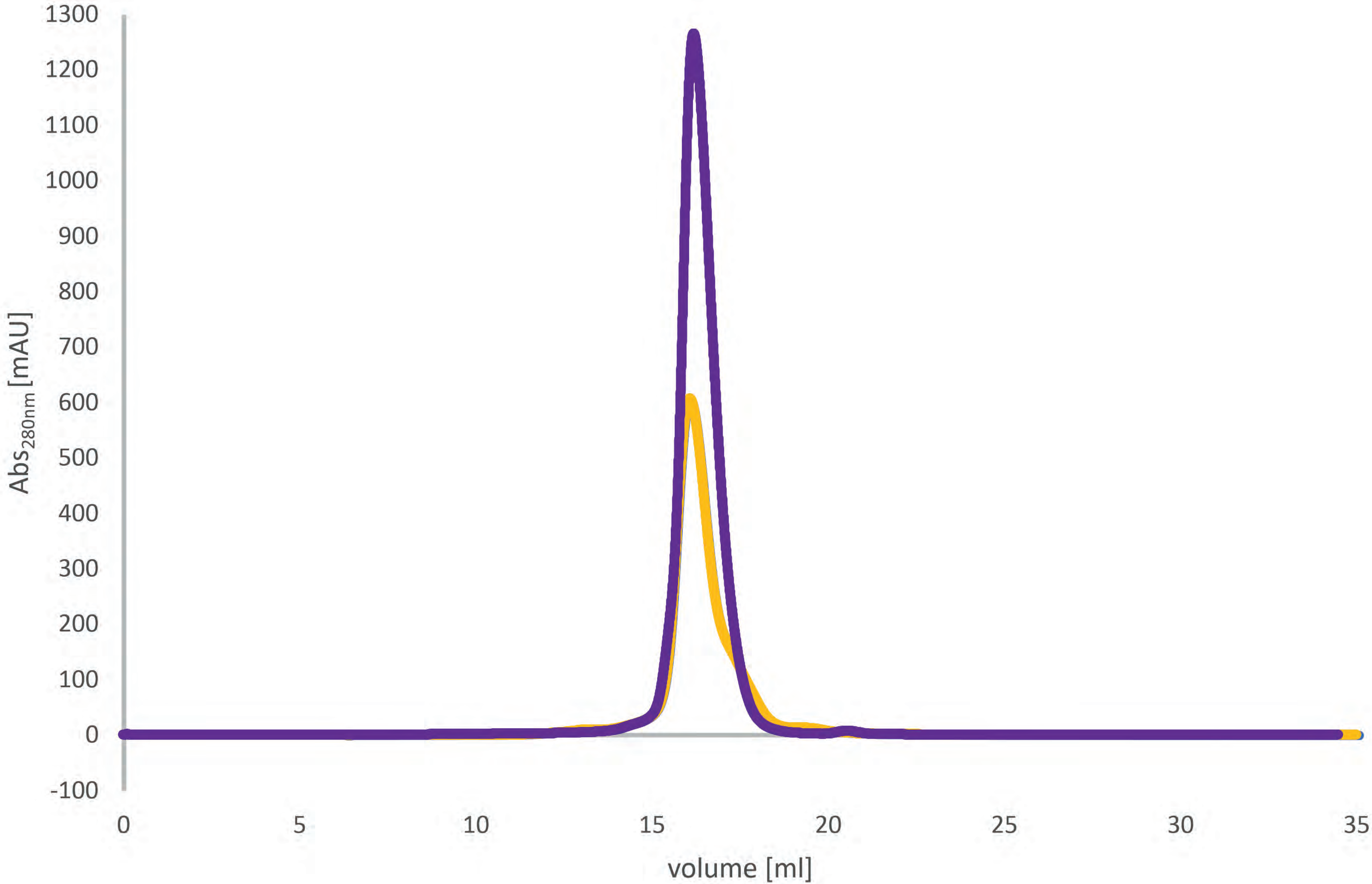
1300
1200
1100
1000
900
800
700
600
500
400
300
200
100
0
-100
Abs280nm [mAU]
0
5
10
15
20
25
30
35
volume [ml]

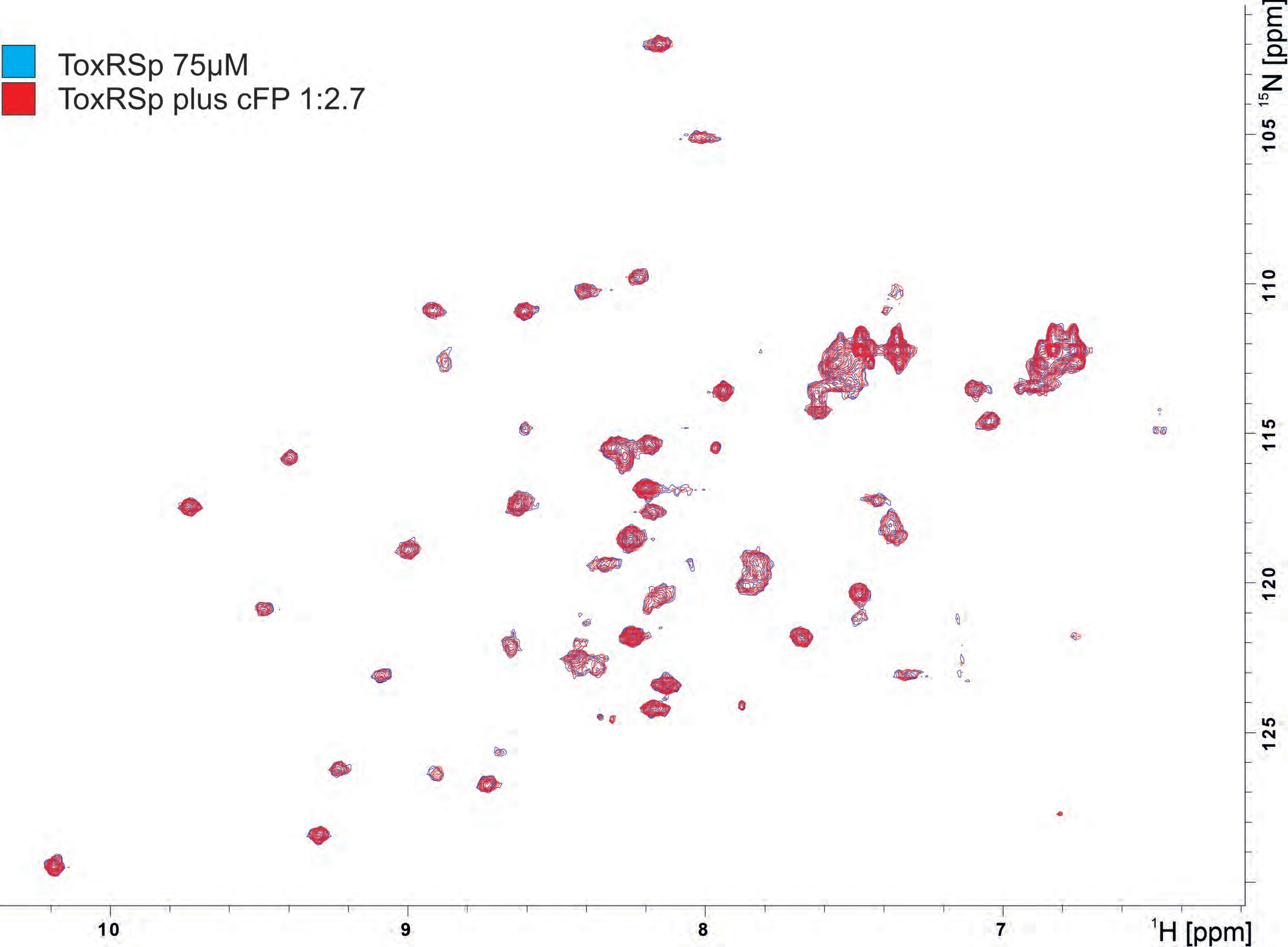
ToxRSp 75µM
ToxRSp plus cFP 1:2.7
105
110
115
120
125
15N [ppm]
10
9
8
7
1H [ppm]

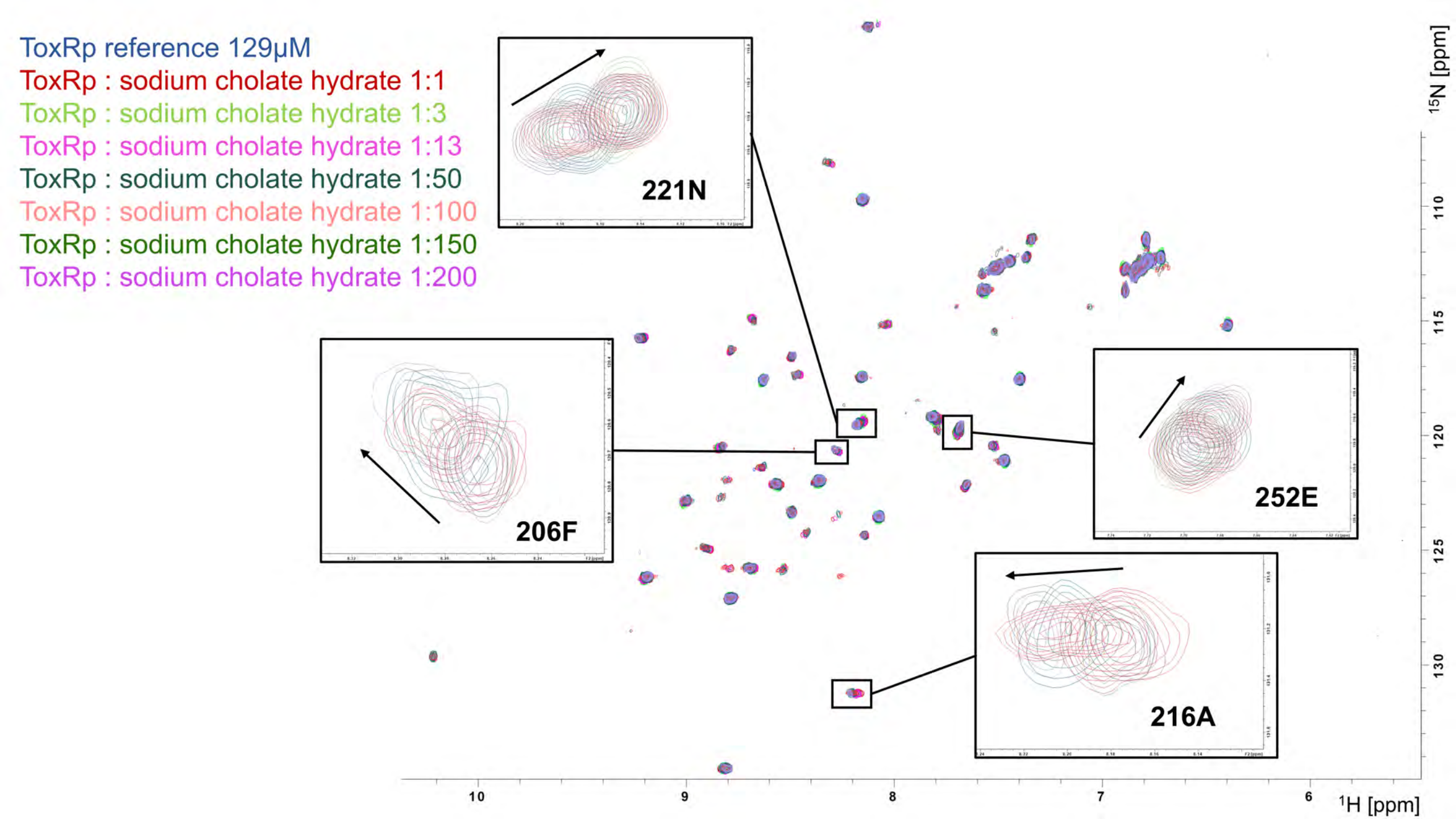
ToxRp reference 129µM
ToxRp : sodium cholate hydrate 1:1
ToxRp : sodium cholate hydrate 1:3
ToxRp : sodium cholate hydrate 1:13
ToxRp : sodium cholate hydrate 1:50
ToxRp : sodium cholate hydrate 1:100
ToxRp : sodium cholate hydrate 1:150
ToxRp : sodium cholate hydrate 1:200
221N
206F
252E
216A
15N [ppm]
110
115
120
125
130
10
9
8
7
6
1H [ppm]

ToxRSp of *Vibrio* species (ToxRp: orange, ToxSp: grey)

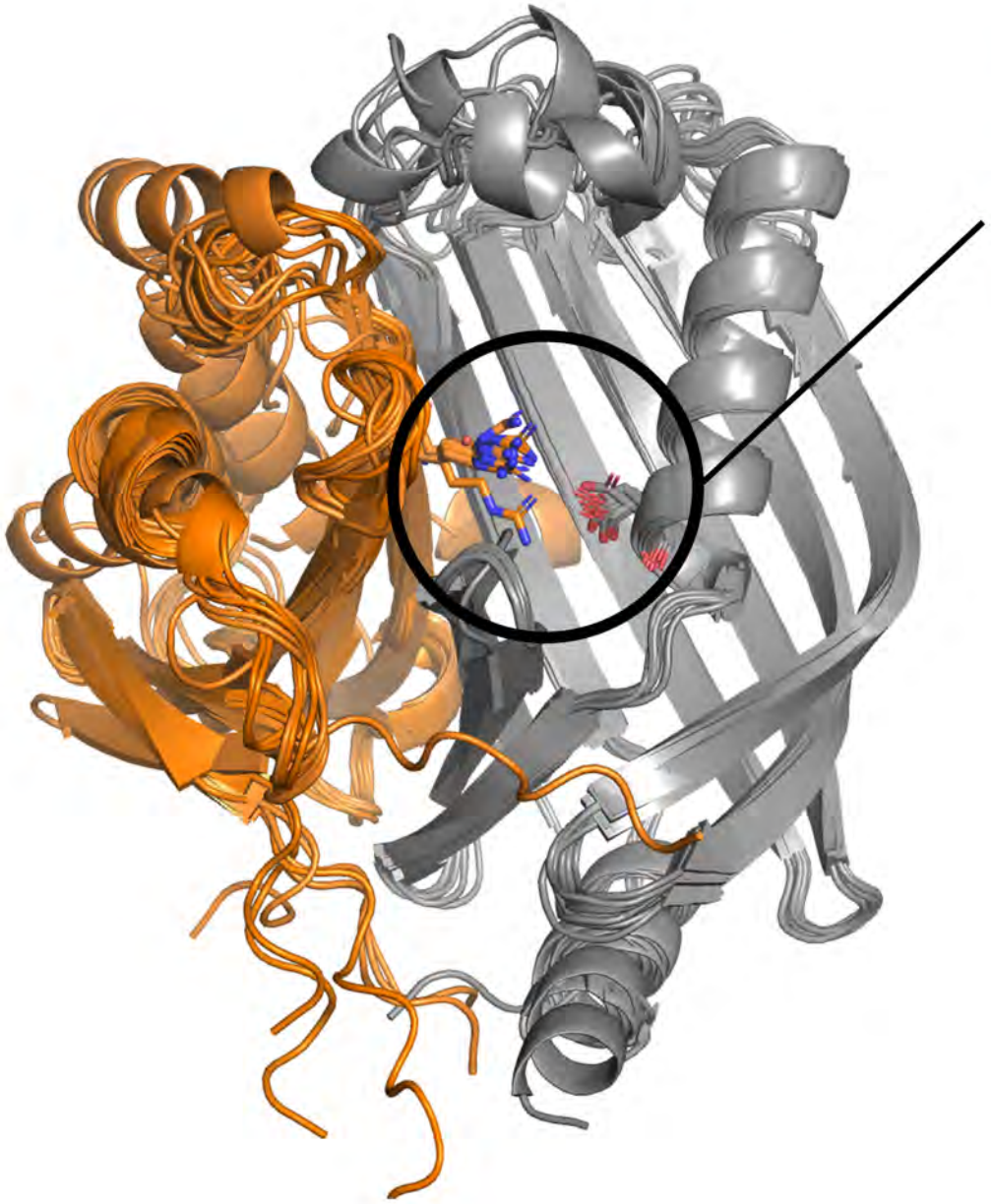

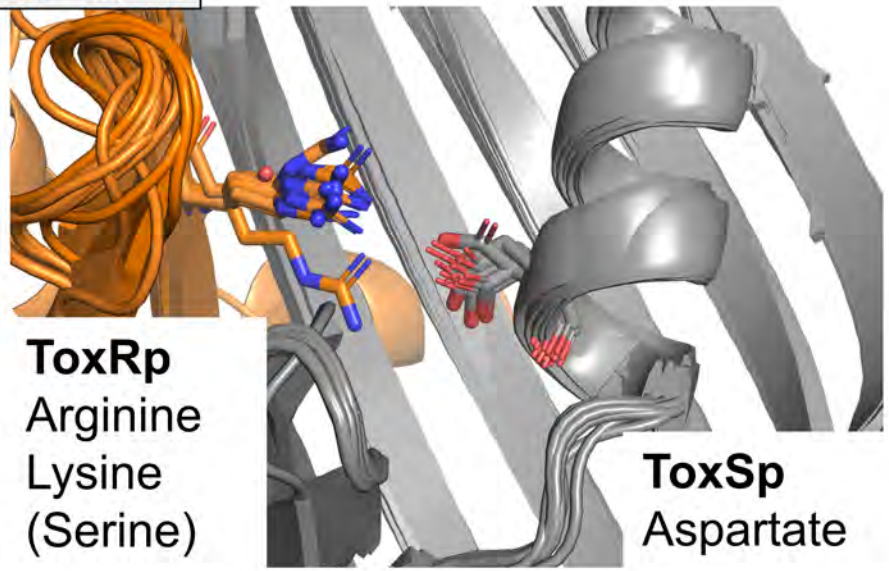

Organism	ToxRp residue	ToxSp residue
V. cholerae	R281	D142
V. fischeri	R	D
V. tapetis	K	D
V. nigripulchritudo	R	D
V. atlanticus	S	D
V. mimicus	R	D
V. vulnificus	R	D
V. parahaemolyticus	R	D
V. diabolicus	R	D
V. rotiferianus	R	D
V. alginolyticus	R	D

Sequential alignment of ToxSp from different *Vibrio* strains

```
fischeri            -----SDSKVEQLLISKEWQSMSTVRID--------TDYEDMGPLKRADIKSNVVYLPNK    47
tapetis             WLYWGSDAQVERVLTSREWQTRMVMRIYADTSTDVLEQDGEIGPLKKATIESNVKYLPNG    60
nigripulchritudo    ---TQTSAKVENVLTSREWQSRMVTRLFIESDS---EQDEVIGPLRKATIDSNVKYLPNG    54
atlanticus          ----GSDAKVERLLTQHEWQSKMVTLIS-----DIK-QEDSIGPLRKVELSSNAKYLPNG    50
cholerae            ------DFKLEQVLTSREWQSKMVSLIK-----TNS-NRPAMGPLSRVDVTSNVKYLPNG    48
mimicus             --------KLEQVLTSREWQSKMVSLIK-----TKS-NSPAMGPLSRVDVSSNVKYLPNG    46
vulnificus          ------DLKVEQVLTSKEWQSYMVTVIT-----DDLQNEGSVGPLRKVTLTSNVKYLPNG    49
rotiferianus        -----SDLKVEQVLTSNEWQSTMVTVIT-----DNLPD-DTVGPLRRVNVESNVKYLPNG    49
parahaemolyticus    ------DLKVEQVLTSNEWQSTMVTVIT-----DNLPD-DTVGPLRRVNVESNVKYLPNG    48
diabolicus          ------DLKVEQLLTANEWQSTMVTVIT-----DSLPD-DTVGPLRRVNVESNVKYLPNG    48
alginolyticus       -----SDLKVEQVLTANEWQSTMVTVIT-----DSLPD-DPVGPLRRVNVESNVKYLPNG    49
                          ::*.:*  .***:  .  :         :   :*** :. : **. ****

fischeri            TYSKSSTLTIYSGLADEIHPLTINVMETGNWDYSGDYLLIDPTEFKDVTASDNKNFSGSQ    107
tapetis             TYLRVSRINLFSESVE--ASSIINVSESGNWEMSDNYLLIEPIEFKEISSNQRQDFTEKQ    118
nigripulchritudo    TYLRVSRINLYTGTHEKNTSSTINVSENGAWELSDNYLLIEPKEFKDISSNQGADFTDKQ    114
atlanticus          TYLRMSVVRLYSTQTA--PANVINISETGQWDINDNYLLISPTEFKDVTSAERQDFSEEQ    108
cholerae            TYLRVSIVKLFSDDNS--AESVINISEFGEWDISDNYLLVTPVEFKDISSNQSKDFTDEQ    106
mimicus             TYLRVSIVKLYSDGNS--AESTINISESGEWDISDNYLLVTPIQFKDISSNQSKDFTDEQ    104
vulnificus          NYVRVSVLKLYSNESS--QEVVINISESGTWDVSDNYLLVTAKEFKDISSSQSKDFSDAQ    107
rotiferianus        DYIRVANIKLFAQGSS--AESTINISERGRWEVSDNYLLVTPSEFKDISSSQSKDFTDEQ    107
parahaemolyticus    DYIRVANIKLFAQGST--AESTINISEKGRWEVSDNYLLVSPSEFKDISSSQSKDFSEAQ    106
diabolicus          DYIRVANIKLFAQGST--AESTINISEKGRWEVSDNYLLVSPSEFKDISSSQSKDFSEAQ    106
alginolyticus       DYIRVANIKLFAQGST--AESTINISEKGRWEVSDNYLLVSPSEFKDISSSQSKDFSEAQ    107
                     * : : : :::         **: * * *: ..:***:   :**:::: :  :*:  *

fischeri            KKLIMRVFRMDAQQSKRVDVVNDKTLLLTSLNYGSGILFSH-  148
tapetis             LGVITQIFKMDSQQSRRVEIINTKALLMTSLDHGSAVFYSH-  159
nigripulchritudo    LKVITQIFKMDAQQSRRVEIINAKALLMTSLDHGSTVLYSH-  155
atlanticus          LELITQVIKMDAEQSRRIDIINQKALLLTSLNHGSTVLFSN-  149
cholerae            LQLITQLFKMDAQQSRRVDIVNERTILFTSLSHGSTVLFSNS  148
mimicus             LQLITQLFKMDAQQSRRVDIVNERTILFTSLNHGSTVLFSNS  146
vulnificus          LKLITKVFKMDAQQSRRIDIVNDQTLLLTSLNHGSSVLFSN-  148
rotiferianus        LRLITQIFRLDAEQSRRIDVVNEKTLLLTSLNHGSTVLFRN-  148
parahaemolyticus    LRLITQIFKLDAEQSRRIDVVNEKTLLLTSLNHGSTVLFRN-  147
diabolicus          LRLITQIFKLDAEQSRRIDVVNEKTLLLTSLNHGSSVLFKN-  147
alginolyticus       LRLITQIFKLDAEQSRRIDVVNEKTLLLTSLNHGSSVLFKN-  148
                      :* :::::*::**:*::::* :::*:***.:** ::: :
```

- Percent Identity Matrix

1: fischeri	100.00	45.21	47.30	49.66	48.61	50.00	52.41	48.97	48.61	48.61	48.28
2: tapetis	45.21	100.00	74.51	57.72	58.50	58.62	56.08	56.76	57.14	55.78	56.76
3: nigripulchritudo	47.30	74.51	100.00	58.22	61.11	62.68	60.00	59.31	59.03	56.94	57.24
4: atlanticus	49.66	57.72	58.22	100.00	59.86	60.69	63.95	58.50	60.27	60.27	59.86
5: cholerae	48.61	58.50	61.11	59.86	100.00	93.15	68.71	69.86	67.12	64.38	65.07
6: mimicus	50.00	58.62	62.68	60.69	93.15	100.00	68.97	70.14	67.36	65.28	65.97
7: vulnificus	52.41	56.08	60.00	63.95	68.71	68.97	100.00	72.11	72.11	71.43	72.11
8: rotiferianus	48.97	56.76	59.31	58.50	69.86	70.14	72.11	100.00	95.24	91.84	91.89
9: parahaemolyticus	48.61	57.14	59.03	60.27	67.12	67.36	72.11	95.24	100.00	96.60	96.60
10: diabolicus	48.61	55.78	56.94	60.27	64.38	65.28	71.43	91.84	96.60	100.00	98.64
11: alginolyticus	48.28	56.76	57.24	59.86	65.07	65.97	72.11	91.89	96.60	98.64	100.00

Sequential alignment of ToxRp from different *Vibrio* strains

```
atlanticus          ----------------------------PSQPTHRLNMSKVNDKTNTFTIESNDPQSKSL     32
fischeri            ----------------------------PKSDAFVE-VANYDN-T-PVFVPVNHPSIERW     29
tapetis             ---------------------------SPSPATFTT-VGTFSD-I-PVKTPENHPDISKW     30
nigripulchritudo    -------------------PFLTYLGSQQKPAKFTT-IAEVAG-I-PVRMPENHPSMQQS     38
cholerae            --------------------------TNPSQTSFKP-LTVVDG-V-AVNMPNNHPDLSNW     31
mimicus             ---------------------------------KFKP-LTVVDD-V-AVNMPINHPDLSNW     25
vulnificus          ----------------------------PSESKFRL-LENVNG-V-EVLTPLNHPPLQAW     29
rotiferianus        --------------------------TKPAESQFRQ-IAEFSG-V-PVMTPANHPQLMQW     31
diabolicus          ------------------------------AESQFRQ-VGEYQN-V-PVMTPVNHPQINSW     28
parahaemolyticus    ---------------------------NPAESQFRQ-IGEYQN-V-PVMTPVNHPQINNW     30
alginolyticus       ASNTINWLPRVIIFLSLLLPVCVLLFTNPAESQFRQ-IGEYQS-V-PVMTPVNHPQINNW     57
                                                  .   :    .    .    *.*

atlanticus          LDRLVSLPELNNSNFYITSNRTRIYVSCIYKENS--TSASQS--------------VNFS     76
fischeri            K------P---------------LIEQCTNFYNSKHTDSLKPIEVIATSGQPNQITLNYI     68
tapetis             I------P---------------SITQCVEVYIARHPNELAPVEVIATGGQNGQIALNYI     69
nigripulchritudo    L------P---------------NIEKCIEHYASQHEGDLAPVQVIATGGQNGQIILNYI     77
cholerae            L------P---------------SIELCVKKYNEKHTGGLKPIEVIATGGQNNQLTLNYI     70
mimicus             L------P---------------SIELCVKKYNEKHTGGLKPVEVIATGGQNNQLTLNYI     64
vulnificus          M------P---------------SIRQCVNKYAETHTGDSAPVKVIATGGQGNQLILNYI     68
rotiferianus        M------P---------------SIEQCVARYVENHTNDVMPVKVIATGGQGNKLVLNYI     70
diabolicus          L------P---------------SIEQCIERYVKYHAEDSMPVEVIATGGQNNQLILNYI     67
parahaemolyticus    L------P---------------SIEQCIERYVKHHAEDSLPVEVIATGGQNNQLILNYI     69
alginolyticus       L------P---------------SIEQCIERYVKHHAEDSLPVEVIATGGQDNQLILNYI     96
                          *                   *                              :*:

atlanticus          V-------DIKRPIAKVVNDIVHECQ-----------------------      95
fischeri            HSEEHSDQSISVRLLIDQKGWIRYVDKQRAVTSIQTFITLNPANYLSNR      117
tapetis             HAPEHSSENVTLKLLAVQPDFNQVCTQ----------------------      96
nigripulchritudo    HSIHYSSENVTLRLFSTQPDFAQVCN-----------------------      103
cholerae            HSPEVSGENITLRIVANPNDAIKVCE-----------------------      96
mimicus             HSPEVSGENITLRIVANPTDAVKVCE-----------------------      90
vulnificus          HTLPHSNENVTLRIFSEQNDLGSICK-----------------------      94
rotiferianus        HDTDHSYENVTLRIFAGQNDPTDICK-----------------------      96
diabolicus          HDSQHSYENVTLRIFAGQNDPTDICK-----------------------      93
parahaemolyticus    HDSNHSYENVTLRIFAGQNDPTDICK-----------------------      95
alginolyticus       HDSNHSYENVTLRIFAGQNDPTDIC------------------------      121
                         .:.  :     .
```

- **Percent Identity Matrix**

1: atlanticus	100.00	15.49	16.90	15.49	25.35	23.88	25.35	18.31	21.43	21.13	21.43
2: fischeri	15.49	100.00	41.05	39.36	45.74	44.44	37.23	37.23	41.94	41.49	40.86
3: tapetis	16.90	41.05	100.00	56.84	48.42	51.11	46.81	48.42	51.61	50.53	50.00
4: nigripulchritudo	15.49	39.36	56.84	100.00	44.79	48.89	50.00	45.83	49.46	49.47	47.06
5: cholerae	25.35	45.74	48.42	44.79	100.00	93.33	54.26	50.00	48.39	50.53	50.53
6: mimicus	23.88	44.44	51.11	48.89	93.33	100.00	54.44	50.00	50.00	51.11	50.56
7: vulnificus	25.35	37.23	46.81	50.00	54.26	54.44	100.00	64.89	59.14	59.57	59.14
8: rotiferianus	18.31	37.23	48.42	45.83	50.00	50.00	64.89	100.00	75.27	74.74	74.74
9: diabolicus	21.43	41.94	51.61	49.46	48.39	50.00	59.14	75.27	100.00	94.62	92.39
10: parahaemolyticus	21.13	41.49	50.53	49.47	50.53	51.11	59.57	74.74	94.62	100.00	97.87
11: alginolyticus	21.43	40.86	50.00	47.06	50.53	50.56	59.14	74.74	92.39	97.87	100.00

Sequential alignment of ToxRp from mostly human colonizing *Vibrio* strains

```
tapetis             -SPSPATFTTVGTFSDIPVKTPENHPDISKWIPSITQCVEVYIARHPNELAPVEVIATGG     59
cholerae            TNPSQTSFKPLTVVDGVAVNMPNNHPDLSNWLPSIELCVKKYNEKHTGGLKPIEVIATGG     60
mimicus             ------KFKPLTVVDDVAVNMPINHPDLSNWLPSIELCVKKYNEKHTGGLKPVEVIATGG     54
vulnificus          --PSESKFRLLENVNGVEVLTPLNHPPLQAWMPSIRQCVNKYAETHTGDSAPVKVIATGG     58
parahaemolyticus    -NPAESQFRQIGEYQNVPVMTPVNHPQINNWLPSIEQCIERYVKHHAEDSLPVEVIATGG     59
diabolicus          ---AESQFRQVGEYQNVPVMTPVNHPQINSWLPSIEQCIERYVKYHAEDSMPVEVIATGG     57
                          *  :   ..: *  * *** :. *:***  *:: *   *     *::******

tapetis             QNGQIALNYIHAPEHSSENVTLKLLAVQPDFNQVCTQ  96
cholerae            QNNQLTLNYIHSPEVSGENITLRIVANPNDAIKVCE-  96
mimicus             QNNQLTLNYIHSPEVSGENITLRIVANPTDAVKVCE-  90
vulnificus          QGNQLILNYIHTLPHSNENVTLRIFSEQNDLGSICK-  94
parahaemolyticus    QNNQLILNYIHDSNHSYENVTLRIFAGQNDPTDICK-  95
diabolicus          QNNQLILNYIHDSQHSYENVTLRIFAGQNDPTDICK-  93
                    *..*: *****    * **:**::.:   *  .:*
```

- **Percent Identity Matrix**

1: tapetis	100.00	48.42	51.11	46.81	50.53	51.61
2: cholerae	48.42	100.00	93.33	54.26	50.53	48.39
3: mimicus	51.11	93.33	100.00	54.44	51.11	50.00
4: vulnificus	46.81	54.26	54.44	100.00	59.57	59.14
5: parahaemolyticus	50.53	50.53	51.11	59.57	100.00	94.62
6: diabolicus	51.61	48.39	50.00	59.14	94.62	100.00